THE FLORIDA STATE UNIVERSITY

COLLEGE OF ARTS AND SCIENCES

A MODEL OF THE SPATIAL STRUCTURE AND PRODUCTIVITY OF PHYTOPLANKTON POPULATIONS DURING VARIABLE UPWELLING OFF THE COAST OF OREGON

By
JOSEPH S. WROBLEWSKI

A Dissertation submitted to the
Department of Oceanography
in partial fulfillment of the
requirements for the degree of
Doctor of Philosophy

Approved:

James J. O'Brien
Professor Directing Dissertation

George A. Knauer

Richard J. Iverson

Lawrence P. Small

Richard S. Iverson

Lawrence P. Small

R. H. Backus

W. D. Sturges 31-8-76
Chairman, Department of Oceanography

December, 1976

ABSTRACT

During the season favorable for coastal upwelling off the western boundary of continents, the local circulation is strongly influenced by occasional wind "events" of several days' duration. Variability in the wind stress affects the rate of upwelling and ultimately the local biological productivity.

To investigate the relationship between wind events and primary production off the coast of Oregon in August 1973, a time-dependent, numerical model of the upwelling circulation was coupled to a complex model of primary and secondary productivity. Primary productivity is a function of nutrient concentration, light intensity and temperature. The model dependent variables (phytoplankton nitrogen, zooplankton nitrogen, nitrate, ammonia and detrital nitrogen) are advected by a flow which is influenced by bottom topography and a variable wind stress.

Advection by a two-cell, upwelling circulation is the major physical mechanism leading to mesoscale patchiness in the phytoplankton, zooplankton, detritus and nutrient fields. The numerical model predicts a phytoplankton and detritus

[illegible]

The numerical model predicts a phytoplankton and detritus plume for which considerable observational evidence exists.

Model predictions of daily primary production (78 to 226 mg N m^{-2} day^{-1}) during intermittent upwelling are paradoxically comparable to production during strong upwelling. When northerly winds are strong, phytoplankton are supplied with more limiting nutrient but experience a shorter euphotic zone residence time. The phytoplankton are advected offshore and down to aphotic zone depths by the lower, cyclonically rotating gyre of the two-cell circulation. Under variable winds downwelling is not as prevalent, enabling the plants to utilize the upwelled nutrients.

A new formulation for herbivore egestion as a function of food availability is proposed. Model herbivore dynamics allow high assimilation efficiency at low grazing rates. In addition inhibition of nitrate uptake by phytoplankton in the presence of ammonia is formulated in a manner consistent with available data. Parameter values of conventional, biological functions for growth, predation and nutrient regeneration are specified from either measurements off Oregon or the literature.

iii

ACKNOWLEDGMENTS

This work was supported primarily by the Office of Naval Research, Ocean Science and Technology Branch under contract N 00014-67-A-0235. The International Decade of Ocean Exploration (IDOE) provided partial support through the Coastal Upwelling Ecosystems Analysis (CUEA) program under NSF Grant No. GX-33502. The author was awarded a National Science Foundation Grant for Improving Doctoral Dissertation Research, Grant No. GA-43265. The National Center for Atmospheric Research, Boulder, Colorado awarded the author a Computing Facilities Grant in support of this research. NCAR is sponsored by the National Science Foundation. Computations were also performed on the CDC 6400 at Florida State University, Tallahassee, Florida.

The accomplishment of this work would not have been possible without the cooperation and encouragement of Dr. J. Dana Thompson. Dr. Thompson provided the physical component of this investigation in a serious effort at interdisciplinary research.

It is with utmost respect and gratitude that I acknowledge my major professor, Dr. James J. O'Brien. Professor O'Brien's achievement in training a scientist in a discipline different than his own is a monument to his scientific

insight. I wish to express my gratitude to Dr. Richard Iverson for many stimulating dialogues over the past four years. Drs. Lawrence Small and James J. O'Brien taught by demonstration the techniques of planning and executing a major oceanographic field program. Other members of my doctoral committee, Drs. Thomas Hallam and George Knauer guided the breadth of this research. Sincere appreciation is extended to my colleagues of the Air-Sea Interaction Group at Florida State University and especially to Messr. John Kindle, Richard Grotjahn and Monty Peffley.

I acknowledge Ms. Elizabeth Smedley and Mr. Dewey Rudd for drafting the figures, and Mrs. Janina Richards for typing the final copy of the manuscript.

Finally, I wish to express my appreciation to my wife, Vena, for her boundless encouragement during my final graduate study years and for typing the draft copies.

This work is dedicated to my father, Mr. S. C. Wroblewski.

v

TABLE OF CONTENTS

	Page
ABSTRACT	ii
ACKNOWLEDGMENTS	iv
TABLE OF CONTENTS	vi
LIST OF TABLES	viii
LIST OF ILLUSTRATIONS	ix
1. INTRODUCTION	1
2. MODEL FORMULATION - THE BIOLOGICAL DYNAMICS	8
2.1 The general equation for mesoscale phytoplankton patchiness	8
2.2 Biological processes included in the model	10
a. The phytoplankton equation	12
b. The herbivore equation	19
c. The detritus equation	21
d. The ammonia and nitrate equations	23
2.3 Scaling of the biological dynamics	23
2.4 Estimation of the biological parameter values	25
a. Steady state solution of the nonspatial model	29
2.5 Formulation of environmental influences on phytoplankton growth	30
a. The temperature function	31
b. The light function	33
c. Phytoplankton growth as a function of light, temperature, and nutrients	34
d. Steady state solution of the (z,t) model	40
of light, temperature, and nutrients	34
d. Steady state solution of the (z,t) model	40
2.6 Calculations of the daily gross primary production	45

Page

3. MODEL FORMULATION - THE PHYSICAL DYNAMICS 47

3.1 Wind forcing and bottom topography . . . 47

3.2 Scaling the physical dynamics 50

3.3 The finite difference scheme 53

3.4 Boundary conditions 57

3.5 Initial conditions 58

4. MODEL RESULTS 63

4.1 The onset of strong upwelling and development of the phytoplankton plume 63

4.2 Cessation of upwelling and decay of the phytoplankton plume 72

4.3 Primary productivity during the strong upwelling case 72

4.4 Plume structure and primary productivity during intermittent upwelling 79

4.5 Model sensitivity analysis 89

4.6 Comparison with observations 94

5. SUMMARY, CONCLUSIONS AND CRITIQUE 100

APPENDIX - DEFINITION OF SYMBOLS AND SCALING RELATIONSHIPS 105

REFERENCES 108

VITA 117

LIST OF TABLES

Page

Table

1. Parameter values of the (x,z,t) mesoscale phytoplankton patchiness model 52

2. Boundary conditions at 50 m depth 59

viii

LIST OF ILLUSTRATIONS

Figure | Page

1. Progressive vector diagram of the winds recorded at the Newport, Oregon, jetty between June 1 and October 1, 1973 5

2. Biological and physical processes included in the spatial model. The biotic components include phytoplankton, herbivores, detritus, and the dissolved nutrients, nitrate and ammonia. Carnivore dynamics are ignored in the model, although the figure shows the probable role of carnivores in the ecosystem. Thin arrows denote pathways of nitrogen between model components. Heavy arrows indicate spatial fluxes 13

3. The exponential reduction in $V_m(NO_3)$ with increasing concentration of ammonia, computed as $V/V_m(NO_3) = e^{-\Psi NH_4}$ where $\Psi = 1.462$ $(\mu gat\ NH_4/\ell)^{-1}$. The four data points summarize four experiments presented in Walsh and Dugdale (1972) 16

4. Uptake rate of nitrate (dotted line), ammonia (dashed line) and total nitrogen uptake (solid line) with increasing concentration of NO_3 and NH_4. Ten micrograms nitrogen per liter on the abscissa means five micrograms of each ionic form are present in solution. It has been

nitrogen per liter on the abscissa means five micrograms of each ionic form are present in solution. It has been

assumed V_m for both nitrate and ammonia is

Figure Page

0.08 hr^{-1} and k_u for both nutrients is 1 μgat N ℓ^{-1}. Uptake of nitrate is inhibited by ammonia in a manner formulated in the text 17

5. Ingestion and egestion rates as functions of phytoplankton concentration. The ingestion rate curve (solid line) for Calanus pacificus is given by a modified Ivlev function where R_m = 0.01 hr^{-1}, Λ = 0.06 (μgat N/ℓ^{-1}) and P_t = 2.5 μgat N ℓ^{-1} (Parsons et al., 1967). Egestion as a constant fraction (0.35) of ingestion is represented by the dotted hyperbolic curve. The sigmoid shaped (dashed) curves for egestion rate result from the function proposed in the text, where $E_m = 3.5\times10^{-3}$ hr^{-1}, $\Delta = 2\times10^{-5}$ hr^{-1}, and τ = 0.15 and 0.10 (μgat N/ℓ)$^{-1}$ 20

6. Assimilation efficiency as a function of food availability. Ingestion rate (I) is defined by the Ivlev grazing curve (solid line) with the same parameter values as in Fig. 5. Egestion rate (E) is determined by the sigmoid curve (dashed line) where τ = 0.15 (μgat N/ℓ)$^{-1}$. Assimilation efficiency (dotted line) is calculated as (I-E)/I. The threshold for superfluous grazing is defined where the assimilation efficiency reaches $(R_m - E_m)/R_m$ 22

Figure Page

7. Time-dependent standing stock concentrations of phytoplankton (P), zooplankton (Z), detritus (D), nitrate (NO_3), and ammonia (NH_4). The abscissa is nondimensional time ($\tau = tV_m$). The ordinate is the concentration of the biotic component as a fraction of the total amount of limiting nutrient in the system, N_t. The nondimensional parameter values for this solution are: $\alpha = 0.03$, $\beta = 0.25$, $\gamma = 0.07$, $\delta = 0.01$, $\lambda = 1.80$, $\xi = 0.05$, $\rho = 0.09$, $\upsilon = 4.50$, $\phi = 0.50$, $\psi = 43.86$, $\omega = 0.02$, and $P^* = 0$ 29

8. Phytoplankton growth rate as a function of temperature. The solid line is calculated from the equation of Lassiter and Kearns (1973), while the dashed line is calculated from Eppley's (1972) general equation 32

9. Relative photosynthesis as a function of light intensity. The solid line is calculated from a modification of the formulation by Vollenweider (1965). The data points are from a laboratory experiment by Ryther (1956) 35

10. Incident radiation as a function of scaled time. The solid line is the positive half of a sine curve. The data points are observations of insolation with comparable time of day recorded in August 1973 off the coast of Oregon 38

11. Steady state oscillation in the phytoplanton profile of the (z,t) model. Plant biomass is expressed as a nondimensional fraction of the total amount of nitrogen in the upwelling profile of the (z,t) model. Plant biomass is expressed as a nondimensional fraction of the total amount of nitrogen in the upwelling ecosystem, N_t 41

Figure Page

12. Light intensity-depth profile at midday in the steady state solution of the (z,t) model 42

13. Steady state vertical profiles of the (z,t) model's dependent variables (herbivores, detritus, nitrate and ammonia) at midday. The dependent variables are expressed as a nondimensional fraction of the total amount of nitrogen in the upwelling ecosystem, N_t . 43

14. Bottom topography assumed in the (x,z,t) upwelling circulation model of Thompson (1974). The rectangular hatched region at the upper right delineates the region of the (x,z,t) model of phytoplankton production 48

15. Stencil showing the grid point locations of the u (squares) and w (crosses) velocities and the dependent variable P (circles) used in integrating the (x,z,t) biological-chemical-physical model. The vertical grid lines in the x-direction are indexed by the letter, j, and the horizontal lines in the z-direction by the letter, k 54

16. (a) The spatial distribution of seawater temperature assumed in the (x,z,t) model of phytoplankton production. Contours are from 7°C at 50 m depth at the coast to 14°C at the surface 50 km offshore. The contour interval is 0.4°C. (b) The steady state gross primary productivity of the water column for the (x,z,t) phytoplankton production model. (c) The steady state phytoplankton spatial distribution for the (x,z,t) model in the

absence of advection. Contour intervals are 0.8 μgat N ℓ^{-1} 60

17. (a) The spatial distribution of the wind stress in the strong upwelling case. The north-south component of the wind stress (solid line) is -0.5 dyne cm^{-2} near the coast. The east-west component of the wind stress is zero everywhere. (b) The temporal variation of the wind stress weighting function in the strong upwelling case 62

18. (a) The upwelling circulation in the transverse plane normal to the coast after 4 days in the strong upwelling case. The bottom topography and the wind stress at day 4 are also shown. The maximum u and w velocities in the field are -2.9 cm sec^{-1} and 1.4×10^{-2} cm sec^{-1}, respectively. (b) The gross primary productivity of the water column after 4 days in the strong upwelling case. (c) The spatial distribution of phytoplankton after 4 days in the strong upwelling case. Contour intervals are 1 μgat N ℓ^{-1} . 65

19. Same as Fig. 18 but for day 7. The maximum u and v velocities in (a) are -5.9 cm sec^{-1} and 4.4×10^{-2} cm sec^{-1}, respectively. Contour intervals in (c) are 1.4 μgat N ℓ^{-1} 67

20. Same as Fig. 18 but for day 10. The maximum u and v velocities in (a) are -6.1 cm sec^{-1} and 5.2×10^{-2} cm sec^{-1}, respectively. Contour intervals in (c) are 1.6 μgat N ℓ^{-1} 68

sec^{-1} and 5.2×10^{-2} cm sec^{-1}, respectively. Contour intervals in (c) are 1.6 μgat N ℓ^{-1} 68

Figure Page

21. (a) Zooplankton field after 10 days in the strong upwelling case. Contour intervals are 1.8 μgat N ℓ^{-1}. (b) Nitrate field after 10 days in the strong upwelling case. Contour intervals are 2 μgat NO_3 ℓ^{-1} . . . 69

22. (a) Ammonia field after 10 days in the strong upwelling case. Contour intervals are 0.6 μgat NH_4 ℓ^{-1}. (b) Spatial distribution of detritus after 10 days in the strong upwelling case. Contour intervals are 0.12 μgat N ℓ^{-1} 71

23. Same as Fig. 18 but for day 15. The maximum u and w velocities in (a) are -3.6 cm sec^{-1} and 1.5×10^{-2} cm sec^{-1}, respectively. Contour intervals in (c) are 2.0 μgat N ℓ^{-1} 73

24. Same as Fig. 18 but for day 20. The maximum u and w velocities in (a) are -2.8 cm sec^{-1} and 7.9×10^{-3} cm sec^{-1}, respectively. Contour intervals in (c) are 1.6 μgat N ℓ^{-1} 74

25. Same as Fig. 21 but for day 20. Contour intervals in (a) are 1.6 μgat N ℓ^{-1} and in (b) are 2 μgat NO_3 ℓ^{-1} 75

26. Same as Fig. 22 but for day 20. Contour intervals in (a) are 0.8 μgat NH_4 ℓ^{-1} and in (b) are 0.1 μgat N ℓ^{-1} 76

27. The north-south component of the wind stress near the coast for the strong upwelling case. The data points show the maximum daily gross primary production calculated for each model day 78

primary production calculated for each model day 78

Figure Page

28. The north-south component of the wind stress calculated from Newport, Oregon, anemometer data recorded during August 1973. The data points show the maximum daily gross primary production predicted for each day by the (x,z,t) productivity model 80

29. The east-west component of the wind stress calculated from the Newport, Oregon, anemometer data recorded during August 1973 . . . 81

30. (a) The spatial distribution of phytoplankton on August 5 in the intermittent upwelling case. Contour intervals are 1.2 μgat N ℓ^{-1}. (b) Same as (a) but on August 15. Contour intervals are 1.4 μgat N ℓ^{-1} . 82

31. Daily gross primary production of the water column within 10 km of the coast as predicted by the (x,z,t) productivity model during August 1973. In (a) the production calculated for August 6, 7 and 8 is shown. In (b) the production for August 11, 12 and 13 is calculated 84

32. Same as Fig. 30 but for August 14 through 17 in (a), and August 18 through 20 in (b) 85

33. (a) Spatial distribution of zooplankton on August 15 in the intermittent upwelling case. Contour intervals are 1.6 μgat N ℓ^{-1}. (b) The nitrate field on August 15 in the intermittent upwelling case. Contour intervals are 2 μgat NO_3 ℓ^{-1} 86

Figure Page

34. (a) The ammonia field on August 15 in the intermittent upwelling case. Contour intervals are 0.6 µgat NH_4 ℓ^{-1}. (b) The spatial distribution of detritus on August 15 in the intermittent upwelling case. Contour intervals are 0.1 µgat N ℓ^{-1} 87

35. The phytoplankton field predicted by the (x,z,t) productivity model for August 23 in the intermittent upwelling case. Contour intervals are 1.8 µgat N ℓ^{-1} 88

36. (a) and (b) as Fig. 20b and c except it has been assumed the temperature field is homogeneous in x. Contour intervals in (b) are 2 µgat N ℓ^{-1} 91

37. (a) The phytoplankton spatial distribution in a transverse plane normal to the coast observed off Oregon on August 7, 1972. Phytoplankton biomass is expressed in terms of mg chlorophyll *a* m^{-3}. (b) Same as (a) except observed on August 9, 1972 (from Small, in preparation) 95

1. INTRODUCTION

The mechanisms controlling phytoplankton patchiness in the ocean are poorly understood. By "patchiness" the author refers to the three-dimensional structure of the phytoplankton population, usually measured as concentration of biomass.

It has long been suspected that the spatial heterogeneity of oceanic plankton is strongly related to the variability of the physical environment (Bainbridge, 1957; Cassie, 1963). Any attempt to parameterize the physical environment in less than its full complexity results in some loss of understanding of the interaction of physical and biological processes in creating phytoplankton patchiness. Yet, parameterization to some extent is necessary, as one cannot look at all relevant spatial and temporal scales simultaneously.

Twenty years elapsed between the first dynamical investigation of patchiness (Kierstead and Slobodkin, 1953) and significant, subsequent progress on the theory of the phenomenon (Platt, 1972). Theory on the distribution of phytoplankton in the vertical dimension has progressed steadily (for a review, see Patten, 1968), in part due to the ease of sampling in the vertical relative to areal

steadily (for a review, see Patten, 1968), in part due to the ease of sampling in the vertical relative to areal sampling. Only recent development of instrumentation and

methodology (Walsh, 1972; Denman and Platt, 1975; Powell et al., 1975) which enables quasi-synoptic sampling of the phytoplankton distribution, has made it possible to field test theories of patchiness. Yet, even the most recent theoretical papers on the spatial structure of phytoplankton populations (Criminale and Winter, 1974; Kamykowski, 1974; Platt and Denman, 1975; Dubois, 1975; Wroblewski and O'Brien, 1976) consider the physical advective and diffusive processes to be homogeneous in the horizontal plane. The few exceptions (Walsh and Dugdale, 1971; Walsh, 1975; O'Brien and Wroblewski, 1976) have been complex numerical models with no analytical solution possible.

Biological processes regulated by the physical and chemical environment can interact with physical transport processes to create large scale features called plumes and tongues. The spatial structure of phytoplankton on scales below several hundred meters is largely controlled by turbulence (Platt, 1972; Denman and Platt, 1975; Powell et al., 1975). This small scale variability is linked to larger scale structures through the continuous turbulent dissipation of the latter (Nihoul, 1975; Platt, 1975). Differences in the physiological character of phytoplankton populations and the existence of microenvironments can also lead to small scale patchiness (Platt and Filion, 1973; Platt and Subba Rao, 1970; Richerson et al., 1970).
lead to small scale patchiness (Platt and Filion, 1973; Platt and Subba Rao, 1970; Richerson et al., 1970).

Above the 1 km length scale phytoplankton biomass no longer behaves merely as a passive scalar subject to

turbulent transport. Advection becomes increasingly important relative to diffusion and biological processes in determining the spatial configuration of the phytoplankton biomass (O'Brien and Wroblewski, 1973; Denman and Platt, 1976).

As often observed length-scale of phytoplankton patchiness in coastal upwelling areas is 5 to 10 km (Beers et al., 1971; Walsh et al., 1974; Kelley et al., 1975). Most biological processes relevant to phytoplankton dynamics occur within the euphotic zone. The time-scales of interest here range from hours (diel periodicity is quite evident in phytoplankton standing crops) to weeks, i.e., several times the fundamental time scale of the mid-latitude upwelling event (Huyer and Pattulo, 1972). The formation and dissipation of plumes and tongues, i.e., water masses rich in phytoplankton biomass with predominant vertical and horizontal extensions respectively[1], is encompassed within these temporal and spatial scales (Beers et al., 1971; Walsh and Dugdale, 1971).

---

[1]The United Nations' Scientific Committee on Ocean Research (SCOR) Working Group 36 during their 1974 meeting in Kiel, Germany, provided new guidelines for terminology used to describe spatial distributions of biological and chemical variables in upwelling regions. The Group recommended use of the term "tongue" to refer to spatial features with a predominant horizontal length scale, such as a shallow coastal bloom of phytoplankton with a seaward protuberance which remains contiguous with the shoreline. "Plumes" should refer to coastal blooms with a significant, offshore directed, vertical extension. Thus the nutrient depleted, thin layer of low salinity water which is discharged from the mouth of the Columbia River and overlies the coastal water off Washington and Oregon should be referred to as the Columbia River "tongue."

During the summers of 1972 and 1973 the Coastal Upwelling Experiment (CUE) was conducted off the Oregon coast. CUE was part of the Coastal Upwelling Ecosystems Analysis Program sponsored by IDOE. Oceanographic data collection efforts during CUE were carried out by four ships; the R/V YAQUINA and R/V CAYUSE from Oregon State University, the National Oceanic and Atmospheric Administration ship R/V OCEANOGRAPHER, and the R/V T.G. THOMPSON of the University of Washington.

Continuous current measurements were made by three types of buoy arrays. An aircraft from the National Center for Atmospheric Research made remote measurements of sea surface temperature and color, in addition to collecting meteorological data. The biological component of CUE consisted of sampling surveys of the primary and secondary production, coordinated by Drs. L. F. Small and C. B. Miller of Oregon State University.

During CUE-I in 1972, it became evident that the local upwelling circulation was significantly affected by wind "events" of 3 or more days' duration. Figure 1 is a progressive vector diagram (PVD) of hourly wind data recorded during the summer of 1973 by an anemometer located on a jetty off Newport, Oregon. The plot is constructed by placing vectors of the wind speed and direction head to tail. The PVD indicates the winds were predominantly from
placing vectors of the wind speed and direction head to tail. The PVD indicates the winds were predominantly from the north during the summer months. Two wind events in

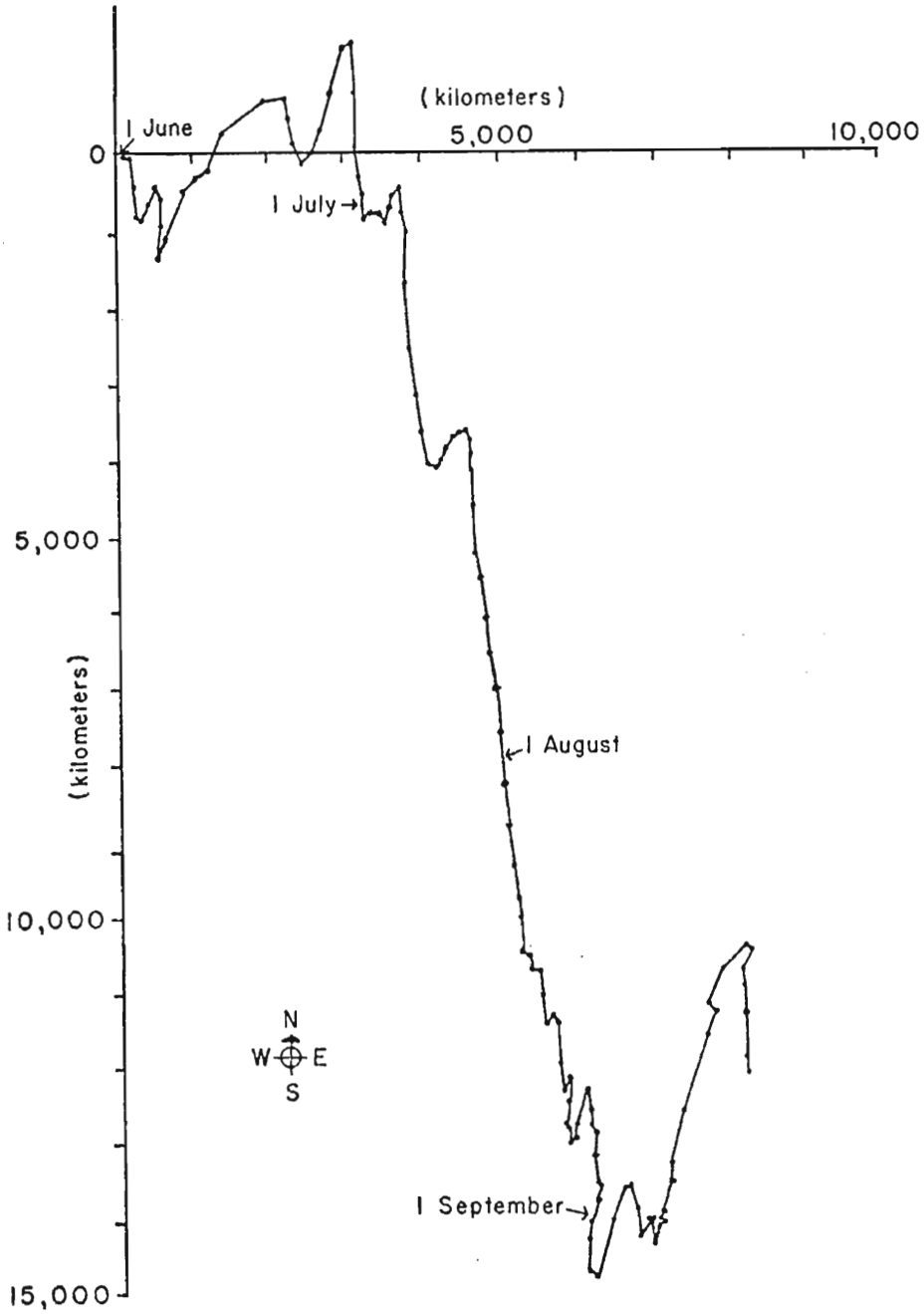

Fig. 1. Progressive vector diagram of the winds recorded at the Newport, Oregon,jetty between June 1 and October 1. 1973.

Fig. 1. Progressive vector diagram of the winds recorded at the Newport, Oregon,jetty between June 1 and October 1, 1973.

July are shown. The first begins July 8 and lasts 7 days, and the second begins July 21 and endures an exceptionally long 20 days.

This paper is an attempt to determine whether our current understanding of coastal upwelling circulation and marine biological processes can be combined into a dynamical explanation of mesoscale phytoplankton patchiness. Nonlinear equations for the distribution of phytoplankton, herbivores, detritus and the nutrients, nitrate and ammonia in a transverse plane normal to the Oregon coast are solved numerically for both strong and intermittent upwelling conditions. Daily primary production of the water column is calculated at 1 km intervals within 50 km of the coast during 20 days of strong upwelling. Daily primary production is also computed for the first 20 days of August 1973 when variable winds induce intermittent upwelling.

The ecosystem dynamics pertinent to patchiness are formulated in Section 2. These dynamics are investigated first without spatial dependence and subsequently with vertical and horizontal dependence. The steady state vertical solutions are utilized as initial conditions for the time-dependent, two-dimensional model of phytoplankton patchiness off Oregon. The numerical scheme, boundary conditions, and physical dynamics of the latter model are carefully discussed in Section 3. Important questions concerning poorly
physical dynamics of the latter model are carefully discussed in Section 3. Important questions concerning poorly
known, biological parameter values and controversial

process formulations are discussed in view of an empirical sensitivity analysis in Section 4. Model water column productivities and dependent variable distributions are compared to observations. Finally, the ability of the model to predict primary production and phytoplankton patchiness during coastal upwelling off Oregon is evaluated.

2. MODEL FORMULATION - THE BIOLOGICAL DYNAMICS

In this section the rationale for the biological and chemical dynamics included in the model is presented. Proper formulation of the problem is the most difficult and important task in modeling research. The ability to reproduce and explain the behavior of oceanic ecosystems requires the inclusion of the important operating mechanisms in the model equations.

2.1 The general equation for mesoscale phytoplankton patchiness

The general equation which describes the distribution of a non-conservative variable in the sea, e.g., phytoplankton biomass, P, is

$$\frac{\partial P}{\partial t} + \nabla \cdot \vec{V}P - \nabla \cdot (K\nabla P) = \text{biological dynamics} \qquad (1)$$

where t is time, $\vec{V}$ represents the horizontal and vertical water velocities, and K is the coefficient of eddy diffusivity. The first term is the local change in P. The divergence represents advection of P, the third term represents turbulent mixing, and "biological dynamics" refers to the biological processes affecting the local change in P.

Three fundamental assumptions are necessary. First, the velocity field is assumed to be nondivergent, i.e., $\nabla \cdot \vec{V} = 0$. This is a requirement for conservation of mass.

Second, the horizontal and vertical coefficients of eddy diffusivity are assumed constant. Third, all derivatives in the longshore direction are neglected. The region of the Oregon coast chosen for the major field experiment CUE is an area where this assumption is more likely to be valid than other upwelling regions currently under study. If one chooses a coordinate system in which y is in the longshore direction, x is positive towards the coast, and z is positive downwards, (1) can be rewritten,

$$\frac{\partial P}{\partial t} + u \frac{\partial P}{\partial x} + w \frac{\partial P}{\partial z} - K_h \frac{\partial^2 P}{\partial x^2} - K_v \frac{\partial^2 P}{\partial z^2} = \text{biological dynamics} \qquad (2)$$

The horizontal velocity, u, is assumed positive towards the coast, and the vertical velocity, w, is positive upwards.

Platt and Denman (1975) examined the relative magnitude of the physical and biological terms in an equation for the mesoscale distribution of phytoplankton in the ocean, similar to (2). They found that given the appropriate conditions, any one of the probable biological and physical processes involved (phytoplankton growth, phytoplankton cell sinking, herbivore grazing, advection or diffusion) can dominate the equation. Thus it is important to specify as exactly as possible the physical and biological dynamics occurring in the region of study.

occurring in the region of study.

2.2 Biological processes included in the model

In the hierarchy of ecosystem modeling (Dugdale, 1975) the (x,z,t) simulation model presented here could be

classified as a productivity model with a detailed consideration of physical influences in both the horizontal and vertical dimensions. Indeed, one of the major concerns of this model is to evaluate the primary productivity, or the rate at which phytoplankton biomass increases, under different upwelling conditions. The author attempts prediction of variances in phytoplankton biomass as well as simulation of the standing crop. Toward this end one must first identify and properly formulate the biological processes influencing primary production.

Neglecting spatial terms for the moment, the local change in the biological variables can be described as

$$\frac{\partial P}{\partial t} = \text{uptake of } NO_3 \text{ and } NH_4 \text{ by growing P} - \text{grazing upon P by Z} - \text{lysis of senescent P cells} \quad (3)$$

$$\frac{\partial Z}{\partial t} = \text{ingestion of P by Z} - \text{metabolic excretion by Z} - \text{egestion of fecal pellets} \quad (4)$$

$$\frac{\partial D}{\partial t} = \text{fecal pellet production} + \text{phytoplankton cell lysis} - \text{bacterial mineralization of detrital nitrogen} \quad (5)$$

$$\frac{\partial NH_4}{\partial t} = \text{bacterial decomposition of detritus} + \text{metabolic excretion by Z} - \text{bacterial oxidation of } NH_4 - \text{uptake of } NH_4 \text{ by P} \quad (6)$$

$$\frac{\partial NO_3}{\partial t} = \text{bacterial oxidation of } NH_4 - \text{uptake of } NO_3 \text{ by P} \quad (7)$$

$$\frac{\partial NO_3}{\partial t} = \text{bacterial oxidation of } NH_4 - \text{uptake of } NO_3 \text{ by P} \quad (7)$$

where P is phytoplankton nitrogen, Z is zooplankton nitrogen, D is detrital nitrogen, NO_3 is dissolved nitrate and nitrite, and NH_4 is dissolved ammonia[2]. All biotic components are expressed in units of concentration of the limiting nutrient, nitrogen. Biological rates are expressed in terms of nitrogen turnover time.

Park (1967) measured a preformed nitrate/phosphate atomic ratio off Oregon of 7:1. Observing the normal assimilation ratio is 16:1, Park suggested nitrogen as the limiting nutrient off Oregon. Field sampling often showed silicate and phosphate present in the euphotic zone where nitrate and ammonia were depleted (Ball, 1970; Atlas, 1973).

In most food chain models, marine species with similar feeding habits are assigned to one trophic level. The individual dynamics of species are lost in this aggregation, except where one organism dominates the trophic level. The phytoplankton community off the Oregon coast during the upwelling season consists mainly of the diatoms Skeletonema costatum, Chaetoceros spp., Rhizosolenia spp. and Thalassiosira spp., with dinoflagellates present but less abundant (Anderson, 1972; Menzies, personal communication). The zooplankton over the Oregon continental shelf in summer are mostly copepoda. The copepods with the highest average biomass are Acartia clausii, A. longiremis, Pseudocalanus minutus, Calanus finmarchicus, and C. plumchrus (Peterson,

mass are Acartia clausii, A. longiremis, Pseudocalanus minutus, Calanus finmarchicus, and C. plumchrus (Peterson,

[2]The charges on the ions NO_3^- and NH_4^+ are omitted for convenience.

1972; Myers, 1975). Over the shelf break the pelagic species, Calanus pacificus and Euphausia pacifica, become important (Smiles and Pearcy, 1971). The collective physiology and behavior of these organisms specify the plankton dynamics included in this model. For example, the zooplankton species over the Oregon shelf exhibit little diel vertical migration (Peterson, 1972), and thus this behavior is not simulated.

Consideration of ecosystem dynamics is limited to two trophic levels and a slowly regenerating detritus component (Fig. 2). Carnivore biomass or predation is not considered. Reproduction or natural death of zooplankton is not dealt with on the short time scale of concern here (days to weeks), although the herbivores can increase in biomass by assimilation of phytoplankton nitrogen. Multiple nutrient limitation of phytoplankton growth is restricted to the dissolved nutrients, NO_3 and NH_4. It is assumed extracellular excretion of nitrogen by growing plants is negligible. Plant growth inhibition or enhancement by trace elements and chelation effects (Johnston, 1964; Barber and Ryther, 1969) are not considered.

2.2a The Phytoplankton equation

Dugdale (1967), Eppley and Coatsworth (1968), MacIsaac and Dugdale (1969), and Caperon and Meyer (1972b) have demonstrated that uptake rates of nitrate and ammonia by marine phytoplankton can be expressed as hyperbolic functions of

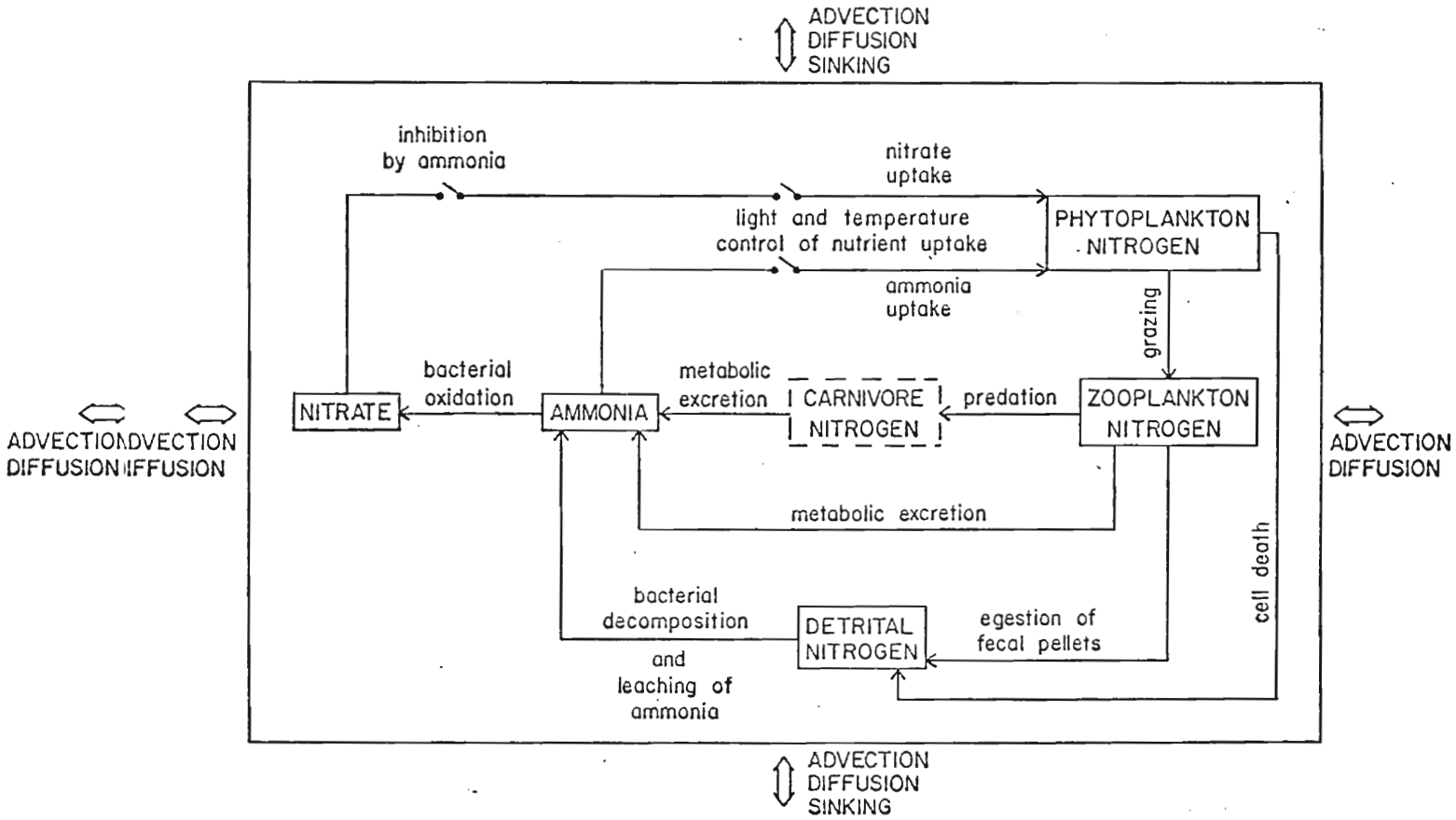

Fig. 2. Biological and physical processes included in the spatial model. The biotic biotic components include phytoplankton, herbivores, detritus, and the dissolved nutrients, nitratenitrate and ammonia. Carnivore dynamics are ignored in the model, although the figure shows tshows the probable role of carnivores in the ecosystem. Thin arrows denote pathways of nitrof nitrogen between model components. Heavy arrows indicate spatial fluxes.

nutrient concentration when that nutrient limits growth. The Michaelis-Menton formulation describing these uptake kinetics is

$$V = \frac{V_m N}{k_u + N}$$

where V is the uptake rate (time^{-1}) of nutrient N (concentration), V_m is the maximum uptake rate, and k_u is the Michaelis or half-saturation constant. The concentration k_u supports half the maximum uptake rate.

Eppley and Thomas (1969) and Caperon and Meyer (1972a) recognized that nutrient uptake and cell growth are indirectly related, as uptake can be separated in time from cell division. Eppley and Thomas have suggested that since cell growth, μ, is a function of cellular content of limiting nutrient, growth is also a hyperbolic function of dissolved nutrient concentration

$$\mu = \frac{\mu_m N}{k_g + N} \quad .$$

Only if the half-saturation constants for uptake, k_u, and growth, k_g, are equal is nutrient uptake equivalent to cell growth. The author makes this assumption here, a not indefensible position when modeling phytoplankton growth in upwelled waters.

Phytoplankton cells preferentially take up ammonia over nitrate. Indeed, the presence of ammonia inhibits the

Phytoplankton cells preferentially take up ammonia over nitrate. Indeed, the presence of ammonia inhibits the activity of the enzyme nitrate reductase essential to the uptake kinetics (Packard and Blasco, 1974) and acts by

reducing V_m (NO_3) (Dugdale and MacIsaac, 1971; Walsh and Dugdale, 1972).

Measurements of V_m (NO_3) versus ammonia concentration in the upwelling regions of Peru and Northwest Africa show a wide scatter of data points (Dugdale and MacIsaac, 1971; MacIsaac et al., 1974). The data presented in Walsh and Dugdale (1972) and in Packard and Blasco (1974) suggest an exponential rather than a linear decrease in V_m (NO_3), with increasing ammonia concentration.

To simulate suppression of nitrate uptake by ammonia, V_m (NO_3) is multiplied by the exponential, $e^{-\Psi NH_4}$. The concentration of ammonia where uptake of nitrate falls to approximately one third V_m (NO_3) is Ψ^{-1}. Figure 3 shows the exponential reduction in V_m (NO_3) with increasing concentration of ammonia found by Walsh and Dugdale (1972).

To be mechanistically correct, perhaps the inhibition phenomenon should be modelled as a competitive inhibition reaction with a threshold effect (Dugdale, personal communication). However, this formulation requires the specification of the dissociation constant for the nitrate reductase-ammonia complex (White et al., 1968) which is difficult to measure. To avoid this complex formulation, nitrate inhibition is modelled in an empirical rather than a mechanistic manner.

In Fig. 4 the theoretical uptake rates of nitrate and manner.

In Fig. 4 the theoretical uptake rates of nitrate and ammonia are shown for increasing concentrations of NO_3 and NH_4. Total nitrogen uptake by phytoplankton is given by

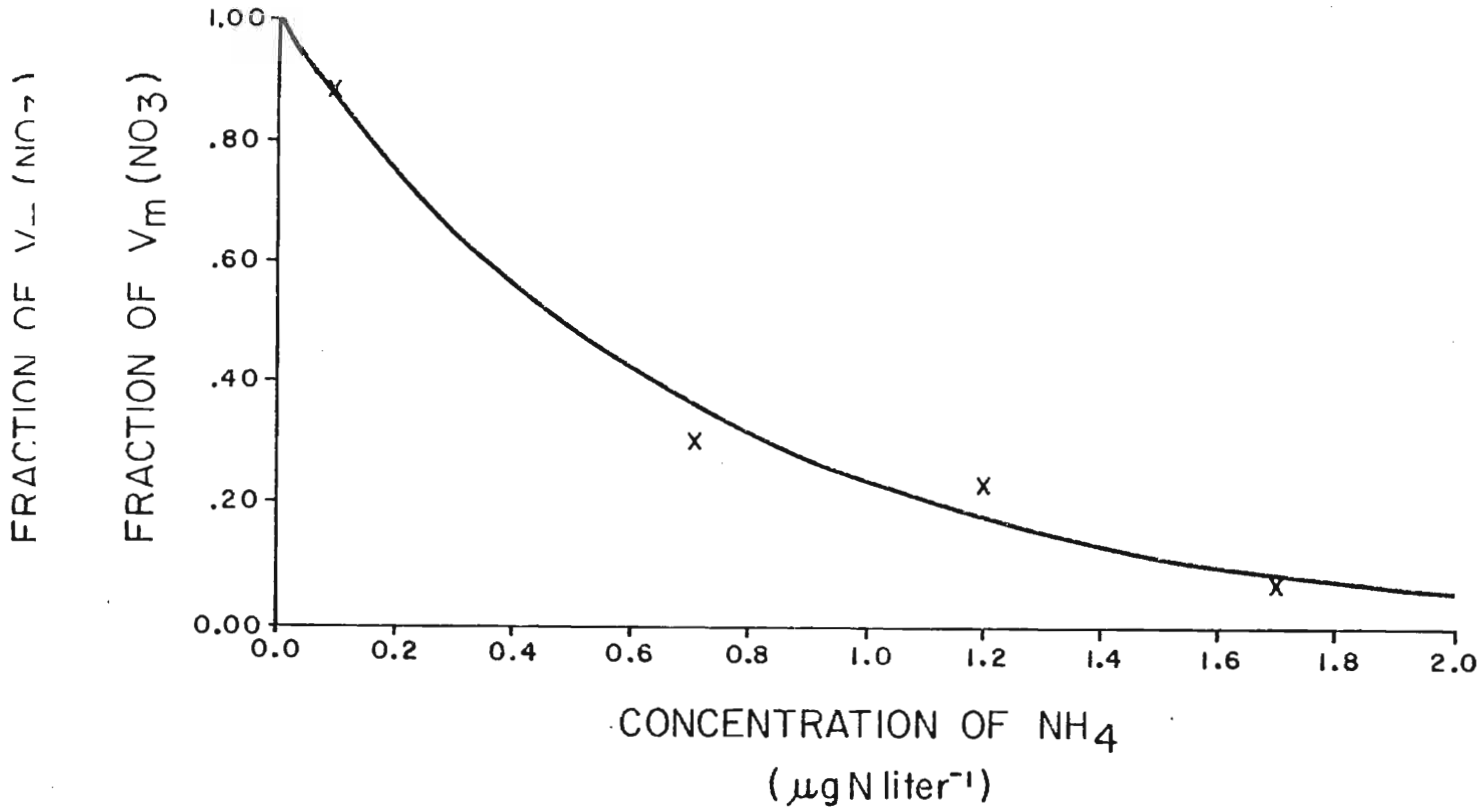

Fig. 3. The exponential reduction in V_m (NO_3) with increasing concentration of ammonia, computed as $V/V_m(NO_3) = e^{-\Psi NH_4}$ where $\Psi = 1.462^m(\mu gat\ NH_4/\ell)^{-1}$. The four data points summarize four experiments presented in Walsh and Dugdale (1972).

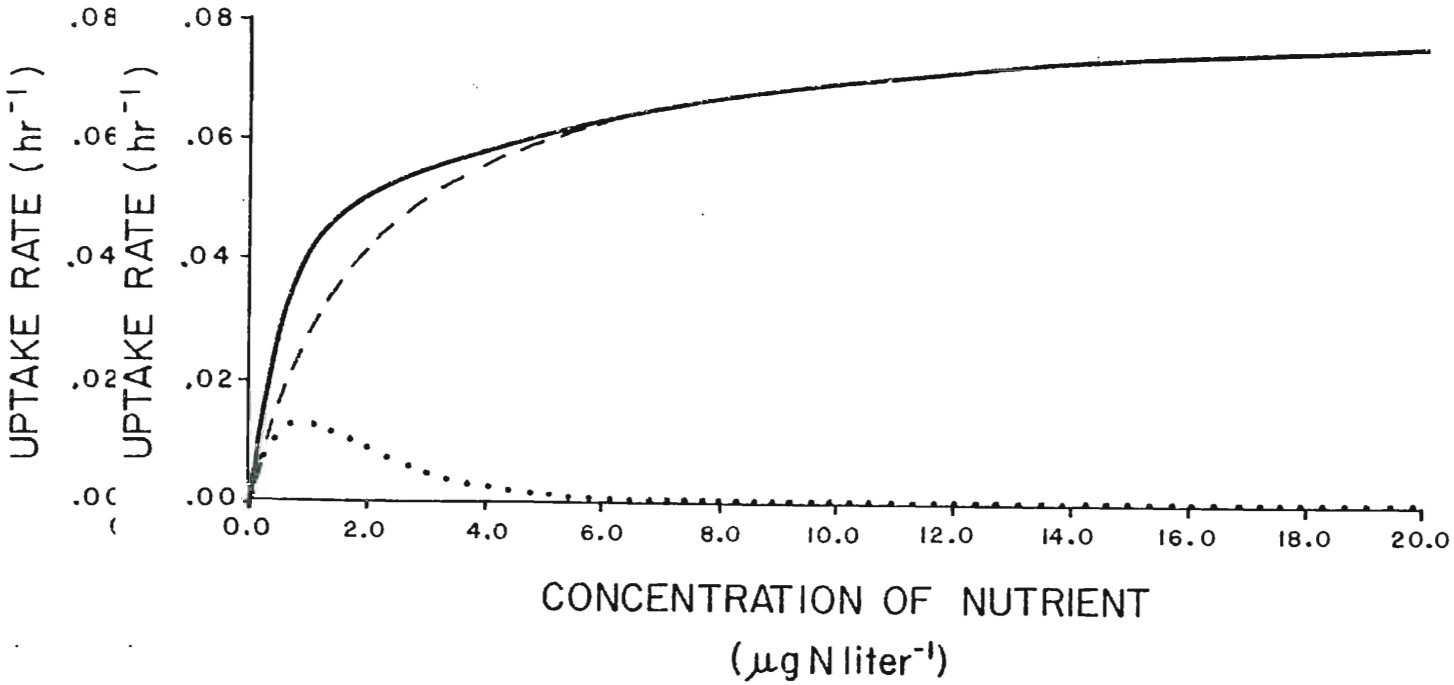

Fig. 4. Uptake rate of nitrate (dotted line), ammonia (dashed line) and total nitrogen uptake uptake (solid line) with increasing concentration of NO_3 and NH_4. Ten micrograms nitrogen pergen per liter on the abscissa means five micrograms of each ionic form are present in soluticsolution. It has been assumed V_m for both nitrate and ammonia is 0.08 hr^{-1} and k_u for both nuboth nutrients is 1 μgat N ℓ^{-1}. Uptake of nitrate is inhibited by ammonia in a manner formulaformulated in the text.

$$V = V_m \left[\frac{NO_3}{k_u + NO_3} e^{-\Psi NH_4} + \frac{NH_4}{k_u + NH_4} \right]$$

where it has been justifiably assumed $V_m\ (NO_3) = V_m\ (NH_4)$ and the half-saturation constants, k_u, for nitrate and ammonia are equal (Eppley et al., 1969; MacIsaac and Dugdale, 1969).

The loss of nitrogen from the phytoplankton population by cell autolysis is represented by a linear loss term, $-\Xi P$, although the process is a complex function of physiological stress. This term is essential in properly modeling the phytoplankton dynamics in the aphotic zone of the water column.

The grazing function is the Ivlev (1945) equation as modified by Parsons et al., (1967).

$$R = R_m \left[1 - e^{-\Lambda(P-P_t)} \right]; \quad P > P_t$$

$$= 0 \qquad\qquad\qquad\qquad ; \quad P \leq P_t$$

where R is the rate of ingestion (hr^{-1}); R_m is the maximum ingestion rate; Λ ($conc^{-1}$) is the Ivlev constant which modifies the rate of change in ingestion with phytoplankton concentration, P; and P_t is the threshold concentration of phytoplankton at which grazing begins. Below the controversial threshold concentration, the zooplankton starve. The values for R_m, Λ and P_t are species-specific (Frost, 1974; Mullin et al., 1975). The grazing rate as a function of

phytoplankton concentration is plotted for Calanus pacificus in Fig. 5.

Upon substitution of these formulations, (3) becomes

$$\frac{\partial P}{\partial t} = V_m \left[\frac{NO_3}{k_u+NO_3} e^{-\Psi NH_4} + \frac{NH_4}{k_u+NH_4}\right] P - R_m \left[1 - e^{-\Lambda(P-P_t)}\right] Z - \Xi P \quad (8)$$

where Z is zooplankton biomass in terms of nitrogen concentration.

2.2b The herbivore equation

Change in zooplankton biomass is taken as the difference between ingestion and the sum of egestion and metabolic excretion. Ingestion is calculated from the Ivlev equation discussed above. Egestion rate as a function of food availability is computed from the proposed expression

$$E = \frac{E_m \Delta e^{T(P-P_t)}}{E_m+\Delta[e^{T(P-P_t)}-1]}$$

where $E_m(hr^{-1})$ is the maximum egestion rate; $\Delta(hr^{-1})$ is the egestion rate at the grazing threshold, P_t; and T $(conc^{-1})$ determines the increase in egestion rate with increasing phytoplankton concentration, P.

Conover (1966) suggests egestion is a constant proportion of food ingested for Calanus hyperboreus feeding over a wide range of diatom food concentration. At low phytoplankton concentrations, however, egestion may no longer be
a wide range of diatom food concentration. At low phytoplankton concentrations, however, egestion may no longer be
a linear function of ingestion. The sigmoid shaped egestion rate curves shown in Fig. 5 were computed from the above

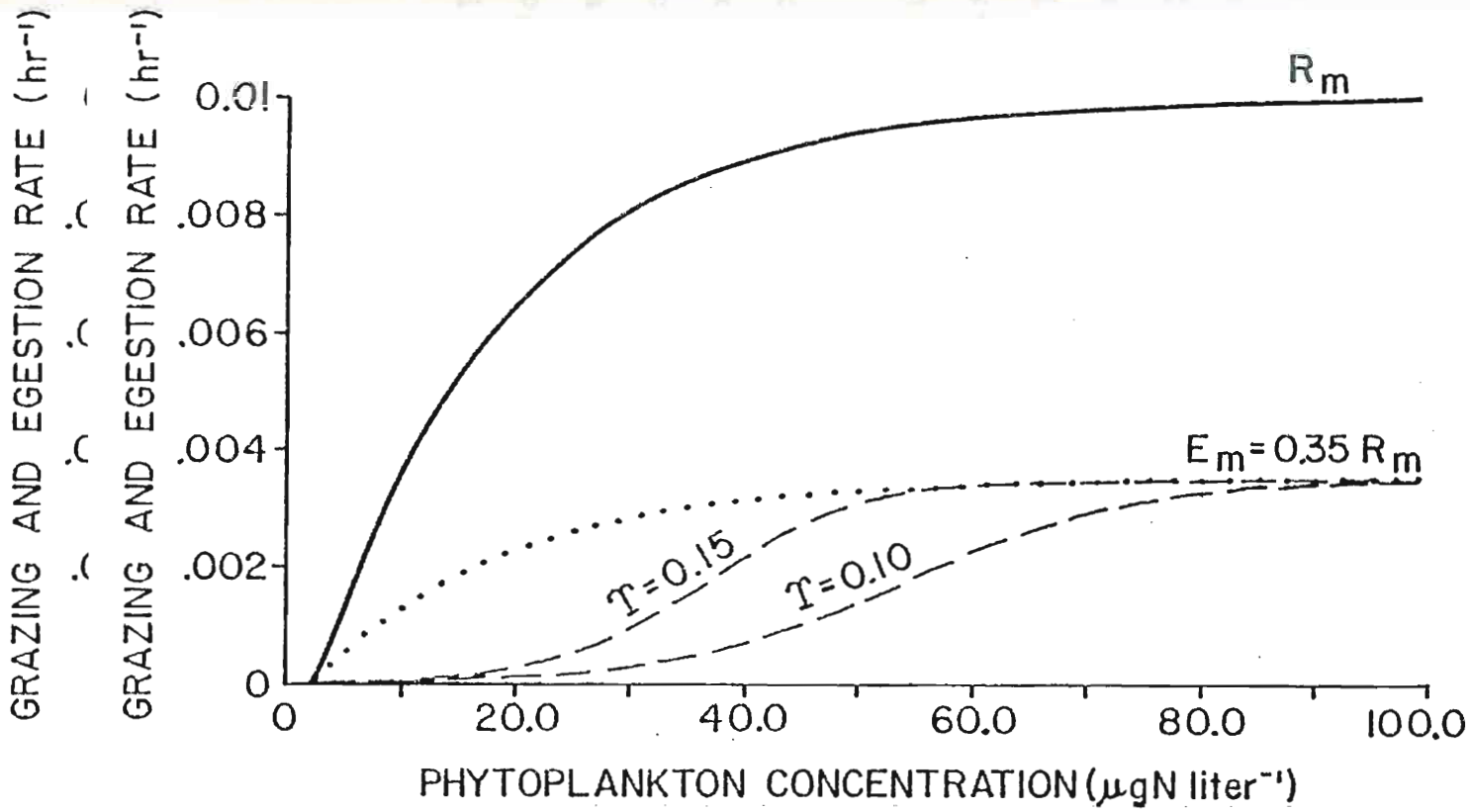

Fig. 5. Ingestion and egestion rates as functions of phytoplankton concentration. The in The ingestion rate curve (solid line) for Calanus pacificus is given by a modified Ivlev functi function where R_m = 0.01 hr^{-1}, Λ = 0.06 (μgat N /ℓ)$^{-1}$ and P_t = 2.5 μgat N ℓ^{-1} (Parsons, et al. et al., 1967). Egestion as a constant fraction (0.35) of ingestion is represented by the do the dotted hyperbolic curve. The sigmoid shaped (dashed) curves for egestion rate result from t from the function proposed in the text, where E_m = 3.5 x 10^{-3} hr^{-1}, Λ = 2 x 10^{-5} hr^{-1}, and T = and T = 0.15 and 0.10 (μgat N/ℓ)$^{-1}$.

proposed expression. Egestion rate as a hyperbolic curve following Conover's hypothesis is also shown for comparison.

Steele (1974) and Frost (1974) recognized that efficiency of assimilation defined as (ingestion-egestion)/ingestion may be high when food is scarce, efficiency possibly decreasing as food concentration increases. In Fig. 6 the assimilation efficiency is calculated for a range of phytoplankton concentration. Ingestion rate is given by the Ivlev grazing curve and egestion rate is expressed by the sigmoid curve. Above the grazing threshold, where the assimilation efficiency is zero by definition, the efficiency rapidly increases and then decreases to a minimum value.

Metabolic excretion of nitrogen varies with grazing activity, temperature and growth stage. Nevertheless, the excretion process is expressed as a linear function of zooplankton biomass, $-\Gamma Z$, where parameter Γ is assigned a value in accord with laboratory measured values for marine copepods under applicable environmental conditions. Equation (4) can then be written as

$$\frac{\partial Z}{\partial t} = R_m \left[1 - e^{-\Lambda(P-P_t)}\right] Z - \frac{E_m \Delta e^{T(P-P_t)} Z}{E_m + \Delta\left[e^{T(P-P_t)}-1\right]} - \Gamma Z \qquad (9)$$

2.2c The detritus equation

Detritus in this model consists of egested copepod fecal pellets and ruptured phytoplankton cells. The term for bacterial remineralization of detrital nitrogen into

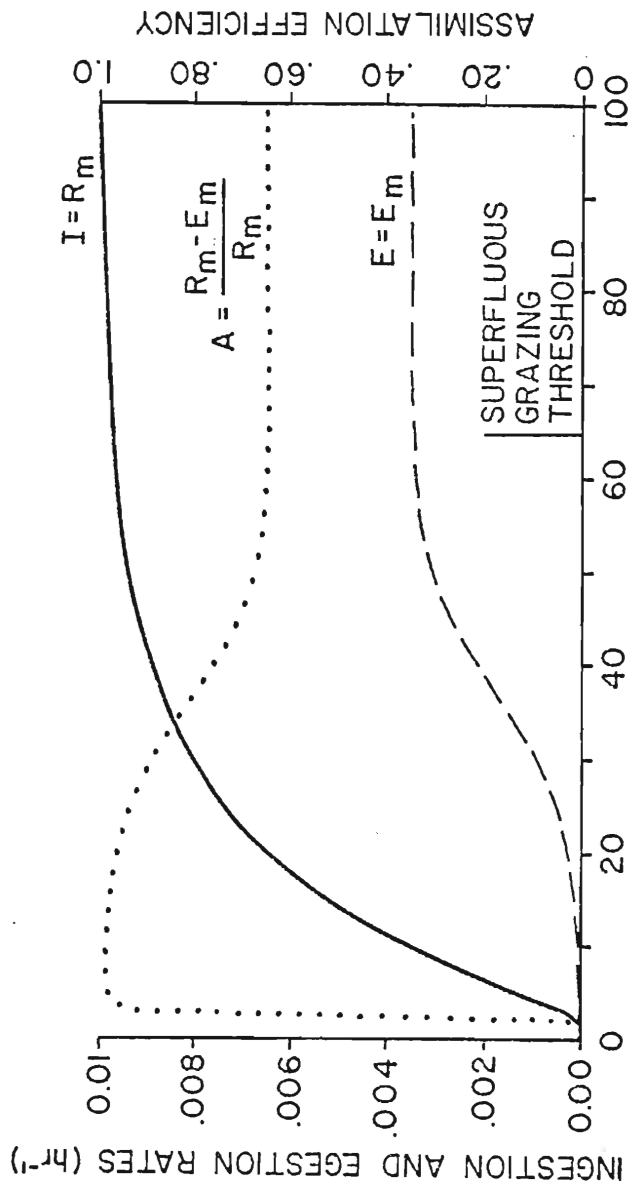

Fig. 6. Assimilation efficiency as a function of food availability. Ingestion rate (I) is defined by the Ivlev grazing curve (solid line) with the same parameter values as in Fig. 5. Egestion rate (E) is determined by the sigmoid curve (dashed line) where $T = 0.15$ (μgat N/ℓ)$^{-1}$. Assimilation efficiency (dotted line) is calculated as $(I-E)/I$. The threshold for superfluous grazing is defined where the assimilation efficiency reaches $(R_m - E_m)/R_m$.

ammonia is $-\Phi D$. Equation (5) in functional form becomes

$$\frac{\partial D}{\partial t} = \frac{E_m \Delta e^{T(P-P_t)Z}}{E_m + \Delta[e^{T(P-P_t)} - 1]} + \Xi P - \Phi D \qquad (10)$$

2.2d The ammonia and nitrate equations

The nutrient equations include the source for uptake by phytoplankton, the sink for excretion of metabolites by herbivores and the remineralization of detritus. The equation for ammonia is

$$\frac{\partial NH_4}{\partial t} = \Phi D + \Gamma Z - V_m \frac{NH_4 P}{k_u + NH_4} - \Omega NH_4 \qquad (11)$$

and that for nitrate is

$$\frac{\partial NO_3}{\partial t} = \Omega NH_4 - V_m \frac{NO_3 P}{k_u + NO_3} e^{-\Psi NH_4} \qquad (12)$$

Bacterial oxidation of ammonia into nitrite and subsequently into nitrate is expressed by the term ΩNH_4. During the CUE data collection effort, NO_2 and NO_3 were measured as total NO_3. Thus, the model does not consider the nitrite intermediate.

2.3 Scaling of the biological dynamics

The biological equations (8) - (12) contain explicitly the parameters V_m, k_u, Ψ, R_m, Λ, P_t, Ξ, E_m, Δ, T, Γ, Φ, and Ω, and implicitly the initial concentrations P, Z, D, NO_3 and NH_4. By scaling the equations the number of parameters Ω, and implicitly the initial concentrations P, Z, D, NO_3 and NH_4. By scaling the equations the number of parameters can be reduced. One nondimensional solution is then equivalent to solving several dimensional cases. To transform

back to dimensional units one multiplies the nondimensional solution by the scaling parameters.

One can examine all biological processes relative to the doubling time of the phytoplankton. If time, t, is scaled by V_m, parameter $\tau = tV_m$, where τ is nondimensional time. Also let P, Z, D, NO_3 and NH_4 be scaled by N_t, the total amount of nitrogen (conc) in all biotic components in the upwelling region.

Using these scaling relationships, (8) - (12) become

$$\frac{\partial P'}{\partial \tau} = \left(\frac{NO_3'}{\alpha + NO_3'} e^{-\psi NH_4'} + \frac{NH_4'}{\alpha + NH_4'} \right) P' - \beta(1 - e^{-\lambda(P-P^*)}) Z' - \xi P' \tag{13}$$

$$\frac{\partial Z'}{\partial \tau} = \beta \left(1 - e^{-\lambda(P-P^*)} \right) Z' - \frac{\rho\delta e^{\upsilon(P-P^*)} Z'}{\rho+\delta[e^{\upsilon(P'-P^*)}-1]} - \gamma Z \tag{14}$$

$$\frac{\partial D'}{\partial \tau} = \frac{\rho\delta e^{\upsilon(P'-P^*)} Z'}{\rho+\delta[e^{\upsilon(P'-P^*)} - 1} + \xi P' - \phi D' \tag{15}$$

$$\frac{\partial NH_4'}{\partial \tau} = \phi D + \gamma Z - \frac{NH_4' P'}{\alpha+NH_4'} - \omega NH_4 \tag{16}$$

$$\text{and } \frac{\partial NO_3'}{\partial \tau} = \omega NH_4 - \frac{NO_3' P'}{\alpha+NO_3'} e^{-\psi NH_4'} \tag{17}$$

where

$P' = P/N_t$ $\quad Z' = Z/N_t$ $\quad D' = D/N_t$

$P' = P/N_t$ $\quad Z' = Z/N_t$ $\quad D' = D/N_t$

$NO_3' = NO_3/N_t$ $\quad NH_4' = NH_4/N_t$ $\quad \alpha = k_u/N_t$

$\beta = R_m/V_m$ $\quad \gamma = \Gamma/V_m$ $\quad \delta = \Delta/V_m$

$$\lambda = \Lambda N_t \qquad \xi = \Xi/V_m \qquad \rho = E_m/V_m$$

$$\upsilon = TN_t \qquad \phi = \Phi/V_m \qquad \psi = \Psi N_t$$

$$\omega = \Omega/V_m \qquad P^* = P_t/N_t \ .$$

The primes are dropped for convenience. All quantities in (13) - (17) are nondimensional. P, Z, D, NO_3 and NH_4 are all fractions; if multiplied by 100 they represent the percent of N_t in that biotic component at time τ, e.g., a standing crop. Time is also nondimensional. For example, if V_m is two doublings per day, then $\tau = 2$ is one dimensional day. The reader must bear in mind these scaling relationships when comparing the nondimensional model results with observational data.

2.4 Estimation of the biological parameter values

Equations (13) - (17) represent a time-dependent, nonspatial, marine plankton model. One must next determine the proper parameter values for application of these equations to the Oregon upwelling ecosystem.

Many of the parameters are limited to a small range after scaling by N_t and V_m. Since newly upwelled waters off Oregon have a maximum total nitrogen concentration of approximately 30 µgat N ℓ^{-1} (mostly as dissolved nitrate), N_t = 30 µgat N ℓ^{-1}. There exists a considerable body of literature on both laboratory and <u>in situ</u> measurement of the maximum growth rate, V_m. Eppley (1972) has summarized the existing data on exponentially growing diatoms.

A maximum growth rate of 2.08 doublings day^{-1} is estimated for neritic diatoms under the environmental conditions of the Oregon upwelling season.

One ratio which arises from the scaling of concentrations in (8) - (12) is $\alpha = k_u/N_t$. A typical value of the half-saturation constant for neritic diatoms in upwelling areas is 1 μgat N ℓ^{-1} for both nitrate and ammonia (Eppley et al., 1969; MacIsaac and Dugdale, 1969). Upon scaling by N_t, the nondimensional half-saturation constant, α, is 0.03. Parameter α typically ranges from 10^{-1} to 10^{-2} for most any oceanic area (O'Brien and Wroblewski, 1973). Lower values of α correspond to phytoplankton utilizing extremely small concentrations of the limiting nutrient.

A fit of the function, $V/V_m(NO_3) = e^{-\Psi NH_4}$, by least squares to the data found in Walsh and Dugdale (1972) gives $\Psi = 1.462$ (μgat $NH_4/\ell)^{-1}$. Figure 2 plots the exponential reduction in $V_m(NO_3)$ using this value for Ψ. After scaling by N_t, nondimensional $\psi = 43.86$.

Phytoplankton physiological death is a significant aphotic zone process (Lehman et al., 1975). One can approximate this loss rate of phytoplankton nitrogen in terms of the time necessary to reduce a light-limited or nutrient-starved population to approximately one third its initial concentration, P_0. Under no growth conditions,

concentration, P_0. Under no growth conditions,

$$\frac{P}{P_0} = e^{-\Xi\tau} = e^{-1} \text{ when } \tau = \Xi^{-1}.$$

The time scale Ξ^{-1} is called the e-folding rate. If it is estimated the phytoplankton standing crop is reduced to $P_0 e^{-1}$ in 10 days, then nondimensional $\xi = 0.05$. It is fortunate that sensitivity analysis (see Section 4.5) shows the model behavior is least influenced by this parameter, for exact determination of Ξ in nature is difficult.

Parameter β is the ratio of the maximum herbivore grazing rate, R_m, to the maximum phytoplankton growth rate, V_m. If β is greater than one, the herbivores can reduce the phytoplankton standing crop through grazing. For continuous grazing Calanus pacificus, $R_m = 0.01$ hr^{-1} (Parsons et al., 1967) and if $V_m = 0.04$ hr^{-1}, $\beta = 0.25$.

Assuming the herbivore population is dominated by calanoid copepods, the species-specific Ivlev constant is in the range 0.01 to 0.1 (μgat N/ℓ)$^{-1}$ and the grazing threshold is less than or equal to 2.5 μgat N ℓ^{-1} (Parsons et al., 1967). Upon scaling, nondimensional $\lambda = 0.3$ to 3.0 and $P^* \leq 0.08$. A value for P^* of zero is used in all the following spatial and nonspatial model solutions.

The maximum egestion rate is chosen to simulate a minimum assimilation efficiency of 65% (Corner and Davies, 1971) under superfluous grazing conditions, i.e., $E_m = 35\%$ of R_m. Thus, $\rho = 0.35\ \beta$. There is currently no published laboratory data on the values of egestion parameters Δ and Υ. Based on unpublished work by Hirota and deduction, Υ laboratory data on the values of egestion parameters Δ and Υ. Based on unpublished work by Hirota and deduction, Υ is chosed as 0.15 (μgat N/ℓ)$^{-1}$ or $\upsilon = 4.5$. For near

complete assimilation of nitrogen at the grazing threshold, Δ is 7.2×10^{-4} hr^{-1} or $\delta = \Delta/V_m = 0.01$.

Calanus finmarchicus grazing on an algal diet in 10°C waters of the Clyde Sea was estimated by Corner et al., (1965) to excrete 8-11% of its body nitrogen per day. A value of 10% of body nitrogen per day is a qualified guess for the metabolic excretion rate of herbivores grazing in the neritic upwelling region off Oregon. Therefore, non-dimensional $\gamma = 0.10$.

Most of the detritus in the model originates from copepod fecal pellet production. Redfield et al., (1963) have suggested that much of the soluble nitrogen in newly formed fecal pellets dissolves before the particle sinks out of the euphotic zone. If it is assumed that 40% of the ammonia in fecal pellets leaches out in 1 day, then parameter $\phi = 0.5$.

The rate of oxidation of ammonia into successively nitrite and nitrate in the ocean is a function of temperature, pressure and bacterial activity (Von Brand et al., 1940). From the data provided by Von Brand et al., (1937), an e-folding time for oxidation of ammonia to nitrite-nitrate appears to be about 25 days. Thus $\omega = 0.02$.

2.4a Steady state solution of the nonspatial model

The initial conditions chosen for P, Z, NO_3, NH_4 and D indicate the behavior of (13)-(17). Figure 7 displays the model's response using the above parameter values and

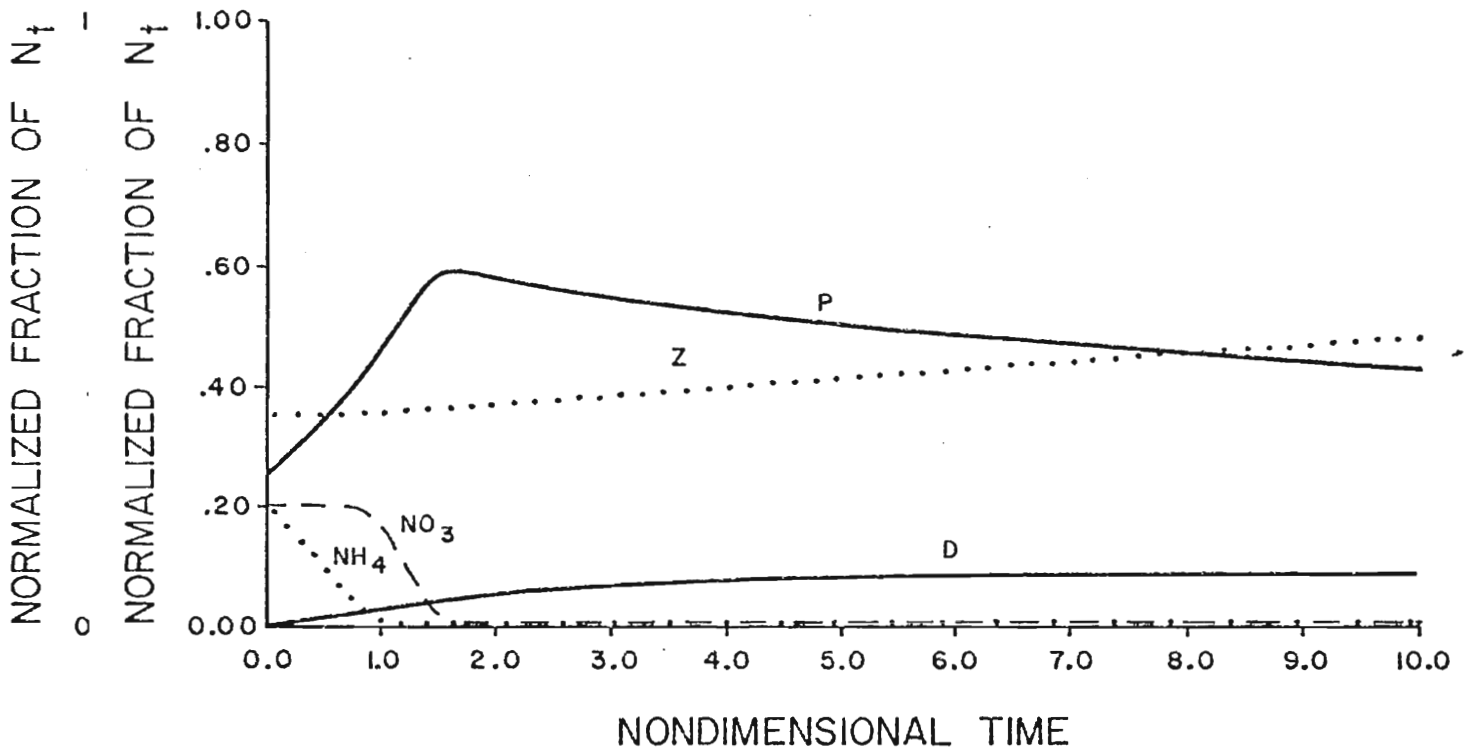

Fig. 7. Time-dependent standing stock concentrations of phytoplankton (P), zoop: zooplankton (Z), detritus (D), nitrate (NO_3), and ammonia (NH_4). The abscissa is nond: nondimensional time ($\tau = tV_m$). The ordinate is the concentration of the biotic comp: component as a fraction of the total amount of limiting nutrient in the system, N_t. The : The nondimensional parameter values for this solution are: $\alpha = 0.03$, $\beta = 0.25$, $\gamma = 0.07$, $\delta = 0.01$, $\lambda = 1.80$, $\xi = 0.05$, $\rho = 0.09$, $\upsilon = 4.50$, $\phi = 0.50$, $\psi = 43.86$, $\omega = 0.02$ and $P^* = 0$.

the initial concentrations P = 0.25, Z = 0.35, NO_3 = NH_4 = 0.20, and D = 0. Ammonia and nitrate are successively depleted by growing phytoplankton. The availability of phytoplankton results in a gradual increase of zooplankton biomass. Grazing results in fecal pellet production and the appearance of detritus.

The steady state eventually achieved is P = 0.245 or 7.35 μgat N ℓ^{-1}, Z = 0.685 or 20.55 μgat N ℓ^{-1}, NO_3 = 0.001 or 0.03 μgat N ℓ^{-1}, NH_4 = 0.014 or 0.42 μgat N ℓ^{-1} and D = 0.055 or 1.65 μgat N ℓ^{-1}. These concentrations are the spatially averaged, standing phytoplankton and zooplankton stocks, concentrations of detritus and dissolved nutrients (ammonia and nitrate), where no perturbations of the system by external forcing functions exist. However, daily variations of light and wind stress forcing of the upper ocean prevent the biological dynamics from ever reaching a steady state, either in time or space.

2.5 Formulation of environmental influences on phytoplankton growth

In addition to nutrient concentration, the growth rate of phytoplankton is influenced by temperature and light intensity. The author has chosen to model phytoplankton growth as a multiplicative factor of nutrients, light, and temperature. Walsh (1975) regarded a single factor as growth limiting. However, Parson and Takahashi (1973) and

temperature. Walsh (1975) regarded a single factor as growth limiting. However, Parson and Takahashi (1973) and Platt et al., (1975) suggest that primary production in the

sea is regulated simultaneously by several environmental variables.

2.5a The temperature function

Where photosynthesis is light saturated and nutrients are not limiting, the rate of plant growth may be a direct function of temperature (Winter et al., 1975). Eppley (1972) found under these conditions the specific growth rate μ (doublings day^{-1}) could be predicted from the empirically derived equation

$$\mu = ab^{cT}$$

where a is 0.851 doublings day^{-1}, b is the constant 1.066, c is $1°C^{-1}$, and T is temperature in °C.

Most marine phytoplankton experience a suppression of the growth rate above some optimum temperature. A formulation proposed by Lassiter and Kearns (1973) well describes the "growth vs. temperature" or μ vs. T curve of many phytoplankton. Their equation is,

$$\mu = \mu_m e^{q(T-T_{opt})} \left\{ \frac{T_m - T}{T_m - T_{opt}} \right\}^{q(T_m - T_{opt})}$$

in which T_{opt} is the optimal temperature; T_m is the temperature above which the growth rate is zero; and q is the constant which modifies the rate of change in μ with T,

ture above which the growth rate is zero; and q is the constant which modifies the rate of change in μ with T,

T_{opt} and T_m. Figure 8 shows the μ vs. T curve for Skeletonema costatum using the above equation with T_{opt} = 20°C,

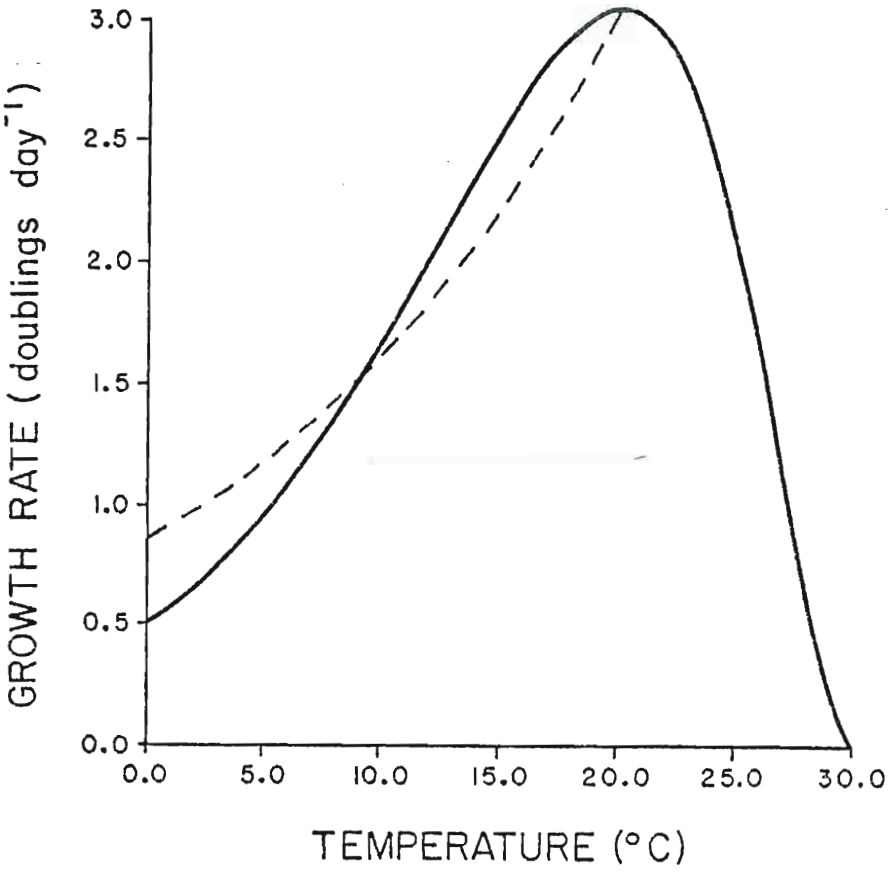

Fig. 8. Phytoplankton growth rate as a function of temperature. The solid line is calculated from the equation of Lassiter and Kearns (1973), while the dashed line is calculated from Eppley's (1972) general equation.

line is calculated from Eppley's (1972) general equation.

T_m = 30°C (Jitts et al., 1964; Curl and McLeod, 1961) and $q = 0.2°C^{-1}$. Eppley's general equation for photoautotrophic algae is shown as the dashed line in Fig. 8. As temperatures are usually less than T_{opt} in an upwelling area, Eppley's empirical relationship is adequate for modelling purposes here.

The highest temperature observed within 50 km of the coast of Oregon during strong upwelling in August 1973 was 14°C. At 14°C the maximum doubling time of the phytoplankton is 2.08 doublings day^{-1} (Fig. 8), provided light and nutrient are not limiting. Phytoplankton growth relative to this maximum is calculated for temperatures less than 14°C by normalizing Eppley's equation by μ_m,

$$\frac{\mu}{\mu_m} = \frac{0.851}{\mu_m} (1.066)^T = ab^{cT}$$

where a = 0.409, b = 1.066 and $c = 1°C^{-1}$. The above equation is used to describe the influence of temperature upon the growth rate of phytoplankton in the following models.

2.5b The light function

Light is another important parameter which affects the growth rate of phytoplankton. The rate of photosynthesis appears linearly related to light at low intensities, becomes constant at optimum intensities, and is suppressed at high intensities. This response is described by the
comes constant at optimum intensities, and is suppressed at high intensities. This response is described by the so-called "photosynthesis vs. light intensity" or P_h vs. I curve (Parsons and Takahashi, 1973). Because the maximum

rate of photosynthesis, P_m, depends on an optimum temperature, nutrient and light regime, plots of P_h vs. I are normalized by P_m (Yentsch and Lee, 1966). A modification of the formulation by Vollenweider (1965),

$$\frac{P_h}{P_{opt}} = \frac{I/I_s}{(1 + (I/I_s)^2)^{1/2}(1 + (\theta I/I_s)^2)^{\eta/2}},$$

is used to describe the rate of phytoplankton growth as a function of light intensity, I. I_s is the irradiance for which $P_h = P_{opt}\ [2(1+\theta^2)^{\eta}]^{-1/2}$. P_{opt} is the maximum photosynthetic rate, P_m, multiplied by a function of θ and η (see Fee, 1969). This complex formulation is adopted here because of its ability to fit P_h vs. I curves exhibiting photoinhibition. Figure 9 shows this equation can reproduce the response of diatom growth to light intensity if I_s = 0.07 cal cm^{-2} min^{-1}, θ = 0.175 and η = 4.3. The data points in Fig. 9 are from the P_h vs. I curve for a mixed culture of the diatoms Skeletonema costatum, Nitzchia closterium, Navicula sp. and Coscinodiscus excentricus, as measured by Ryther (1956) in the laboratory. Model experiments (not shown) demonstrate primary production would be greatly overestimated if one used a hyperbolic P_h vs. I curve, ignoring photoinhibition effects at high light intensities.

2.5c Phytoplankton growth as a function of light, temperature and nutrients

As nutrient uptake is coupled (albeit indirectly) to photosynthesis (Goering et al., 1964; Dugdale and Goering,

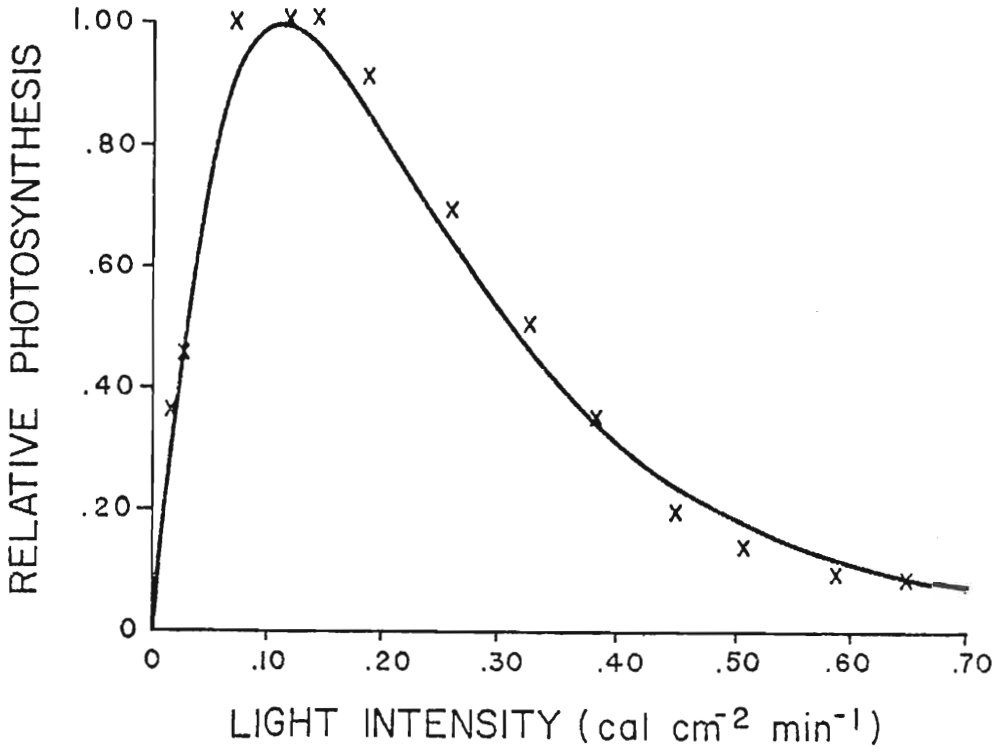

Fig. 9. Relative photosynthesis as a function of light intensity. The solid line is calculated from a modification of the formulation by Vollenweider (1965). The data points are from a laboratory experiment by Ryther (1956).

of the formulation by Vollenweider (1965). The data points are from a laboratory experiment by Ryther (1956).

1967) one can equate relative photosynthesis with relative nutrient uptake, V/V_m.

The relation of light, temperature and nutrient to the growth rate of phytoplankton in the model is formulated as

$$\frac{\partial P}{\partial \tau} = P \left[\frac{NO_3}{\alpha + NO_3} e^{-\psi NH_4} + \frac{NH_4}{\alpha + NH_4} \right] \left[\frac{I/I_s}{[1 + (I/I_s)^2]^{1/2} [1 + (\theta I/I_s)^2]^{\eta/2}} \right] (ab^{cT})$$

where all terms are nondimensional and the units of the growth functions cancel.

Light attenuation with depth in the ocean follows the Beers-Lambert law

$$I = I_0 e^{-\kappa z}$$

where I is the light intensity (cal cm^{-2} min^{-1}) at depth z, I_0 is the light intensity immediately below the sea surface, and κ is the extinction coefficient (m^{-1}) (Parsons and Takashi, 1973). I_0 varies with time of day, cloud cover, and season. The diel periodicity in I_0 may be expressed as

$$I = I_m \sin \left[\frac{\pi \bmod (t, 24)}{d} \right]$$

where I_m is the light intensity at local apparent noon, d is the daylength fraction of a day, and t is time. When the sine function becomes negative, I_0 is set equal to zero. Periodicity is enforced by the modulo.
the sine function becomes negative, I_0 is set equal to zero. Periodicity is enforced by the modulo.

Solar radiation measurements made from a surface buoy 13 km off Sand Lake, Oregon, during CUE II indicate the

daylength, d, is 13 hrs in August. The shortwave radiation penetrating the sea surface at local noon on a cloudless day, I_m, is about 1.25 cal cm^{-2} min^{-1} (Reed and Halpern, 1974). The fit of a sine curve to this insolation data is shown in Fig. 10 where a daylength of 12 hrs has been assumed for simplicity and scaled time begins at dawn.

In coastal waters incident radiation, I_0, is reduced by a factor of two within the first few centimeters of the water column as ultraviolet and infrared radiation is absorbed (Parsons and Takahashi, 1973). The penetration of the photosynthetically active 400 to 700 nm wavelength is then described by Beer's law. Combining Beer's law with a sine function, the photosynthetically active light intensity at a given depth and time of day is

$$I\ (z,t) \;=\; 0.5\ I_m \sin\left[\frac{\pi \bmod (t,\ 24)}{d}\right] e^{-\kappa z}\ .$$

The extinction coefficient κ is dependent on the absorption of pure seawater and the scattering and absorption of suspended particles. Lorenzen (1972) expressed κ as

$$\kappa \;=\; \kappa_w + \kappa_p P + \kappa_d D$$

where κ_w (m^{-1}) is the extinction coefficient of pure seawater; κ_p (m^2/mg N) describes the extinction by phytoplankton, P; and κ_d (m^2/mg N) is the extinction by colored dissolved substances, tripton, and detritus, D.

P_h vs. I_o curves in conjunction with Beer's law have

dissolved substances, tripton, and detritus, D.

P_h vs. I curves in conjunction with Beer's law have long been used to estimate the primary production in the ocean (for a review, see Patten,1968). However, the

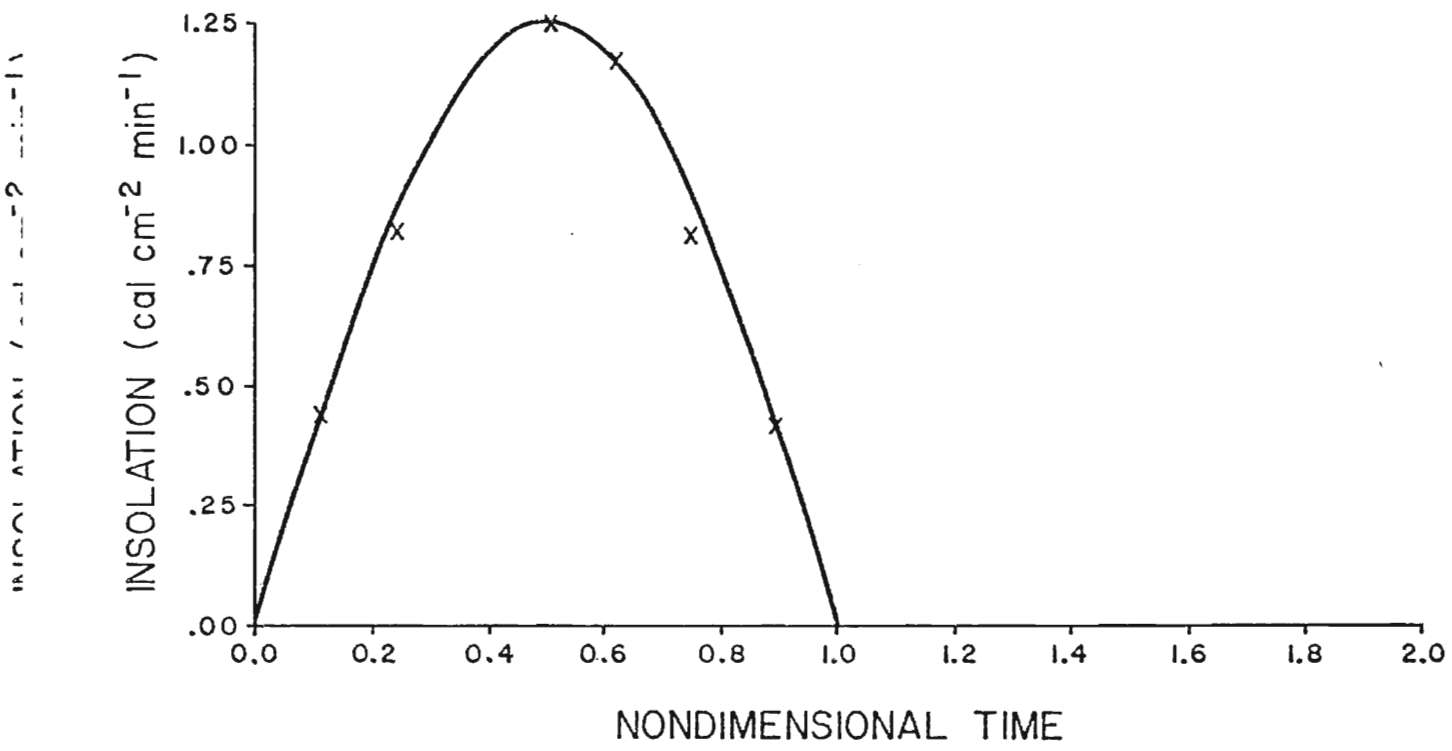

Fig. 10. Incident radiation as a function of scaled time. The solid line is the positive half of a sine curve. The data points are observations of insolation with comparable time of day recorded in August 1973 off the coast of Oregon.

assumptions of a vertically homogeneous phytoplankton distribution and a constant κ, often made in these calculations, is invalid. The self-shading phenomenon of phytoplankton necessitates numerical integration of production with depth (Fee, 1969).

If the distribution of phytoplankton, P, with depth, z, is known at time, t, then

$$I(z,t) = 0.5\ I_m \sin\left[\frac{\pi \bmod (t,24)}{d}\right] e^{-[\kappa_w z + \kappa_p \int_0^z P(z)dz]}$$

where P(z) is the concentration (mg N m^{-3}) of phytoplankton at depth z (m), κ_p (m^2/mg N) is the extinction coefficient per unit concentration of phytoplankton, and κ_w (m^{-1}) is the extinction coefficient of the seawater in the absence of any phytoplankton (Platt et al., 1975).

Small and Curl (1968) integrated $1/z_0 \int_0^z P(z)\ dz$, where z_0 is the depth of 1% incident light penetratration to determine $\overline{P}$, the average concentration of phytoplankton in the euphotic zone during the 1965 Oregon upwelling season. Regressing κ upon $\overline{P}$, they found

$$\kappa = 0.067 + 0.076\ \overline{P}$$

where $\overline{P}$ is expressed in mg chlorophyll a m^{-3}. The value for κ_w, 0.067 m^{-1}, is higher than expected for the absorption of light by pure seawater (0.04 m^{-1}) due to nonchlorophyllous, colored, dissolved substances from the Columbia River tongue. Tripton, or nonliving suspended matter, from local river runoff was not as important as these colored

soluble substances (Small and Curl, 1968). If one assumes a chl a/N ratio of 1/8 for vigorously growing phytoplankton with excess nitrate in the water (Antia et al., 1963), then κ_p off Oregon during upwelling is 0.095 cm^2 $(\mu gat\ N)^{-1}$. The chl a/N ratio is quite variable in nature, weakening the estimate of κ_p.

2.5d Steady state solution of the (z,t) model

The ability of the above formulations to simulate plankton and nutrient dynamics in a neritic water column off Oregon is tested by comparing model solutions to observational data. The initial conditions for the solutions shown in Figs. 11 and 13 are the steady state values for P, Z, NO_3, NH_4 and D from the nonspatial model (Fig. 7). The (z,t) model includes diffusion of the dependent variables in the vertical, with a value for K_v of 1 cm^2 sec^{-1}. A temperature profile corresponding to that specified for a water column 50 km offshore (see Section 3.5) is assumed.

Figure 11 displays the phytoplankton vertical profiles which result when plant growth varies with depth. The profile fluctuates about a steady state as incident radiation follows the sinusoid curve (Fig. 10) and photosynthetically active light penetrating the surface is attenuated with depth. A phytoplankton maximum occurs at a depth of 21 m. Sampling profiles taken 50 km offshore during CUE often

depth. A phytoplankton maximum occurs at a depth of 21 m. Sampling profiles taken 50 km offshore during CUE often

showed a chlorophyll maximum between 10 and 25 m.

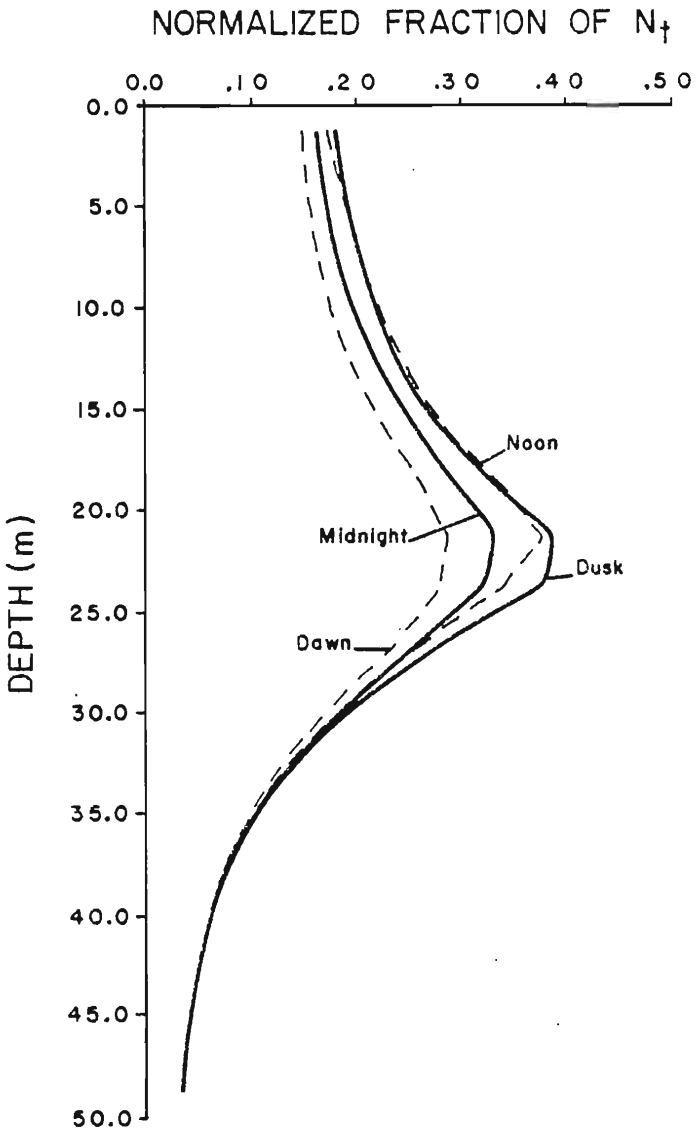

Fig. 11. Steady state oscillation in the phytoplankton profile of the (z,t) model. Plant biomass is expressed as a nondimensional fraction of the total amount of nitrogen in the upwelling ecosystem, N_t.

upwelling ecosystem, N_t.

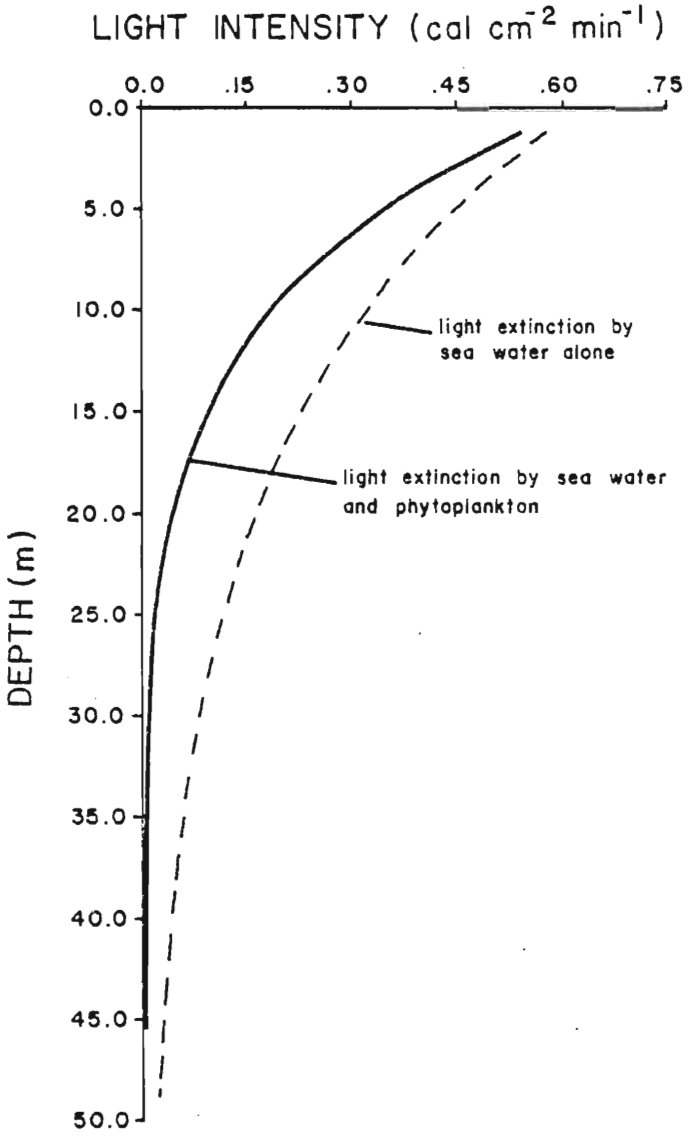

Fig. 12. Light intensity-depth profile at midday in the steady state solution of the (z, t) model.

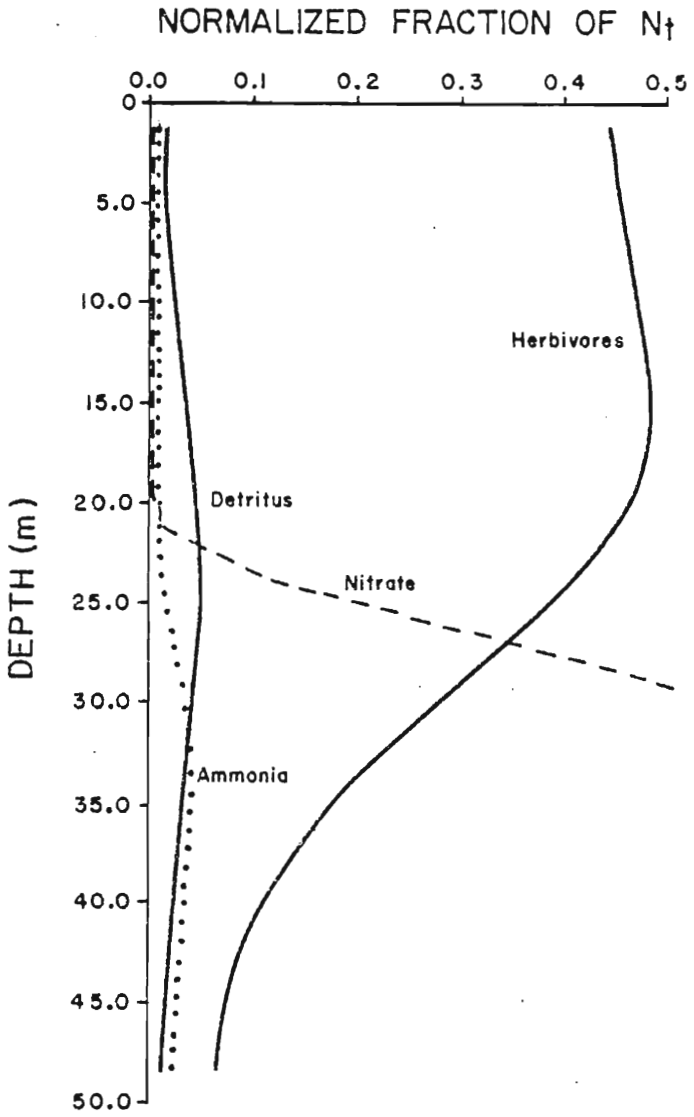

Fig. 13. Steady state vertical profiles of the (z,t) model's dependent variables (herbivores, detritus, nitrate and ammonia) at midday. The dependent variables are expressed as a non-dimensional fraction of the total amount of nitrogen in the upwelling ecosystem, N_t.

dimensional fraction of the total amount of nitrogen in the upwelling ecosystem, N_t.

Figure 12 shows the light intensity-depth profile at midday. If light absorption by phytoplankton were not considered, i.e., if $\kappa_p = 0$, the 1% I_0 light intensity would reach 68 m instead of 33 m. Suppression of phytoplankton rate by light intensities greater than 0.13 cal cm^{-2} min^{-1} occurs at midday in the upper 12 m. Suppression of phytoplankton growth at local noon in the summer has been observed to depths of at least 10 m (Small, personal communication). Below 15 m, the availability of light becomes growth limiting.

The nutrients, detritus, and zooplankton profiles at midday are shown in Fig. 13. Oscillations similar to that shown in the phytoplankton profile (Fig. 11) are found in the nitrate and ammonia profiles but are not depicted. The ammonia and nitrate profiles indicate nutrient depletion in the upper 20 m of the water column, both nutrients increasing in concentration below this depth as uptake by phytoplankton is reduced. The zooplankton maximum occurs at 16 m. The zooplankton standing stock quickly decreases below the euphotic zone. Zooplankton biomass is directly related to the concentration of its prey through the Ivlev grazing term. Detritus, which is assumed to sink at a rate of 8 m day^{-1} (see Section 3.2) shows a maximum at 26 m. If a sinking rate of zero were assumed, the shape of the detritus profile would more closely correspond to the zooplankton profile, since egestion of herbivore fecal pellets is the main source of detritus.

2.6 Calculation of the Daily Gross Primary Production

Given the phytoplankton vertical distribution, one can calculate the rate, V, at which inorganic nitrogen is incorporated into phytoplankton nitrogen, P. Integration of the growth of phytoplankton over depth, $\int_z VP$, where V is a function of light, temperature and nutrients gives the gross primary productivity (mg N m^{-2} hr^{-1}) of the water column. Models where the functional expression for V is not too complicated can be integrated analytically, provided the vertical distribution of P is homogeneous, or at best a smooth function (Fee, 1970; Platt et al., 1975). In the present model one must resort to numerical integration.

To find the daily gross primary production of the water column (mg N m^{-2}), one integrates over depth and time the expression,

$$V_m P \left[\frac{NO_3\, e^{-\Psi NH_4}}{k_u + NO_3} + \frac{NH_4}{k_u + NH_4}\right] \left[\frac{I/I_s}{[1 + (I/I_s)^2]^{1/2}[1 + (\theta I/I_s)^2]^{\eta/2}}\right] (ab^{cT})$$

where

$$I(z,t) = 0.5\, I_m \sin\left[\frac{\pi \bmod (t,24)}{d}\right] e^{-[\kappa_w z + \kappa_p \int_0^z P(z)dz]} .$$

The daily gross primary production calculated for the

The daily gross primary production calculated for the phytoplankton profile shown in Fig. 11 is 100 mg N m^{-2}. Anderson (1964) observed a daily net primary production of

between 0.3 and 1.2 g C m^{-2} day^{-1} in oceanic waters 50 km off Oregon during the 1962 upwelling season. Assuming a C/N ratio of 7 (Small and Ramberg, 1971), this production in terms of nitrogen is 43 to 171 mg N m^{-2} day^{-1}. It appears the biological and chemical dynamics formulated in this model can correctly simulate primary production off Oregon.

3. MODEL FORMULATION - THE PHYSICAL DYNAMICS

In this section the physical dynamics of upwelling are formulated for incorporation into the spatial, primary productivity model in an attempt to simulate mesoscale phytoplankton patchiness observed during upwelling off Oregon.

3.1 Wind forcing and bottom topography

Thompson (1974) has developed an (x,z,t) model of the transverse circulation off the Oregon coast for the same period in 1973 during which an intensive biological sampling program was conducted. Thompson's model was run with an observed wind stress profile (Fig. 27) to simulate upwelling events which occurred in August 1973. The forecast time-dependent velocity field was used to advect the biotic variables in what will henceforth be referred to as the "intermittent upwelling case." A "strong upwelling case" was also run with a steady wind stress driving the upwelling model.

Thompson's circulation model delineates the position of the pycnocline, the localities of upwelling, convergences and divergences all of which are influenced by bottom topography and a variable wind stress. Thompson assumed a free surface and the bottom topography shown in Fig. 14. This slope is a linearized version of the actual bottom topography

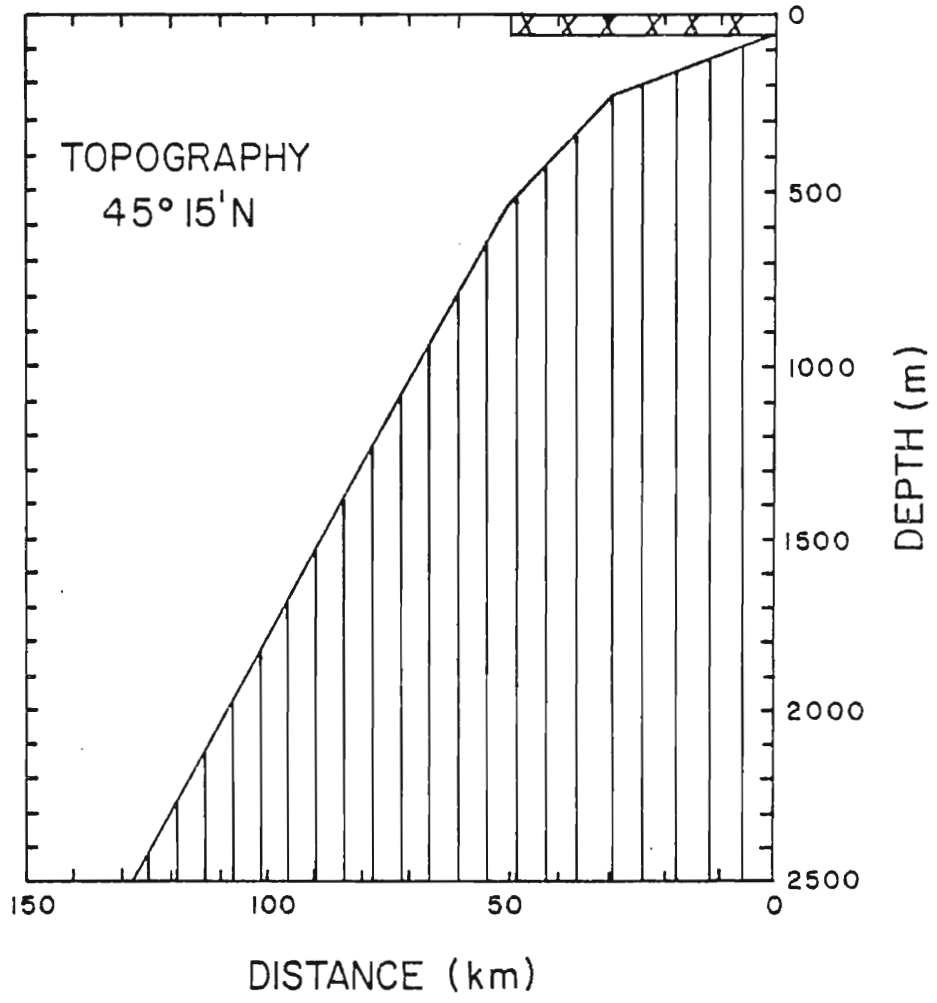

Fig. 14. Bottom topography assumed in the (x,z,t) upwelling circulation model of Thompson (1974). The rectangular hatched region at the upper right delineates the region of the (x,z,t) model of phytoplankton production.

upwelling circulation model of Thompson (1974). The rectangular hatched region at the upper right delineates the region of the (x,z,t) model of phytoplankton production.

off Oregon. Bottom depths from the coast to 150 km offshore between 44°55'N and 44°15'N were digitized from bathymetry charts, averaged in the longshore direction, and finally linearized to obtain a bottom slope characteristic of the CUE region. A bottom depth of 50 m at the coast is assumed to simplify computations.

A basic assumption of both the physical and biological spatial models is no longshore variation in the coastline, bottom topography or velocity field. This assumption makes for computational economy. It also simplifies the spatial dynamics to a degree that fundamental features in the physical circulation and in the biological and chemical fields can be examined without the confusion imposed by longshore variability. The importance of longshore variation in coastline and bottom topography upon the upwelling circulation has been discussed by Hurlburt (1974), Shaeffer (1974), and Peffley and O'Brien (1976). However, the author leaves consideration of longshore derivatives in (2) to future, more ambitious, undertaking.

All biological simulations are confined to the upper 50 m of the water column in a region within 50 km of the coast. The modeled cross section is shown as the thin hatched area in Fig. 14. This area is divided into a grid of 50 by 20 rectangles in the x and y directions, respectively. The dimensions of each grid box are 2.5 m in depth and 1 km in

rectangles in the x and y directions, respectively. The dimensions of each grid box are 2.5 m in depth and 1 km in width. The first biological grid point is 1.25 m below the sea surface.

3.2 Scaling of the physical dynamics

The equation governing phytoplankton patchiness in a transverse plane normal to the Oregon coast is again

$$\frac{\partial P}{\partial t} + u\,\frac{\partial P}{\partial x} + w\,\frac{\partial P}{\partial z} - K_h\,\frac{\partial^2 P}{\partial x^2} - K_v\,\frac{\partial^2 P}{\partial z^2} = \text{biological terms} \quad (2)$$

where "biological terms" refer to the phytoplankton dynamics developed in the previous section.

If one scales (2) so all terms are nondimensional, one can compare the relative influence of the physical and biological processes in determining the spatial distribution of phytoplankton. Let

$$x = Lx' \qquad u = Uu'$$

$$z = Hz' \qquad w = Ww'$$

where L and H are characteristic horizontal and vertical length scales, U is a typical value of the organized horizontal flow, and W is a typical value of the vertical velocity. Using the scaling relations put forth in the previous section, (2) becomes nondimensional,

$$\frac{\partial P'}{\partial \tau} + \left[\frac{U}{LV_m}\right] u'\,\frac{\partial P'}{\partial x'} + \left[\frac{W}{HV_m}\right] w'\,\frac{\partial P'}{\partial z} - \left[\frac{K_h}{L^2 V_m}\right]\frac{\partial^2 P'}{\partial x'^2}$$

$$- \left[\frac{K_v}{H^2 V_m}\right]\frac{\partial^2 P'}{\partial z'^2} = \text{scaled biological dynamics.} \quad (18)$$

Once again the primes are dropped for convenience. The scaling of the equations for herbivores, detritus, ammonia and nitrate is similar.

Scaling parameters L and H can be regarded as the length scales within which the patchiness phenomenon occurs. The resolution of patchiness is determined by the choice of Δx and Δz. Since the author is interested in resolving features less than 50 km horizontal length and less than 50 m vertical length, Δx and Δz must be several factors smaller than these scales. Based on these horizontal and vertical length scales, a value for K_h of 5×10^5 cm^2 sec^{-1} and for K_v of 1 cm^2 sec^{-1} is assumed (Okubo, 1971). The dimensional value of all parameters used in the (x,z,t) model for both the strong upwelling case and the intermittent upwelling case is presented in Table 1.

Platt and Denman (1975) performed a similar scaling of (2), although they elected not to divide through by V_m to retain units of frequency. The characterstic time scale of each term is then the reciprocal of its coefficient. The nondimensional coefficients in (18) define the importance of the advective terms relative to the diffusive and growth terms in the equation. When $U/(LV_m)$ or $W/(HV_m)$ >> 1, advection plays a dominant role in determining the spatial configuration of the phytoplankton biomass (O'Brien and Wroblewski, 1973). If one evaluates the magnitude of these coefficients using the values presented in Table 1, it becomes evident that vertical advection is twice as important

- [illegible] using the values presented in Table 1, it becomes evident that vertical advection is twice as important

as horizontal transport in determining the spatial configuration of the phytoplankton. The diffusion terms are two orders of magnitude smaller than the advective terms.

Table 1

Parameter values of the (x,z,t) mesoscale phytoplankton patchiness model

Parameter	Value	Parameter	Value
a	4.09×10^{-1}	V_m	2.4×10^{-5} sec^{-1}
b	1.07	w_s	0.01 cm sec^{-1}
c	1.0°C^{-1}	W	2.0×10^{-2} cm sec^{-1}
d	4.32×10^{4} sec	Δx	1.0×10^{5} cm
E_m	1×10^{-6} sec^{-1}	Δz	2.5×10^{2} cm
H	5.0×10^{3} cm	Γ	2.4×10^{-6} sec^{-1}
I_s	1.2×10^{-3} cal cm^{-2} sec^{-1}	Δ	2.1×10^{-7} sec^{-1}
I_m	2.1×10^{-2} cal cm^{-2} sec^{-1}	η	4.30
K_h	5.0×10^{5} cm^2 sec^{-1}	θ	0.175
K_v	1.0 cm^2 sec^{-1}	κ_p	9.5×10^{-2} cm^2 (μgN)$^{-1}$
k_u	1.0 μgN liter^{-1}	κ_w	6.7×10^{-4} cm^{-1}
L	5.0×10^{6} cm	Λ	0.06 (μgN/liter)$^{-1}$
N_t	30.0 μgN liter^{-1}	Ξ	1.2×10^{-6} sec^{-1}
P_t	0.0 μgN liter^{-1}	Υ	0.15 (μgN/liter)$^{-1}$
R_m	2.8×10^{-6} sec^{-1}	Φ	1.2×10^{-5} sec^{-1}
Δt	8.6×10^{2} sec	Ψ	1.46 (μgN/liter)$^{-1}$
U	10.0 cm sec^{-1}	Ω	4.7×10^{-7} sec^{-1}

Detritus (i.e., ruptured phytoplankton cells and egested copepod fecal pellets of floccular composition) is assumed to have a constant sinking rate, w_s. The nutrients, NH_4 and NO_3, are totally passive, i.e., $w_s = 0$. Phytoplankton cells may be neutrally buoyant in nutrient rich waters (Smayda, 1970) permitting one to omit a sinking term in (2). The detritus sinking rate, w_s, is scaled in the same manner as the vertical velocity, w,

$$w_s = W w_s' .$$

The total derivative for detritus may then be expressed as,

$$\frac{\partial D}{\partial \tau} + S_1 u \frac{\partial D}{\partial x} + S_2 (w + w_s) \frac{\partial D}{\partial z} - E_h \frac{\partial^2 D}{\partial x^2} - E_v \frac{\partial^2 D}{\partial z^2} = \text{scaled biological dynamics} \qquad (19)$$

where $S_1 = U/(LV_m)$, $S_2 = W/(HV_m)$, $E_h = K_h/(L^2V_m)$, and $E_v = K_v/(H^2V_m)$.

3.3 The finite difference scheme

The final nondimensional equations are expressed in finite difference form and solved for each spatial grid point using the scaled u and w velocities derived from the physical upwelling circulation model. If the vertical grid lines in the x-direction are indexed by the letter, j; the horizontal lines in the z-direction, by the letter, k; and nondimensional time is denoted by the index, n; then, $P^n_{j,k} = P(n\Delta\tau, j\Delta x, k\Delta z)$.
and nondimensional time is denoted by the index, n; then, $P^n_{j,k} = P(n\Delta\tau, j\Delta x, k\Delta z)$.

Refer to the stencil shown in Fig. 15. The values of the scaled u and w velocities are determined for the center

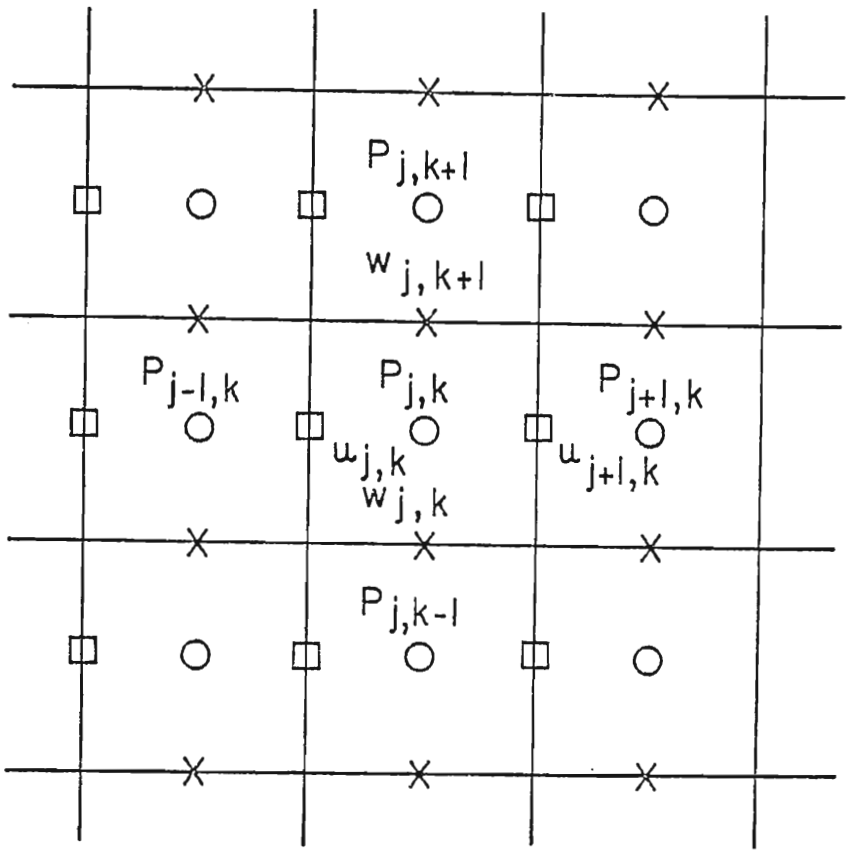

Fig. 15. Stencil showing grid point locations of the u (squares) and w (crosses) velocities and the dependent variable P (circles) used in integrating the (x,z,t) biological-chemical-physical model. The vertical grid lines in the x-direction are indexed by the letter, j, and the horizontal lines in the z-direction by the letter, k.

z-direction by the letter, k.

of the grid walls to increase computational stability. The computed concentration of P, Z, D, NO_3 or NH_4 represents an average over the grid box. The change in concentration of a biotic component is dependent on the amount present within the grid box, the concentration in the nearest four adjacent boxes, the transport into and out of the box, and the biological dynamics occurring within the box.

The finite differencing of the equations for the biological variables P, Z, D, NO_3 and NH_4 incorporates a leap-frog scheme in time, a quadratic conservative advective scheme suggested by Piacsek and Williams (1970) and an explicit scheme for the diffusive terms. The diffusive and biological terms are lagged in time. For example, (18) is rewritten,

$$P^{n+1}_{j,k} = P^{n-1}_{j,k} - \frac{2\Delta\tau U}{\Delta x L V_m}\left[\frac{(P^n_{j+1,k} + P^n_{j,k})}{2} u^n_{j+1,k} - \frac{(P^n_{j-1,k} + P^n_{j,k})}{2} u^n_{j,k}\right] - \frac{2\Delta\tau\, W}{\Delta z\, H V_m}\left[\frac{(P^n_{j,k+1} + P^n_{j,k})}{2} w^n_{j,k+1} - \frac{(P^n_{j,k} + P^n_{j,k-1})}{2} w^n_{j,k}\right] - \frac{2\Delta\tau\, K_h}{(\Delta x)^2 L^2 V_m}\left[P^{n-1}_{j+1,k} + P^{n-1}_{j-1,k} - 2P^{n-1}_{j,k}\right] + \frac{2\Delta\tau\, K_v}{(\Delta z)^2 H^2 V_m}\left[P^{n-1}_{j,k+1} + P^{n-1}_{j,k-1} - 2P^{n-1}_{j,k}\right] + 2\Delta\tau\, B^{n-1}_{j,k}$$

where

$$(\Delta z)^2 H^2 V_m \left[\quad \right]$$

where

$$B_{j,k}^{n-1} \equiv \mu_1 \left[(NO_{3j,k}^{n-1} \; P_{j,k}^{n-1} \; e^{-\psi NH_{4j,k}^{n-1}}) / (\alpha + NO_{3j,k}^{n-1}) \right.$$

$$\left. + \; (NH_{4j,k}^{n-1} \; P_{j,k}^{n-1}) / (\alpha + NH_{4j,k}^{n-1}) \right]$$

$$- \beta \left[1 - e^{-\lambda (P_{j,k}^{n-1} - P^*)} \right] Z_{j,k}^{n-1} - \xi P_{j,k}^{n-1}$$

and

$$\mu_1 \equiv \frac{I_{j,k}^{n+1}/I_s}{\left[1+(I_{j,k}^{n+1}/I_s)^2\right]^{1/2} \left[1+(\theta I_{j,k}^{n+1}/I_s)^2\right]^{\eta/2}} \; (ab^{cT_{j,k}}) \; .$$

When advection and diffusion are neglected, the finite differencing scheme reduces to the common Euler method.

Conditions necessary for stability are:

$$\Delta\tau < \frac{\Delta x}{\sqrt{2}\; u_m} \qquad \text{where } u_m = \text{Max}_{j,k,n} \left| \frac{U}{LV_m} u \right|$$

$$\Delta\tau < \frac{\Delta z}{\sqrt{2}\; w_m} \qquad \text{where } w_m = \text{Max}_{j,k,n} \left| \frac{W}{HV_m} w \right|$$

$$\Delta\tau < \frac{(\Delta x)^2 L^2 V_m}{4\; K_h}$$

$$\Delta\tau < \frac{(\Delta z)^2 H^2 V_m}{4\; K_v} \; .$$

In this model the advective criteria are the more stringent. The stability criterion for the Euler method is $\Delta\tau < \sigma^{-1}$ where σ is the largest biological rate parameter. The accuracy of the finite differencing scheme in approximating its analogous continuous derivative increases with smaller

racy of the finite differencing scheme in approximating its analogous continuous derivative increases with smaller

values of $\Delta\tau$. The time step, $\Delta\tau$, used was 0.02 which converts to 0.01 days in real time.

3.4 Boundary conditions

No advective mass flux is allowed across the solid coast or the air-sea interphase. At the water column bottom boundary, the direction of the flow determines the advective boundary condition. If water is upwelling, the boundary values for P, Z, NO_3, NH_4 and D are specified from observational data. If water is downwelling, the concentration of the variable just inside the boundary determines the value at the boundary. A one-sided derivative is used for the advective terms. The offshore boundary is treated similarly. No diffusive mass flux is allowed through any boundary.

These boundary conditions are such that limiting nutrient can become stored within the model region as either P, Z, NO_3, NH_4 or D. Yet, the total amount of nutrient is conserved in a balance between what is advected into and out of the region and what is stored as standing stock or dissolved nutrient.

Sampling profiles of phytoplankton nitrogen, nitrate and ammonia taken 50 km seaward of the Oregon coast in 1972 and 1973 closely approximate the steady state profiles of these variables shown in Figs. 11 and 13. Continuous profiles of zooplankton biomass and detrital nitrogen at 50 km offshore were not taken, but the zooplankton net tows and the particulate nitrogen data do indicate the model's
offshore were not taken, but the zooplankton net tows and the particulate nitrogen data do indicate the model's
steady state profiles for zooplankton and detritus are reasonable. The steady state values of these variables at

50 m are taken as the boundary condition concentrations in upwelling water entering the model region from below. (Table 2).

3.5 Initial conditions

Presently, there does not exist adequate field data to specify the initial conditions of the biological and chemical dependent variables for all x and z at the onset of the model case runs. For lack of a better alternative, the initial conditions are taken as the steady state solution of the (x,z,t) primary productivity model in the absence of advection.

The temperature field is specified from observations made during August 1973. Sea surface temperatures were found to decrease from 14°C at an offshore distance of 50 km to 9°C at the coast during strong upwelling. Temperatures below the surface mixed layer decreased rapidly with depth, especially where cold slope water moved onto the continental shelf. A polynomial function was fit to the observed temperature data to give a time-invariant, smoothed temperature field evaluated at each grid location in the model region (Fig. 16a).

The influence of this temperature distribution on the steady state, daily primary production of the water column is shown in Fig. 16b. Fig. 16c shows the initial conditions
steady state, daily primary production of the water column is shown in Fig. 16b. Fig. 16c shows the initial conditions
for the phytoplankton field. The phytoplankton spatial distribution differs from the steady state profiles shown in

Table 2

Boundary conditions at 50 meters depth

Variable	Observed (μgat N ℓ^{-1})	Simulated (μgat N ℓ^{-1})
P	0.5 - 1.5	1.0
Z	1.0 - 10.0	3.0
NO_3	25.0 - 30.0	25.0
NH_4	0.3 - 0.5	0.6
D	0.5 - 1.5	0.4

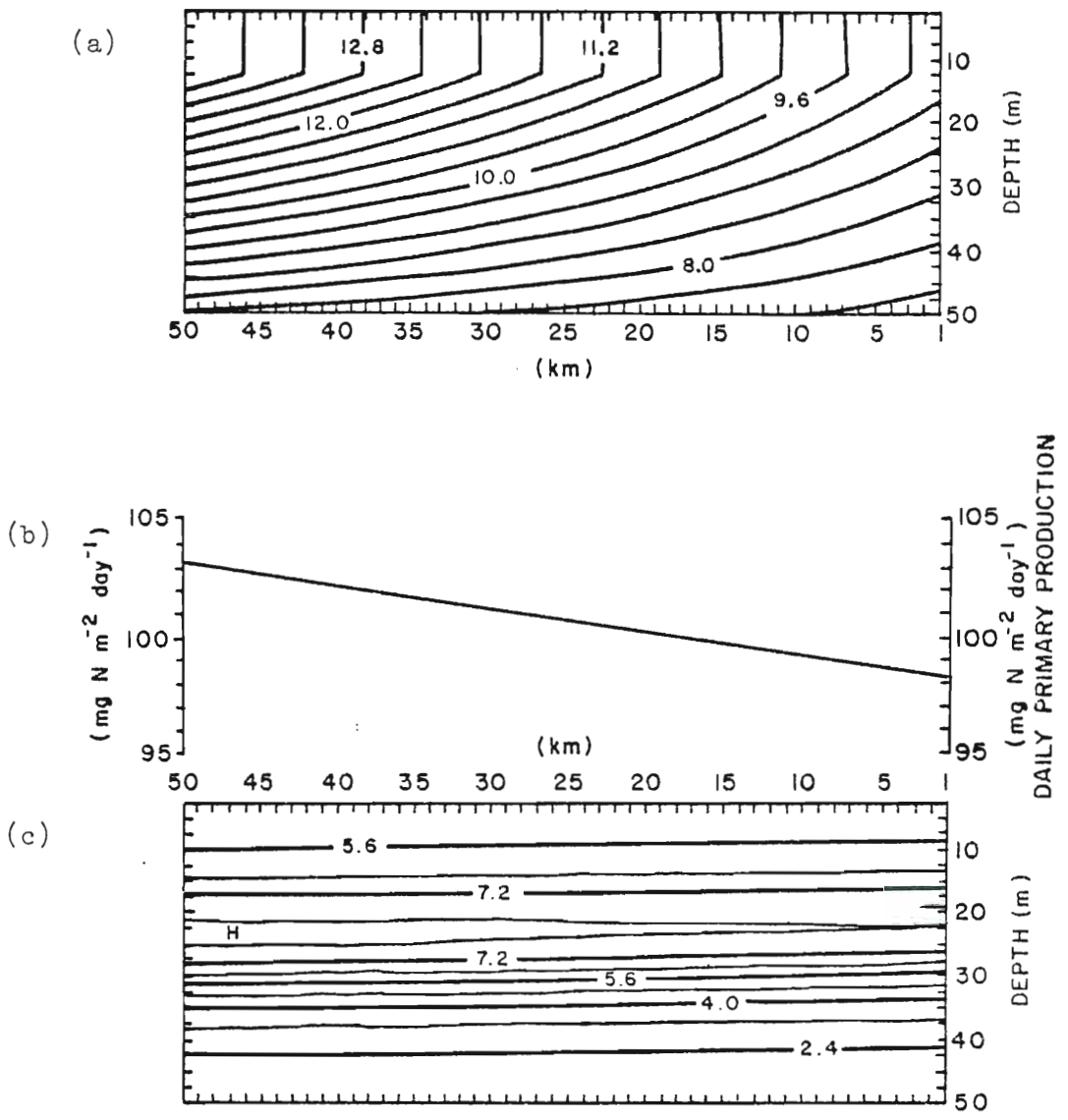

Fig. 16. (a) The spatial distribution of seawater temperature assumed in the (x,z,t) model of phytoplankton production. Contours are from 7°C at 50 m depth at the coast to 14°C at the surface 50 km offshore. The contour interval is 0.4°C. (b) The steady state gross primary productivity of the water column for the (x,z,t) phytoplankton production model. (c) The steady state phytoplankton spatial distribution for the (x,z,t) model in the absence of advection. Contour intervals are 0.8 μgat N ℓ^{-1}.

Fig. 11 only in that plant growth as a function of temperature varies in x as well as z (Fig. 16b). If the temperature field (Fig. 16a) showed no variation with distance offshore, the initial phytoplankton field would appear homogeneous in x, although stratified in z.

At the beginning of the modeled 20-day period of the strong upwelling case, a spatially variable wind stress is specified which linearly increases from zero at time zero to -0.5 dyne cm^{-2} from the north (Fig. 17a and b). The wind stress remains at this magnitude from day 1 to day 10, then linearly decreases to zero during day 11. It remains zero for the rest of the 20-day period (Fig. 17b). The wind stress used in the physical circulation model for the intermittent upwelling case is derived from actual wind measurements recorded by an anemometer located on the south jetty off Newport, Oregon (Figs. 27 and 28).

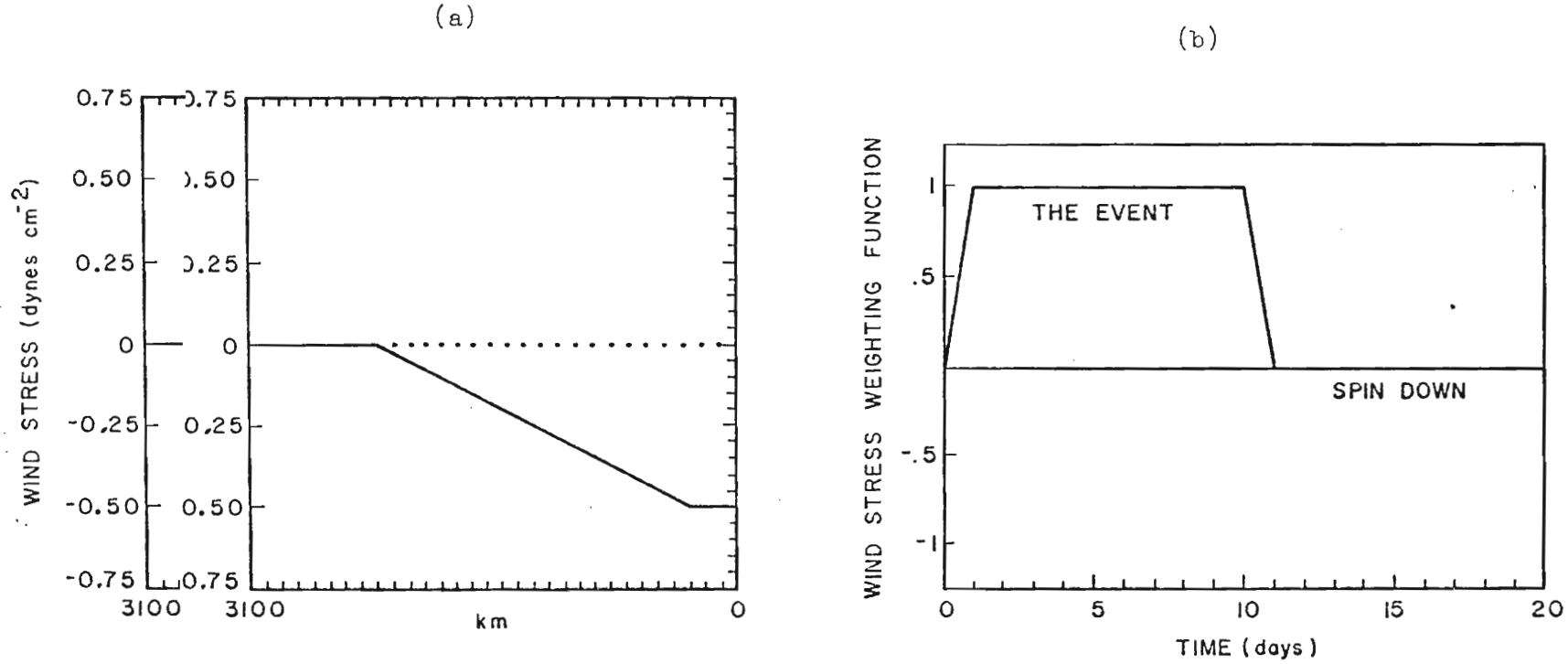

Fig Fig. 17. (a) The spatial distribution of the wind stress in the strong upwelling case. The north- north-south component of the wind stress (solid line) is -0.5 dyne cm^{-2} near the coast. The east-w east-west component of the wind stress is zero everywhere. (b) The temporal variation of the wind s wind stress weighting function in the strong upwelling case.

4. MODEL RESULTS

In this section simulations of mesoscale phytoplankton patchiness during strong upwelling and during intermittent upwelling in August 1973 are presented. Results from both model runs are subsequently compared with observations made during CUE and with the literature. The goal is to investigate the biological, chemical and physical dynamics involved, rather than to merely reproduce the observed features numerically. A sensitivity analysis of the (x,z,t) model is performed to ascertain which of the mechanisms involved are the most important in determining the spatial solutions.

4.1 The onset of upwelling and development of the phytoplankton plume

It is difficult to graphically represent the time-dependent nature of the velocity field and the corresponding spatial features of the biological and chemical dependent variables. In the following "snapshot" displays of these fields, the reader should remember many functions (such as growth of phytoplankton) vary with time of day. For example, a diel periodicity occurs in the concentration of ammonia and nitrate which is not apparent in the following pictures. As a convention, the velocity field and the corresponding and nitrate which is not apparent in the following pictures. As a convention, the velocity field and the corresponding spatial distribution of the dependent variables are

displayed at the end of a model day. The nondimensional model solutions have been multiplied by N_t to regain units of concentration and thus help the reader compare the model results with observations.

The velocity field after 4 days elapsed time in the strong upwelling case is presented in Fig. 18a. The linearized bottom topography and the wind stress at the time of the velocity field snapshot are also shown. The wind stress vector has a magnitude of -0.5 dyne cm^{-2} and points southward. The velocity field is visualized by vectors representing the position and instantaneous velocity of tracer particles which have been advected by the flow. Only the vectors within 25 km of the coast are shown, although the circulation is calculated out to 3100 km. The vector arrows are scaled by the maximum vector occurring in the field at that time. It should be remembered that each vector's horizontal and vertical scales differ by two orders of magnitude. Two cyclonically rotating circulation cells are evident in Fig. 18a. The lower cell advects water towards the coast along the bottom and up into the euphotic zone within 5 km of the coast. This upwelled water either continues to rise to the surface or moves offshore beneath the second counterclockwise rotating circulation cell. In this second cell the flow is weakly onshore at 30 m depth and strongly offshore near the surface. This two-cell circulation is similar to the conceptual diagram of coastal upwelling off Oregon presented in Fig. 16 of Mooers, Collins, and Smith (1976).

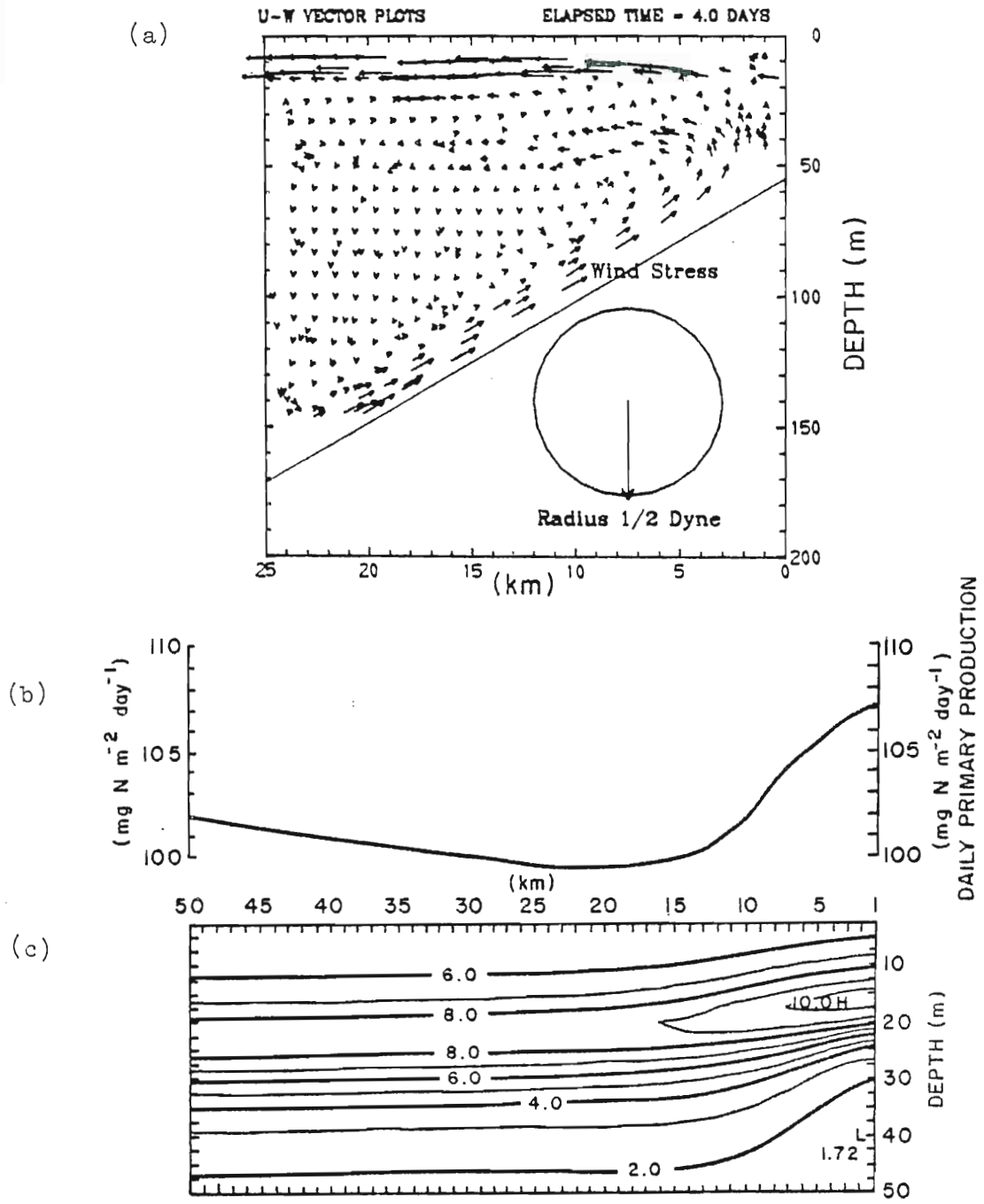

Fig. 18. (a) The upwelling circulation in the transverse plane normal to the coast after 4 days in the strong upwelling case. The bottom topography and the wind stress at day 4 are also shown. The maximum u and w velocities in the field are -2.9 cm sec^{-1} and 1.4×10^{-2} cm sec^{-1}, respectively. (b) The gross primary productivity of the water column after 4 days in the strong upwelling case. (c) The spatial distribution of [illegible] maximum u and w velocities in the field are -2.9 cm sec^{-1} and 1.4×10^{-2} cm sec^{-1}, respectively. (b) The gross primary productivity of the water column after 4 days in the strong upwelling case. (c) The spatial distribution of phytoplankton after 4 days in the strong upwelling case. Contour intervals are 1 μgat N ℓ^{-1}.

Figure 18b displays the daily gross primary production of the water column calculated at each 1 km grid point in the model region at day 4. The distribution of phytoplankton within 50 km of the coast and within 50 m of the surface after 4 days elapsed time is shown in Fig. 18c.

Figure 18 shows that a high in phytoplankton biomass develops near the coast with the onset of upwelling. The formation of a plume is apparent in the phytoplankton field. The upwelling of water high in nitrate concentration into the euphotic zone leads to the increase in plant biomass. Even though the growth rate of phytoplankton is slower near the coast due to the colder temperatures there (Fig. 16a), the nutrient-limited plants bloom with the supply of nitrate (Fig. 18c).

After 7 days the two-cell circulation (Fig. 19a) and the phytoplankton plume (Fig. 19c) are well developed. A maximum plant biomass occurs at 17 m depth between 6 and 11 km offshore (Fig. 19c). This maximum has been advected away from the coast and closer to the surface. The maximum also occurs at a shallower depth than the steady state profile maximum (Fig. 11) because of self-shading by the rapidly growing phytoplankton (Fig. 19b).

As upwelling at the coast intensifies, downwelling develops in the region between 10 and 25 km offshore (Fig. 20a). The contours of the phytoplankton and nitrate fields near the water column bottom boundary clearly show the downwelling (Figs. 20c and 21b). The phytoplankton maximum

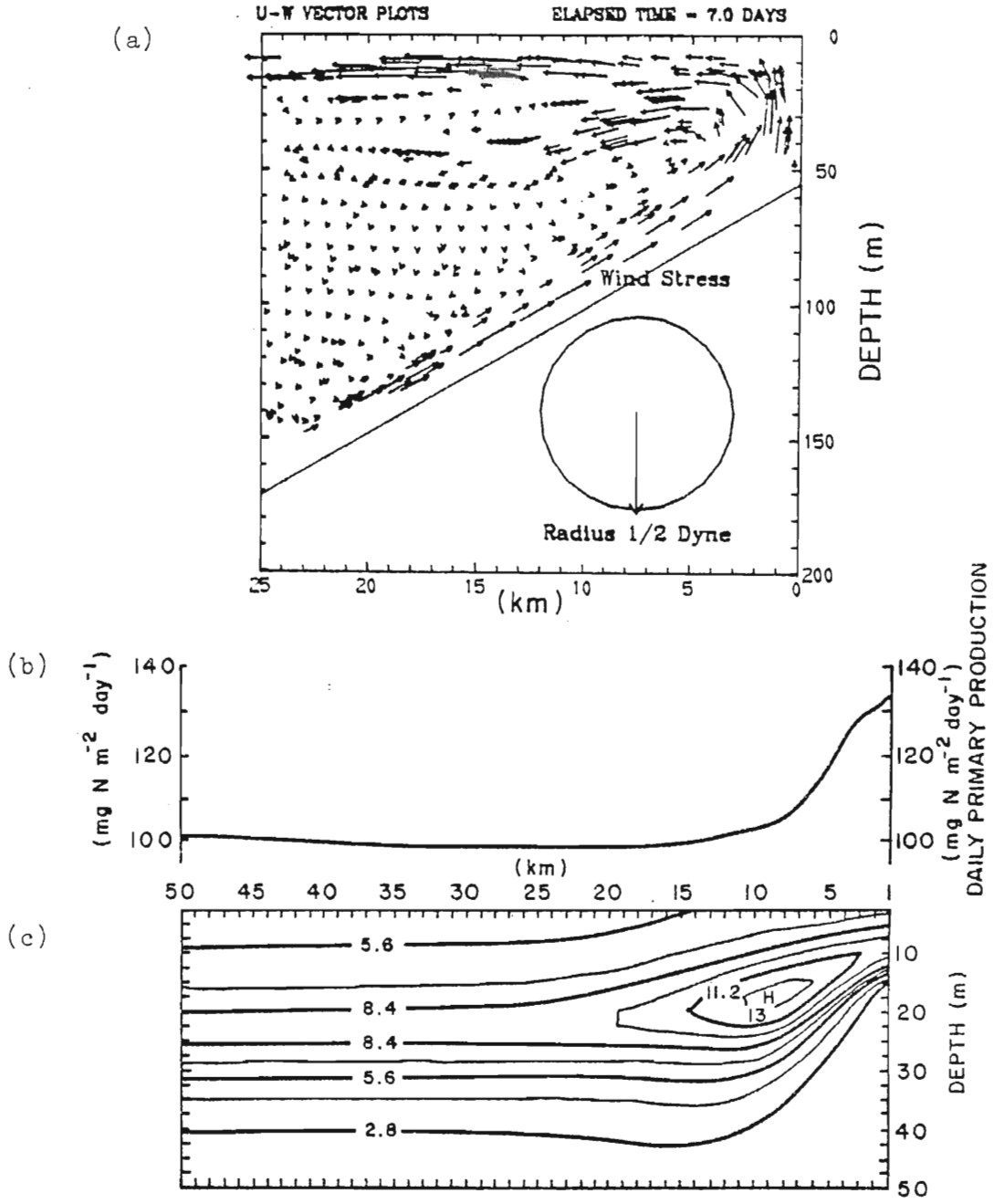

Fig. 19. Same as Fig. 18 but for day 7. The maximum u and w velocities in (a) are -5.9 cm sec^{-1} and 4.4 x 10^{-2}

Fig. 19. Same as Fig. 18 but for day 7. The maximum u and w velocities in (a) are -5.9 cm sec^{-1} and 4.4 x 10^{-2} cm sec^{-1}, respectively. Contour intervals in (c) are 1.4 µgat N ℓ^{-1}.

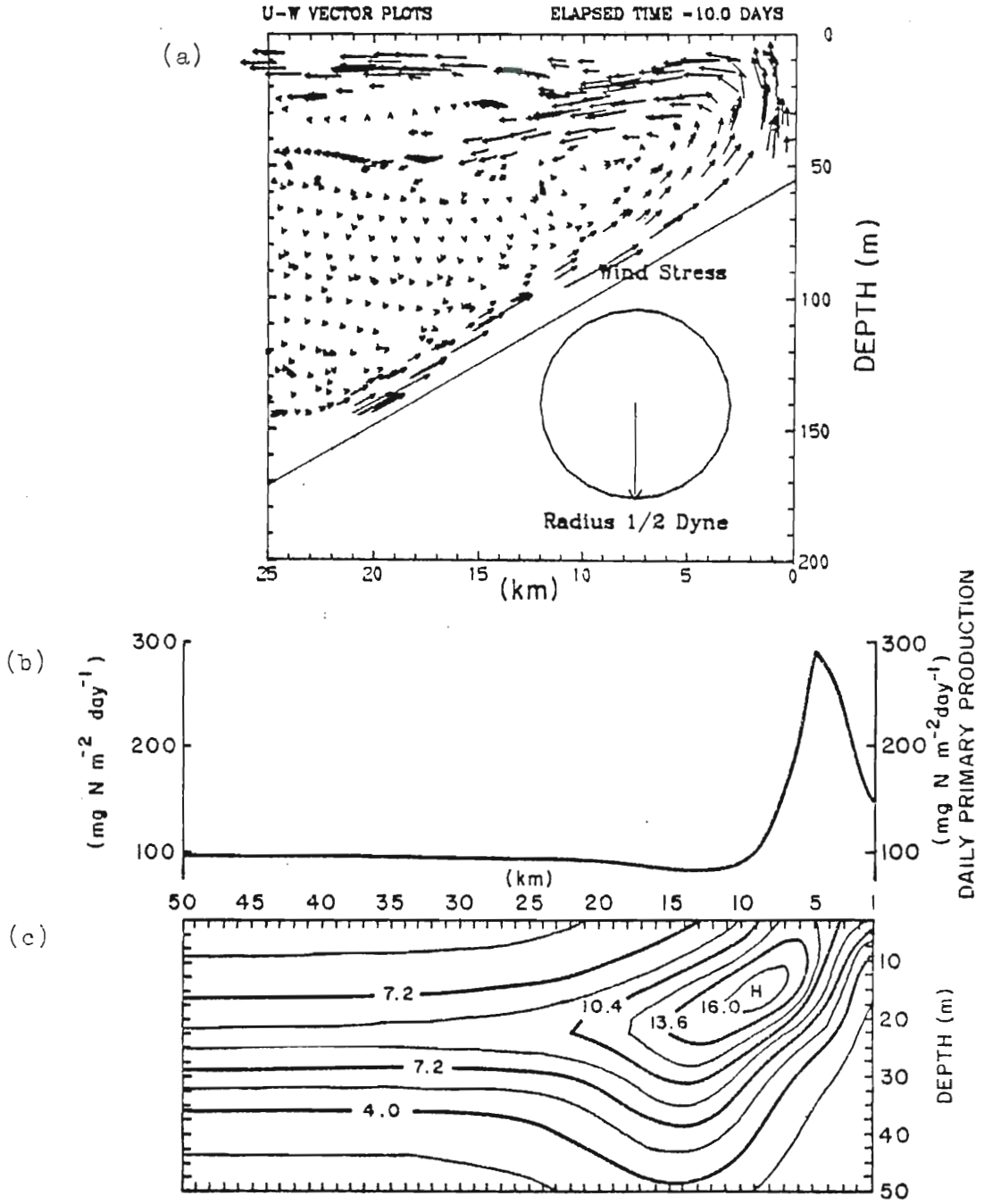

Fig. 20. Same as Fig. 18 but for day 10. The maximum u and w velocities in (a) are -6.1 cm sec^{-1} and 5.2 x 10^{-2} cm sec^{-1}, respectively. Contour intervals in (c) are 1.6 µgat N ℓ^{-1}.

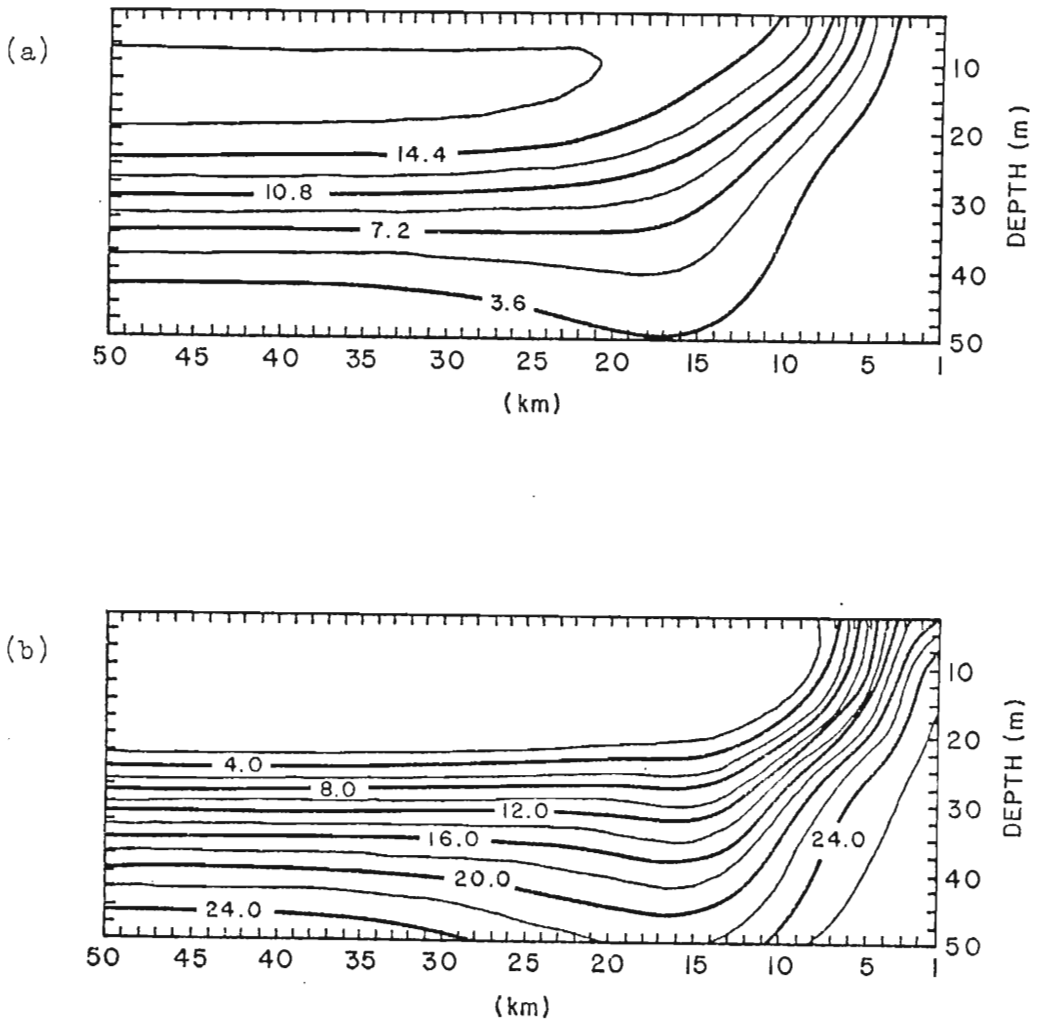

Fig. 21. (a) Zooplankton field after 10 days in the strong upwelling case. Contour intervals are 1.8 µgat N ℓ^{-1}. (b) Nitrate field after 10 days in strong upwelling case. Contour intervals are 2 µgat NO_3 ℓ^{-1}.

1.8 µgat N ℓ^{-1}. (b) Nitrate field after 10 days in strong upwelling case. Contour intervals are 2 µgat NO_3 ℓ^{-1}.

increases as it is advected further offshore and closer to the surface (Fig. 20c).

The zooplankton field shows the upwelling and offshore transport of water low in herbivore biomass (Fig. 21a). The highest zooplankton concentrations occur seaward of the phytoplankton plume.

The concentration of nitrate in the euphotic zone is kept low by plant production. Only where strong upwelling occurs does the supply of NO_3 exceed its utilization, allowing high concentrations of nitrate to reach the surface (Fig. 21b).

In the steady state ammonia profile, the maximum concentration occurs at 35 m (Fig. 13). During the strong upwelling case, this maximum intensifies as nutrient supply to the euphotic zone leads to increased phytoplankton production, zooplankton grazing and fecal pellet production. The slow oxidation of ammonia into nitrite-nitrate is exceeded by the nutrient input from decomposing fecal pellets, resulting in high concentrations of NH_4 at 35 to 45 m depth (Fig. 22a). Upwelling of water low in ammonia concentration within 10 km of the coast and between 33 and 50 km offshore further intensifies the ammonia gradient.

Figure 22b shows the development of a plume in the detritus field. The detritus maximum at day 10 in the strong upwelling case occurs several meters below and several kilo-

detritus field. The detritus maximum at day 10 in the strong upwelling case occurs several meters below and several kilo-

meters seaward of the phytoplankton plume. The main source of this detritus is fecal pellets produced by herbivores

(a)

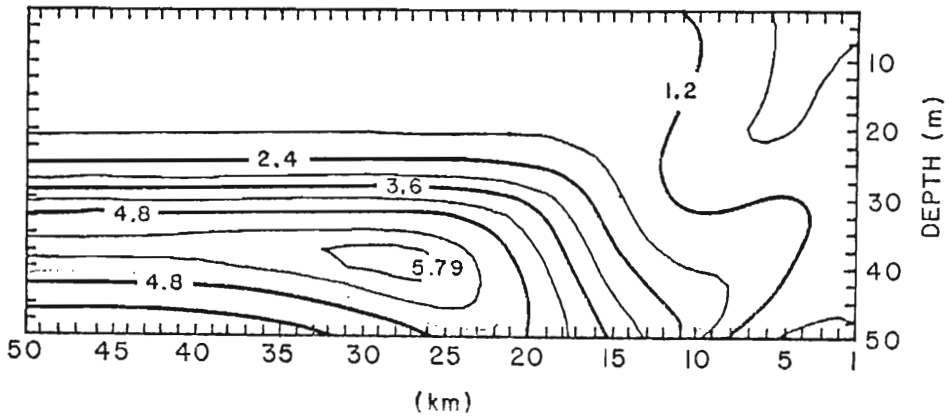

(b)

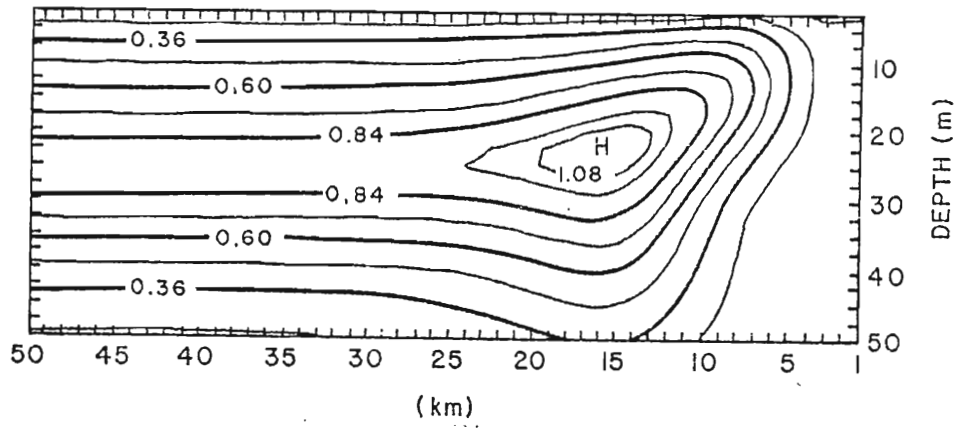

Fig. 22. (a) Ammonia field after 10 days in the strong upwelling case. Contour intervals are 0.6 µgat NH_4 ℓ^{-1}. (b) Spatial distribution of detritus after 10 days in the strong upwelling case. Contour intervals are 0.12 µgat N ℓ^{-1}.

grazing in the phytoplankton plume. The fecal pellets sink as they are advected offshore.

4.2 Cessation of upwelling and decay of the phytoplankton plume

When the wind linearly decrease to zero during day 11, the upwelling at the coast begins to decline and the offshore downwelling slowly relaxes (Figs. 23a, 24a). The upwelled water is not as strongly advected offshore and below the euphotic zone as before. This allows the phytoplankton to bloom on the nitrate which remains longer in the euphotic zone. The highest plant concentration, 23 μgat N ℓ^{-1}, occurs on day 13, two days after the wind stress falls to zero. As upwelling subsides the phytoplankton maximum recedes toward the coast and deepens (Fig. 23c).

After 20 days the plant maximum has decreased to 15.4 μgat N ℓ^{-1} and occurs contiguous with the coast at a depth of 15 m (Fig. 24c). With no wind forcing, upwelling ceases (Fig. 24a) and the euphotic zone becomes depleted of nutrients (Fig. 25b). The zooplankton standing stock declines nearshore (Fig. 25a). The detritus maximum decays as fecal pellet production lessens (Fig. 26b). The ammonia maximum offshore begins to decrease at day 20 (Fig. 26a) as more NH_4 is oxidized to NO_3 than is added by decomposing fecal pellets.

4.3 Daily primary production of the water column
pellets.

4.3 Daily primary production of the water column during the strong upwelling case

The daily gross primary production of the water column

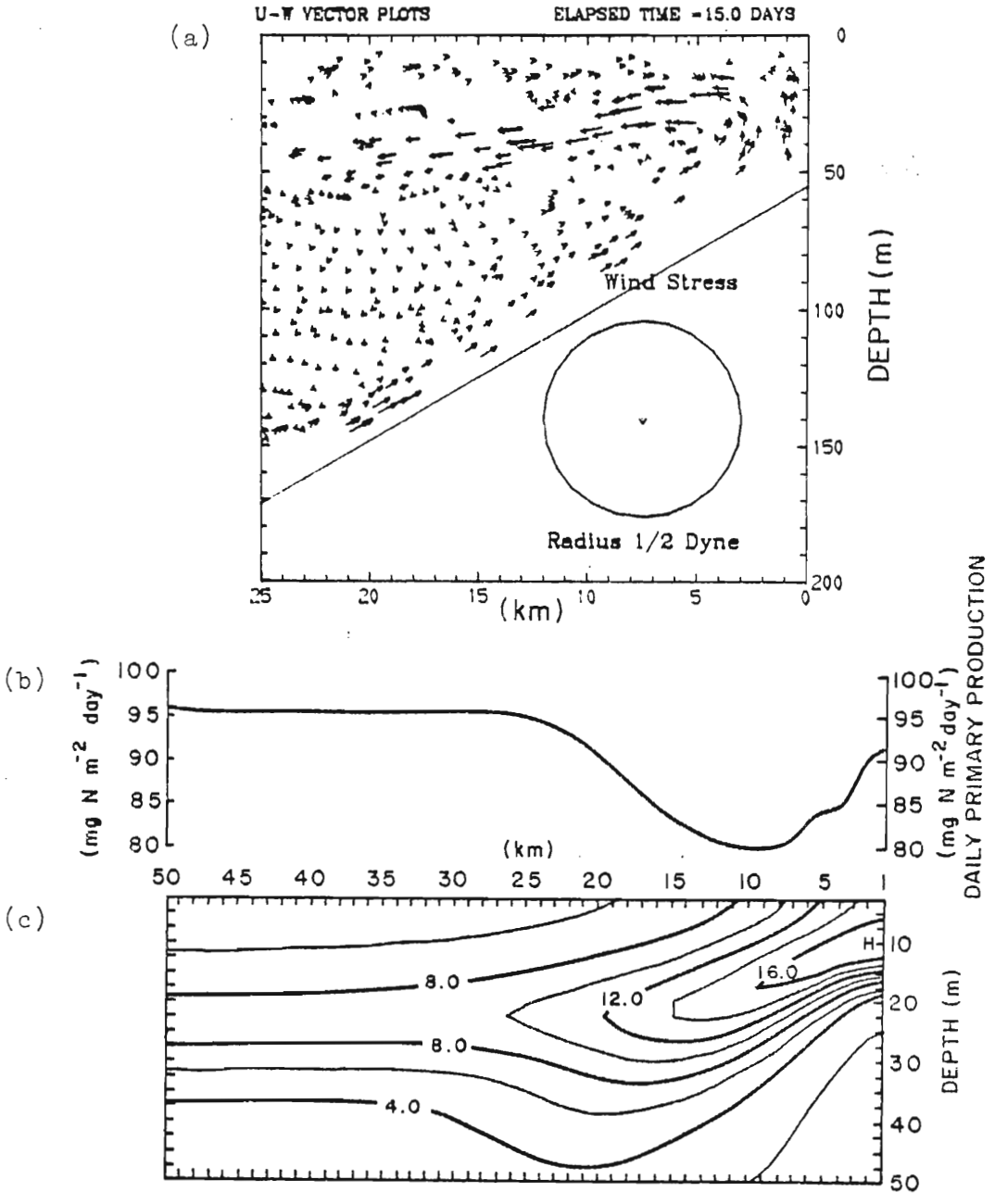

Fig. 23. Same as Fig. 18 but for day 15. The maximum u and w velocities in (a) are -3.6 cm sec^{-1} and 1.5 x 10^{-2} cm sec^{-1}, respectively. Contour intervals in (c) are

Fig. 23. Same as Fig. 18 but for day 15. The maximum u and w velocities in (a) are -3.6 cm sec^{-1} and 1.5 x 10^{-2} cm sec^{-1}, respectively. Contour intervals in (c) are 2.0 μgat N ℓ^{-1}.

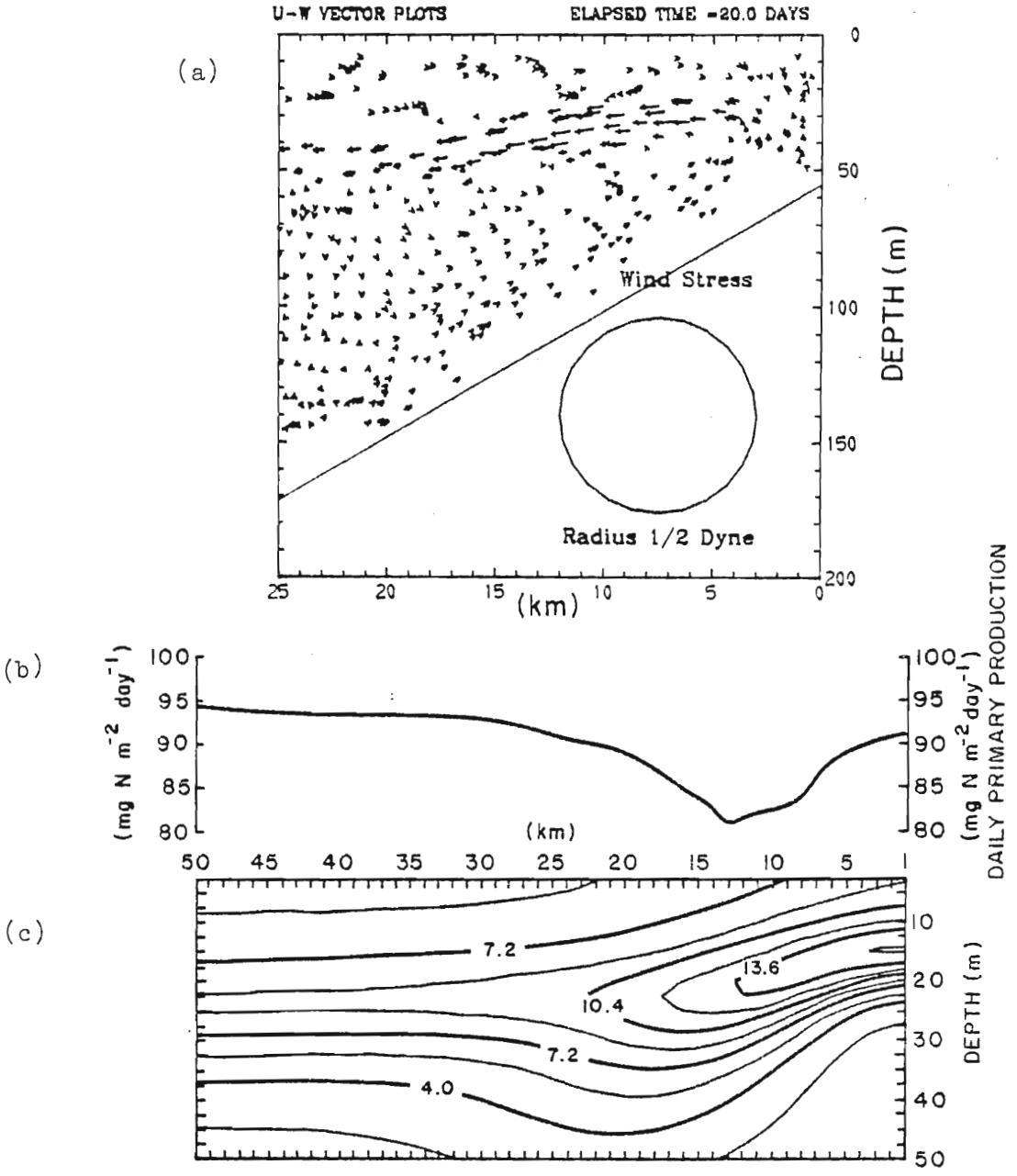

Fig. 24. Same as Fig. 18 but for day 20. The maximum u and w velocities in (a) are -2.8 cm sec^{-1} and 7.9 x 10^{-3} cm sec^{-1}, respectively. Contour intervals in (c) are 1.6 µgat N ℓ^{-1}.

cm sec^{-1}, respectively. Contour intervals in (c) are 1.6 µgat N ℓ^{-1}.

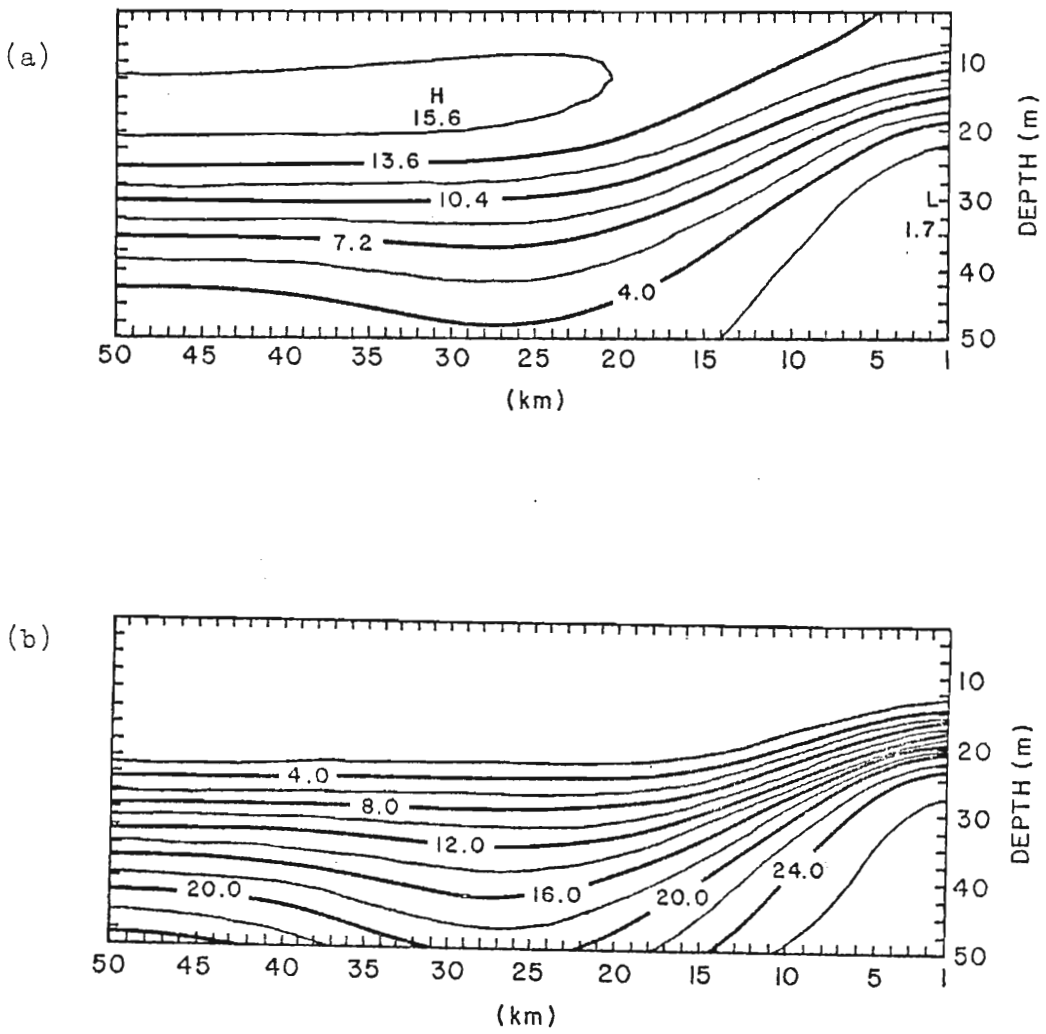

Fig. 25. Same as Fig. 21 but for day 20. Contour intervals in (a) are 1.6 µgat N ℓ^{-1} and in (b) are 2 µgat NO_3 ℓ^{-1}.

Contour intervals in (a) are 1.6 µgat N ℓ^{-1} and in (b) are 2 µgat NO_3 ℓ^{-1}.

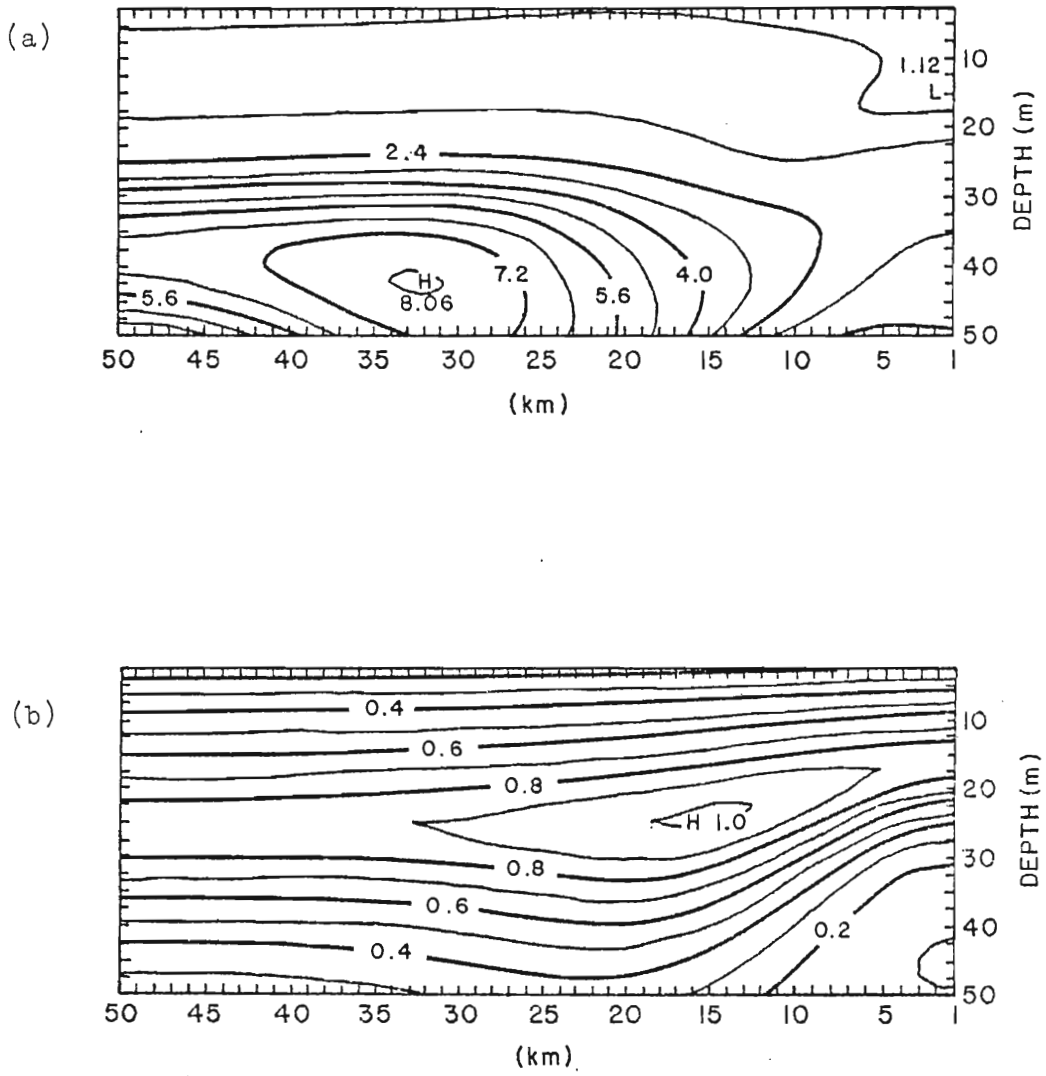

Fig. 26. Same as Fig. 22 but for day 20. Contour intervals in (a) are 0.8 µgat NH_4 ℓ^{-1} and in (b) are 0.1 µgat N ℓ^{-1}.

is plotted above the corresponding phytoplankton field for days 4, 7, 10, 15, and 20 (Figs. 18b, 19b, 20b, 23b, and 24b). These figures show that as upwelling supplies nitrate to the nutrient-limited euphotic zone, primary productivity increases. The plants grow fastest where the supply of nutrients is greatest. The maximum daily primary production occurs on day 10 (Fig. 20b) when upwelling is strongest (Fig. 20a). Primary production increases not only at the locus of upwelling, but also in surface waters which are advected seaward. While the highest daily primary production occurs in the region of most intense upwelling (Figs. 20a and b), the maximum phytoplankton standing crop is found offshore (Fig. 20c).

Figure 27 depicts the relationship between the north-south component of the wind stress and daily primary production. The increasing amplitude of the production curve in Fig. 27 reflects the growing concentration of phytoplankton biomass in the plume. Productivity continues to increase during upwelling conditions, but declines when the northerly wind stress decays on day 11. With no further wind forcing of upwelling, phytoplankton growth becomes nutrient-limited.

Residual upwelling accounts for the shoreward increase in the productivity curves in Figs. 23b and 24b. Residual downwelling in the region 10 to 25 km offshore reduces the productivity by as much as 9 mg N m^{-2} day^{-1} as plants are downwelling in the region 10 to 25 km offshore reduces the productivity by as much as 9 mg N m^{-2} day^{-1} as plants are advected to aphotic zone depths. The reduction in productivity in this region is also due to lower temperatures.

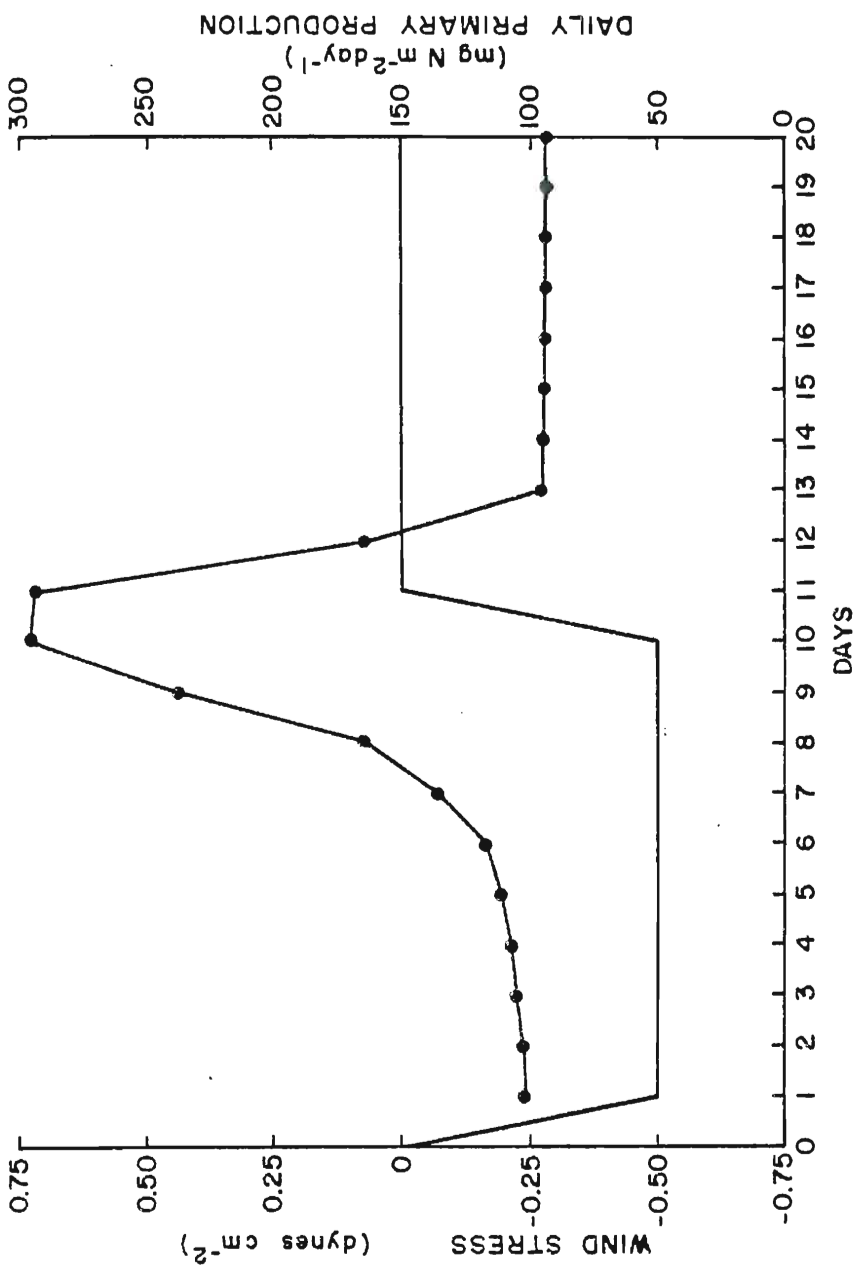

Fig. 27. The north-south component of the wind stress near the coast for the strong upwelling case. The data points show the maximum daily gross primary production calculated for each model day.

4.4 Plume structure and primary productivity during intermittent upwelling

To investigate the response of primary production to intermittent upwelling, Thompson's (1974) numerical circulation model was run with a variable wind stress calculated from the August 1973 recordings of an anemometer located on the south jetty off Newport, Oregon. The wind stresses in the north-south and east-west directions are shown in Figs. 28 and 29, respectively. The circulation model was driven from rest on August 1, 1973 with initial conditions specified from observational hydrographic data. The resulting time dependent u, v, and w velocities were used to advect the biological and chemical dependent variables. Initial conditions for the biological simulation model were the same as for the strong upwelling case, i.e., the steady state solution of the (x,z,t) biological-chemical model in the absence of advection.

The two-cell circulation found in the strong upwelling case develops during the first five days of August (not shown). The north-south wind stress during this period (Fig. 28) is similar in magnitude to the northerly wind stress of the strong upwelling case (Fig. 27). A phytoplankton plume similar to that of the strong upwelling case develops by August 5 (Fig. 30a). Daily primary production (Fig. 28) is comparable to that calculated for the fifth

develops by August 5 (Fig. 30a). Daily primary production

(Fig. 28) is comparable to that calculated for the fifth day of the strong upwelling case (Fig. 27).

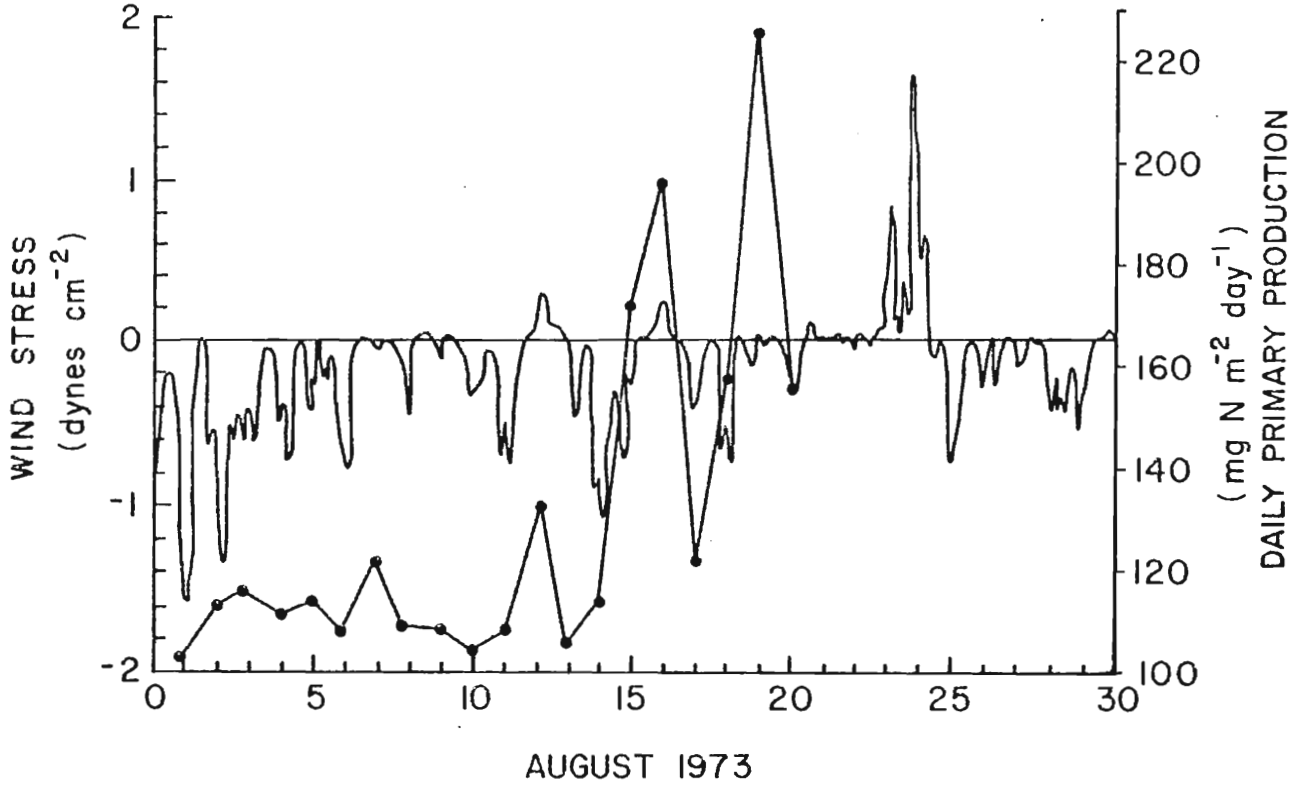

Fig. 28. The north-south component of the wind stress calculated from Newport, Oregon, anemometer data recorded during August 1973. The data points show the maximum daily gross primary production predicted for each day by the (x,z,t) productivity model.

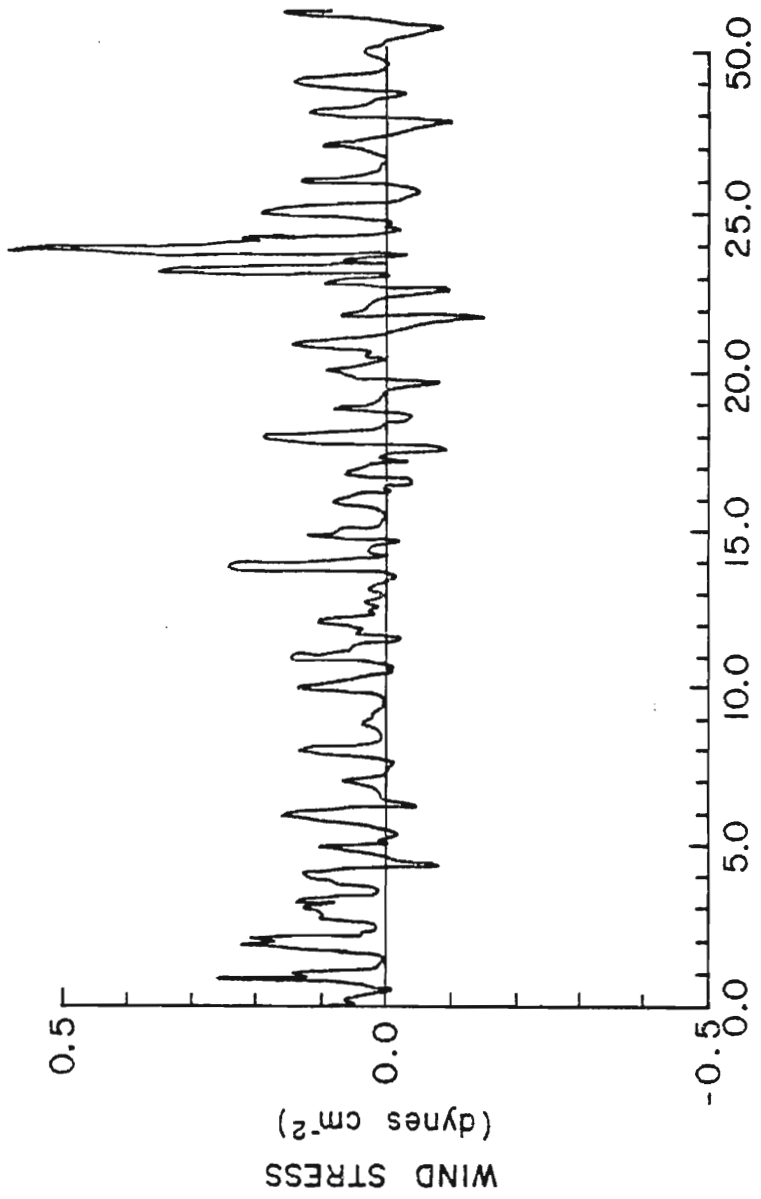

Fig. 29. The east-west component of the wind stress calculated from the Newport, Oregon, anemometer data recorded during August 1973.

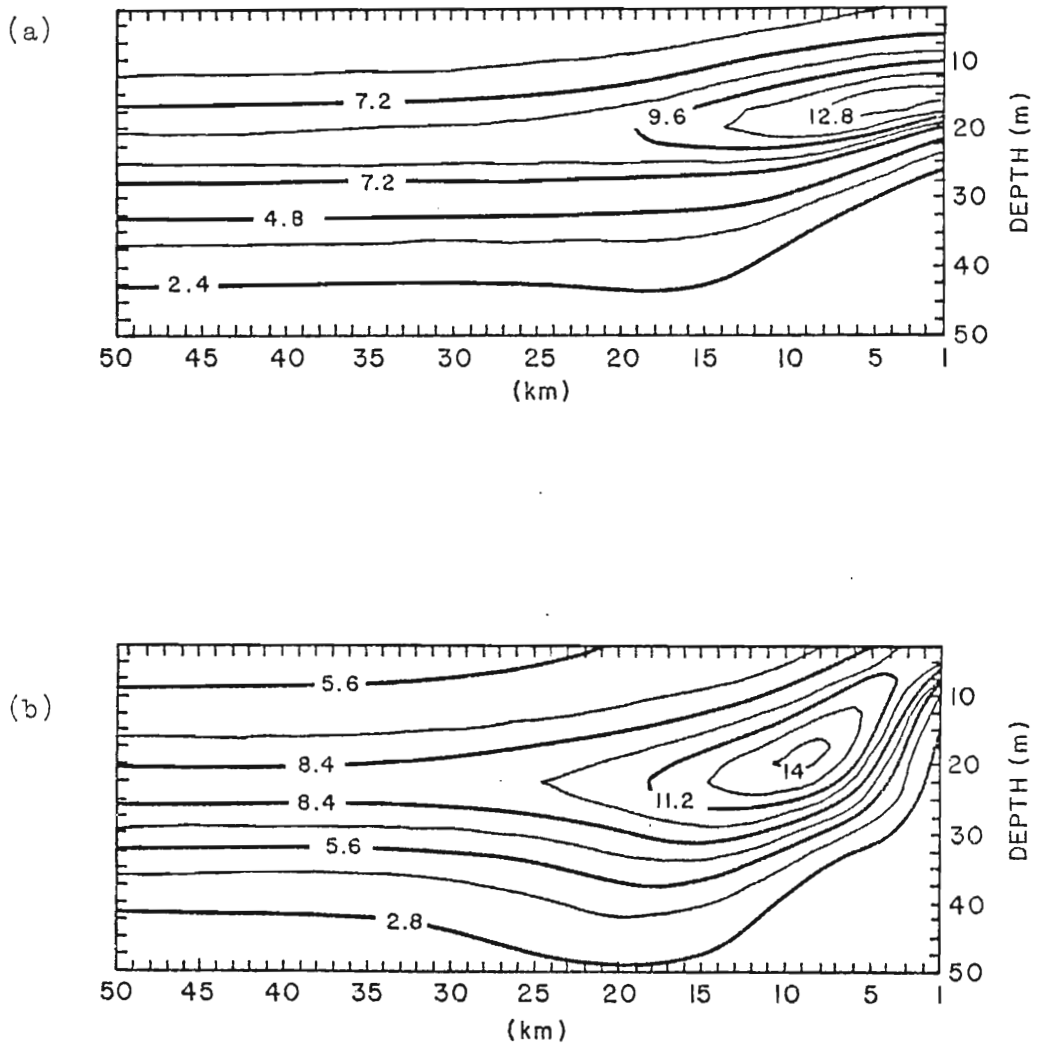

Fig. 30. (a) The spatial distribution of phytoplankton on August 5 in the intermittent upwelling case. Contour intervals are 1.2 μgat N ℓ^{-1}. (b) Same as (a) but on August 15. Contour intervals are 1.4 μgat N ℓ^{-1}.

(b) Same as (a) but on August 15. Contour intervals are 1.4 μgat N ℓ^{-1}.

The two-cell circulation decays into a more confused upwelling circulation after August 6 when periods of prolonged relaxation of the wind stress occur (Fig. 28). While primary production steadily increased with continuous wind forcing in the strong upwelling case (Fig. 27), calculations of daily primary production from August 5 to August 20 show a variability which is related to fluctuations in the north-south component of the wind stress (Fig. 28). Each major intensification of the longshore wind component is followed by an increase in primary production (Figs. 31 and 32). Upon relaxation of the wind stress, the rate of upwelling slows and the primary productivity decreases. The wind event of August 13 to 15 (Fig. 28) results in advection of the phytoplankton maximum away from the coast (Fig. 30b), much as observed after 10 days in the strong upwelling case.

The spatial structure of the dependent variables (P, Z, NO_3, NH_4 and D) all develop features during intermittent upwelling similar to that found in the strong upwelling case. The zooplankton, nitrate, ammonia and detritus fields as they appear on August 15 are shown in Figs. 33 and 34.

The quiescent period from August 19 to 23 is followed by a reversal in the north-south wind component. Downwelling develops at the coast. The contours of the phytoplankton field on August 23 (Fig. 35) clearly show the
welling develops at the coast. The contours of the phytoplankton field on August 23 (Fig. 35) clearly show the
downwelling within 4 km of the coast.

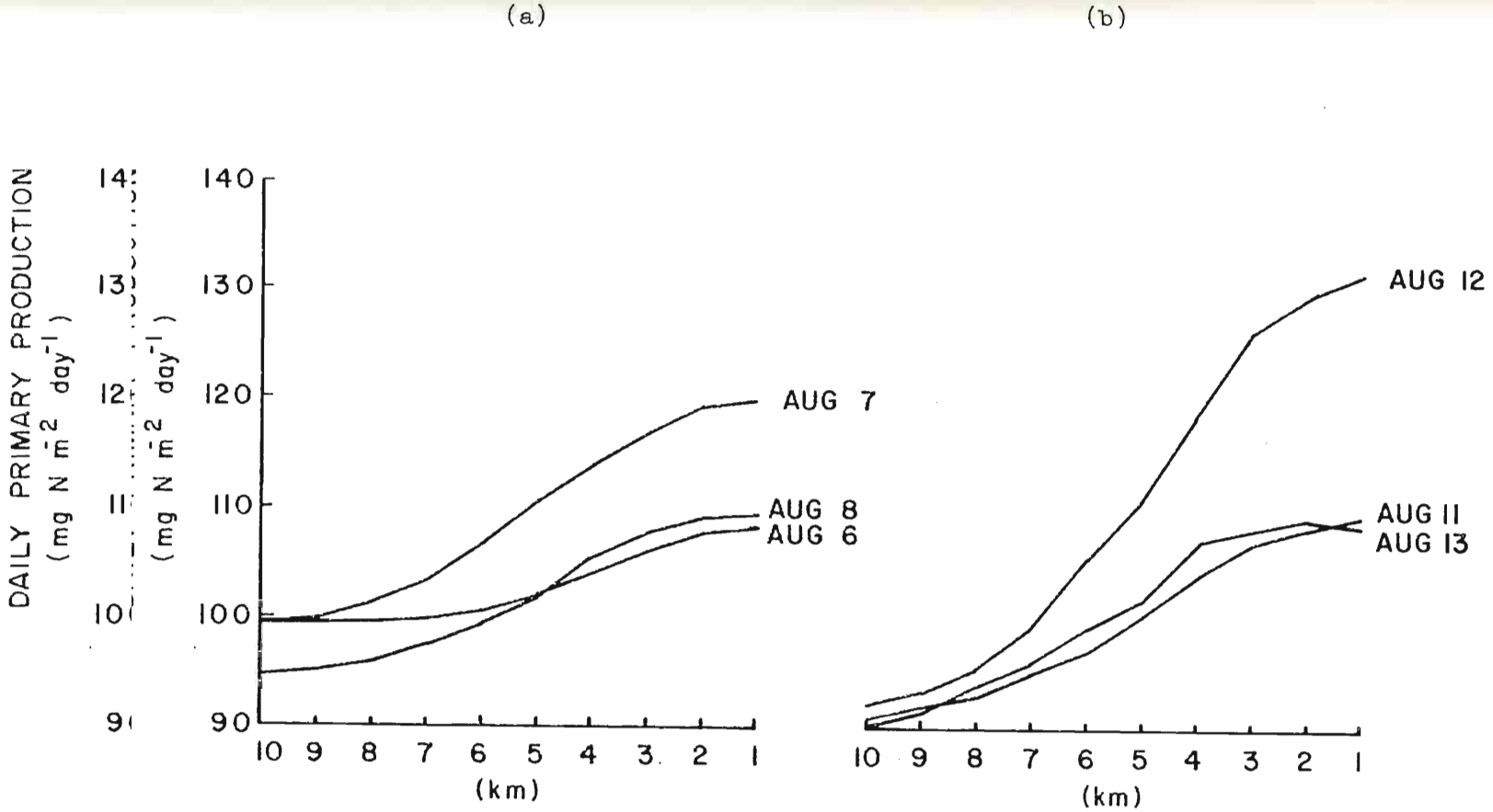

Fig. 31. Daily gross primary production of the water column within 10 km of the coast as predicted by the (x,z,t) productivity model during August 1973. In (a) the production calculated for August 6, 7 and 8 is shown. In (b) the production for August 11, 12 and 13 is calculated.

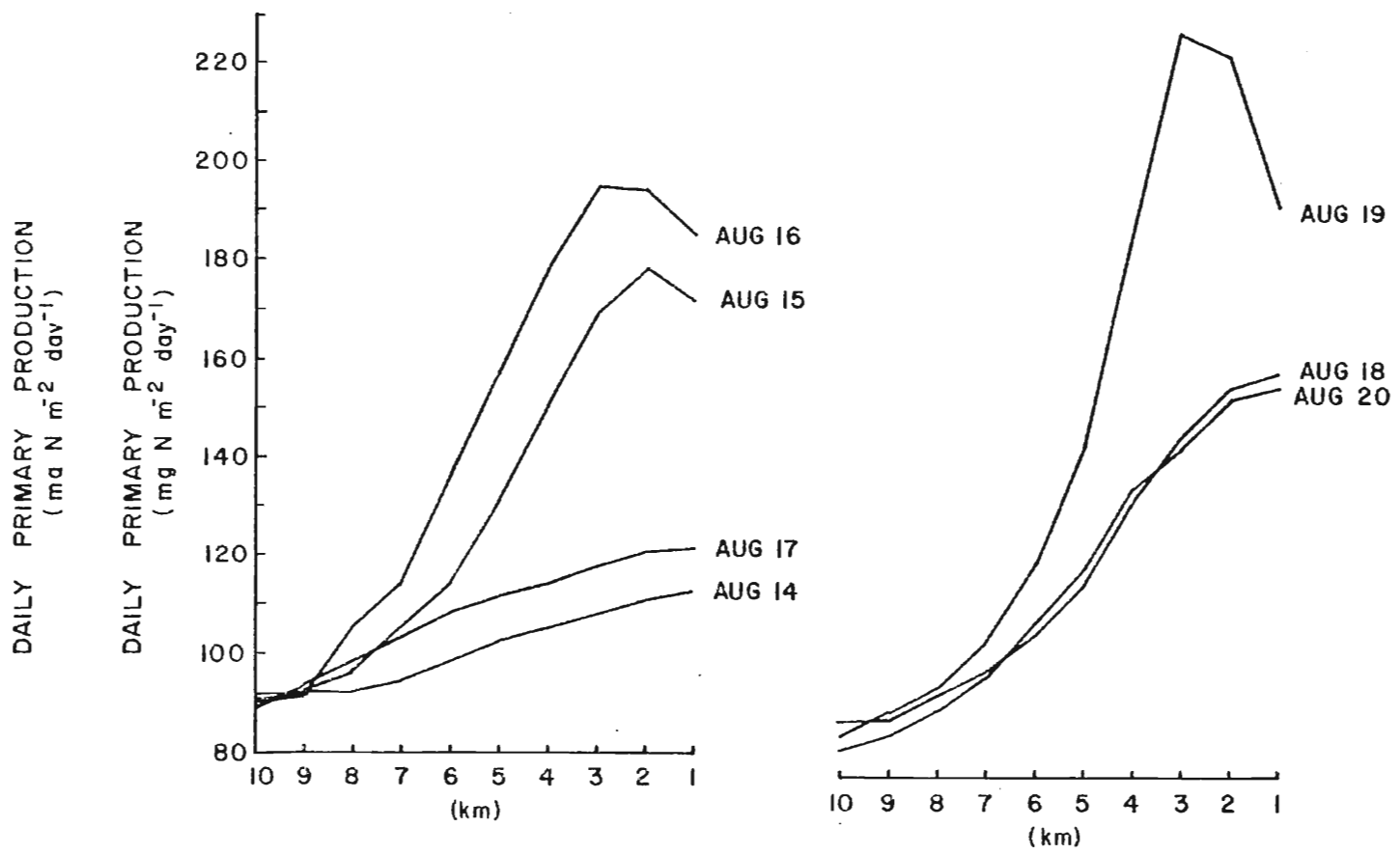

Fig. 32. Same as Fig. 30 but for August 14 through 17 in (a), and August 18 through 20 in (b).

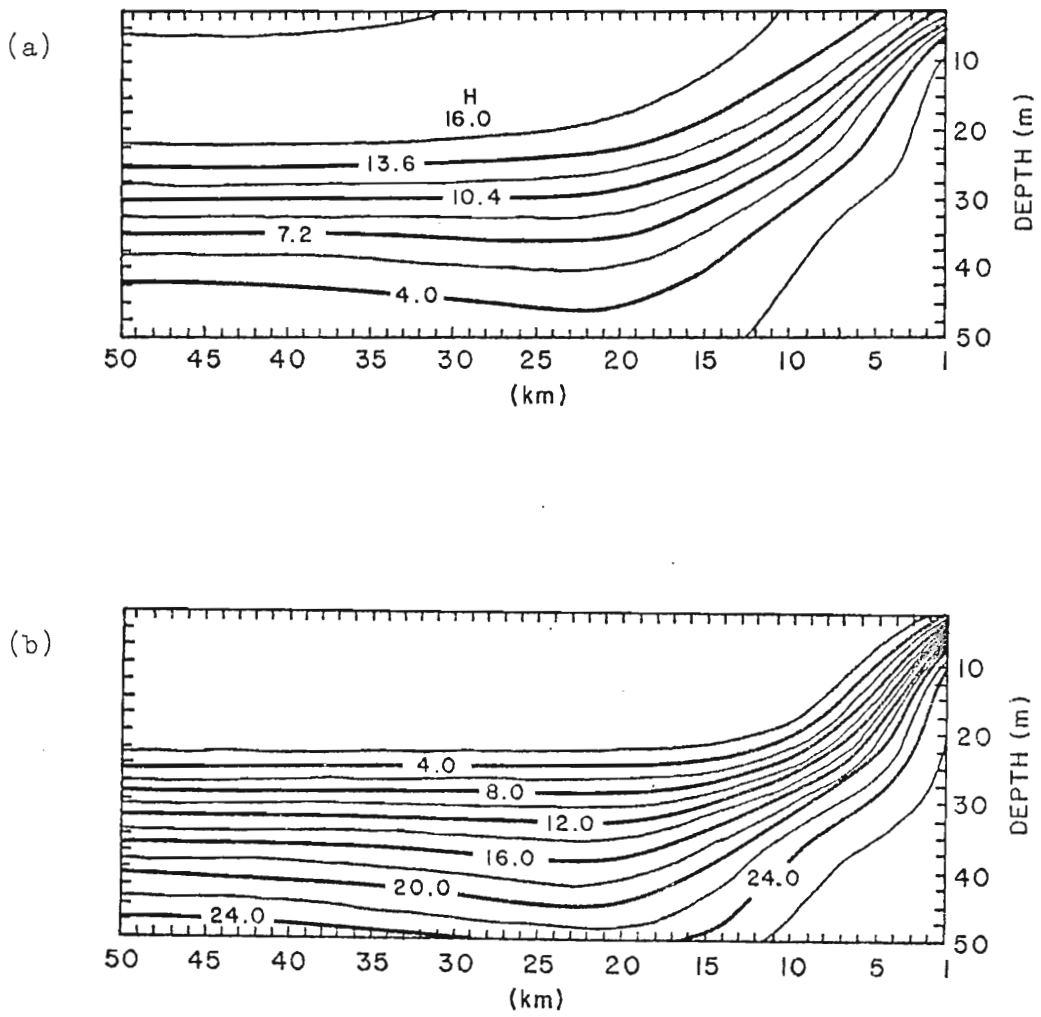

Fig. 33. (a) Spatial distribution of zooplankton on August 15 in the intermittent upwelling case. Contour intervals are 1.6 μgat N ℓ^{-1}. (b) The nitrate field on August 15 in the intermittent upwelling case. Contour intervals are 2 μgat NO_3 ℓ^{-1}.

welling case. Contour intervals are 2 μgat NO_3 ℓ^{-1}.

(a)

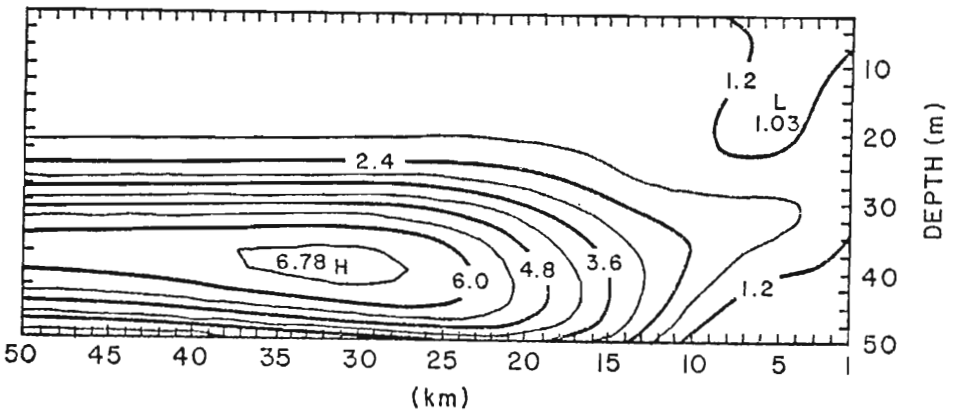

(b)

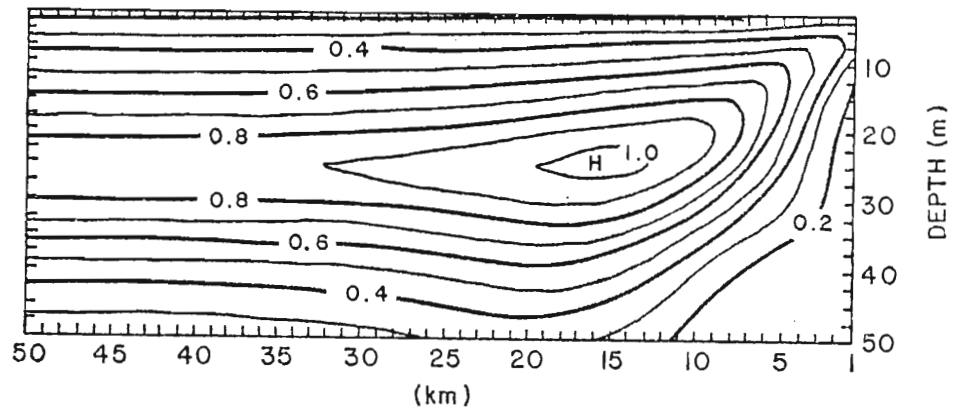

Fig. 34. The ammonia field on August 15 in the intermittent upwelling case. Contour intervals are 0.6 µgat $NH_4 \ell^{-1}$. (b) The spatial distribution of detritus on August 15 in the intermittent upwelling case. Contour intervals are 0.1 µgat N ℓ^{-1}.

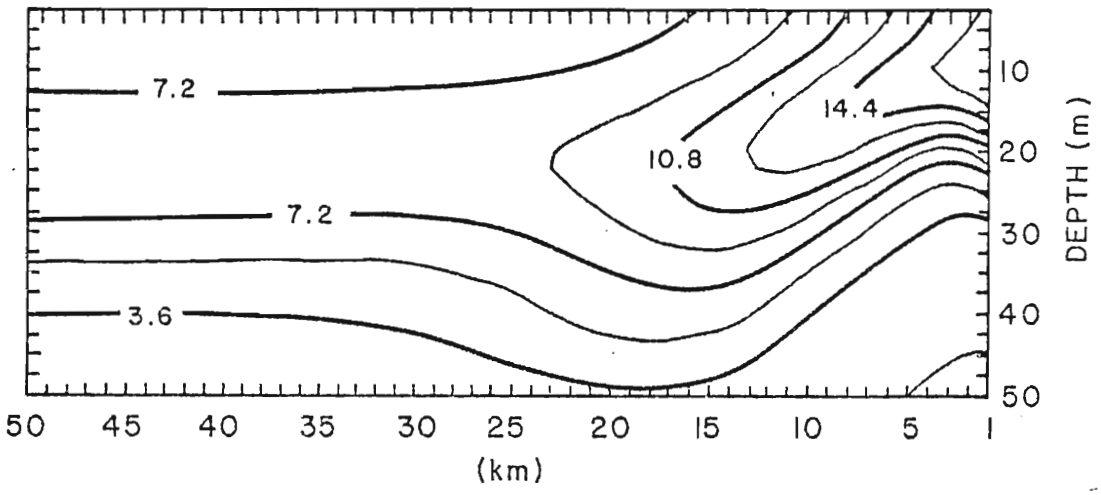

Fig. 35. The phytoplankton field predicted by the (x,z,t) productivity model for August 23 in the intermittent upwelling case. Contour intervals are 1.8 μgat N ℓ^{-1}.

4.5 Model sensitivity analysis

The (x,z,t) patchiness simulation model contains 34 independent or specified parameters (Table 1). The values of many of these parameters are chosen from observational and laboratory data and the remaining are deduced from biological and physical oceanographic theory. It is critical to understand the response of the model to variation in the parameter values, especially for those parameters whose value is controversial.

The ideal method of parameter value investigation is an analytical sensitivity analysis. However, the theory of sensitivity analysis is well developed only for steady state one-box models (Tomovic, 1963). There is an obvious need to develop analytical tools to investigate the time dependent nature of spatial models. For the present, one must resort to an empirical sensitivity analysis for complex spatial models, such as the one described here.

One begins an empirical sensitivity analysis with the best estimate for all parameter values, and then conducts a qualitative investigation of the model's response to variation of an individual parameter. For the sake of brevity the results of an extensive empirical sensitivity analysis will be only summarized in the following.

The spatial distributions of the dependent variables P, Z, NO_3, NH_4 and D are quite sensitive to the value of

The spatial distributions of the dependent variables P, Z, NO_3, NH_4 and D are quite sensitive to the value of

the vertical diffusion coefficient, K_v. Increased diffusion in the vertical smooths the gradient structure. With an

increased value of K_v, the phytoplankton plume deepens and its vertical profile is more smooth. Nutrients are supplied to the euphotic zone by vertical diffusion at a faster rate and daily gross primary production increases. The spatial model is less responsive to an increase in the horizontal diffusion coefficient, K_h, although smoothing in the horizontal structure of all variables does occur.

The sinking rate of dead organic matter has been reviewed by Smayda (1969) and more recently measured in the laboratory by Smayda (1970) and by Fowler and Small (1972). Depending on the shape and density of the particle, sinking rates range between one and several hundred meters per day for dead phytoplankton and fecal pellets. Envisioning detritus in this model as lysed phytoplankton cells and floccular,newly egested copepod fecal pellets, the author has used a detritus sinking rate, w_s, of 0.01 cm sec^{-1} or 8.6 m day^{-1} in all spatial solutions shown in Section 4. An increase in w_s results in a deepening of the maximum in the steady state detritus profile and a more rapid loss of limiting nutrient from the euphotic zone in the form of decomposing detritus.

The response of primary production to variation in the temperature field was explored by assuming no offshore variation in temperature. With 20°C surface temperatures at the coast, daily gross primary production increased by 65%

tion in temperature. With 20°C surface temperatures at the coast, daily gross primary production increased by 65%

(compare Figs. 20b and 36a). The standing crop of phytoplankton at day 10 in the strong upwelling case increased

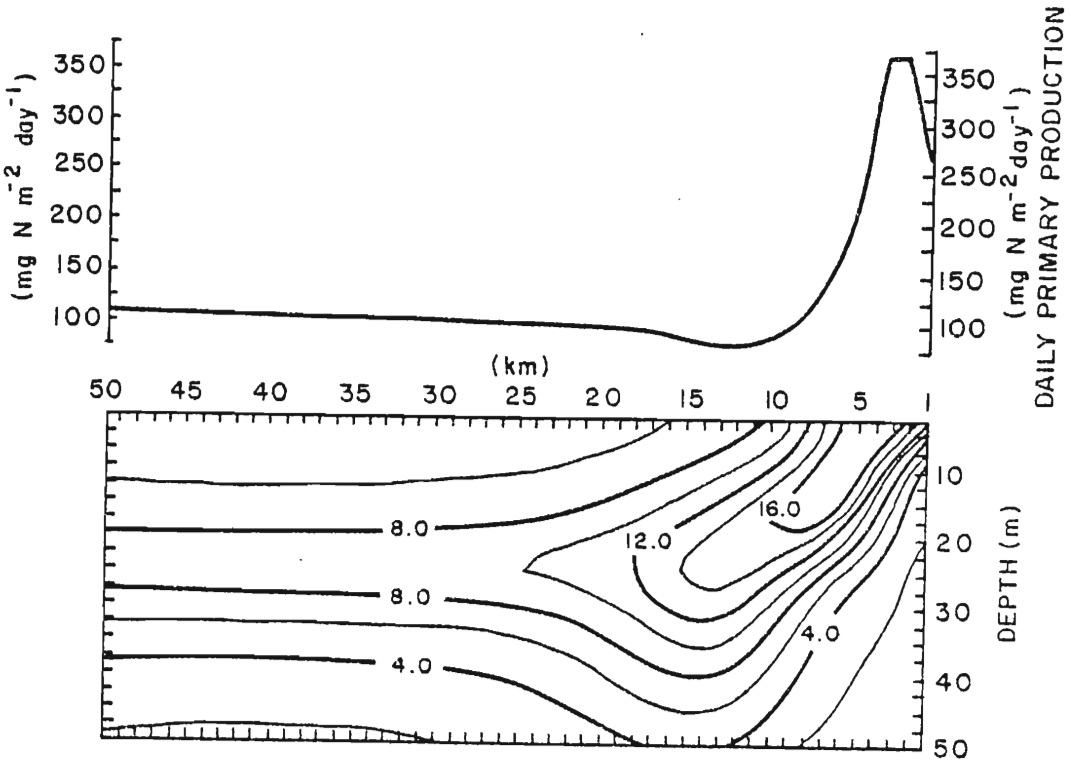

Fig. 36. (a) and (b) as Fig. 20b and c except it has been assumed the temperature field is homogeneous in x. Contour intervals in (b) are 2 μgat N ℓ^{-1}.

Fig. 36. (a) and (b) as Fig. 20b and c except it has been assumed the temperature field is homogeneous in x. Contour intervals in (b) are 2 μgat N ℓ^{-1}.

by 2 μgat N ℓ^{-1} over the standing stock observed in Fig. 20c. The phytoplankton plume maximum occurred closer to the coast and to the surface (Fig. 36b). Thus a proper specification of the temperature field is necessary to prevent overestimation of the primary production. Thompson's (1974) model predicts the offshore variation in temperature of two distinct, density layers off Oregon. Given the sensitivity of primary productivity to the temperature field, future modeling efforts will incorporate this time-dependent temperature prediction.

Phytoplankton growth is quite sensitive to the availability of light. Greater incident radiation at the surface results not only in an enhancement of the light inhibition effect, but paradoxically in an increase in daily primary production. The depth of the euphotic zone does not increase when the dense phytoplankton bloom becomes self-shading. Only a reduction in the self-shading coefficient, κ_p, or the light extinction coefficient for seawater, κ_w, would allow an increased euphotic zone depth.

The sensitivity of the model to the biological rate processes, such as the grazing coefficient, R_m, is best determined by an analytical sensitivity analysis of the one-box, nonspatial nondimensional model. Empirical analysis of (13) - (17) show the parameters describing the zooplankton dynamics: i.e., grazing, egestion and excretion

ysis of (13) - (17) show the parameters describing the zooplankton dynamics; i.e., grazing, egestion and excretion

are most important relative to the phytoplankton growth rate, V_m, in determining the steady state concentration of the

dependent variables P, Z, NO_3, NH_4 and D. O'Brien and Wroblewski (1976) showed conclusively phytoplankton growth and nutrient recycling by zooplankton are the most important and crucial processes in their (x,z,t) spatial ecosystem model for the west Florida continental shelf.

Almost the same steady state solution of nonspatial (13) - (17) is attained using a zooplankton egestion formulation as recommended by Conover (1966) where egestion is a constant fraction of ingestion. In the (z,t) or (x,z,t) model where small concentrations of phytoplankton occur, the choice of formulation does lead to important differences in egestion rate.

The detritus regeneration rate parameter, Φ, and the ammonia oxidation rate parameter, Ω, have long e-folding time scales, yet their values are important in the time-dependent, spatial solutions. Increasing the rate of decomposition of detritus into ammonia, for example, liberates more nutrient for plant growth in the euphotic zone and results in a higher plant standing crop. Increasing the rate of oxidation of ammonia can prevent the development of an ammonia maximum in the spatial solutions. The importance of the small valued, senescent cell lysis coefficient, Ξ, becomes evident in the (z,t) and (x,z,t) solutions, where this term leads to the low concentrations of plants in the aphotic zone.

this term leads to the low concentrations of plants in the aphotic zone.

A positive grazing threshold, P_t, is not necessary to prevent phytoplankton from being locally grazed to

extinction. Diffusion of plants from areas of high concentration to low concentration keeps a finite amount of phytoplankton standing crop present at each grid point. This is an important result. In essence, P_t is a parameterization of turbulent diffusion in nonspatial models (Wroblewski and O'Brien, 1976).

4.6 Comparison with observations

To establish credibility of the model, the spatial solutions in Sections 4.1 to 4.4 are compared with actual observations. It should be remembered that this model is an idealized description of the complex upwelling ecosystem whose irregular physical boundaries are three-dimensional. Nevertheless, if the model is to be a pedagogic tool, its major features must be verifiable by observations.

Many of the features found in the model solutions have been observed off the Oregon coast during the Coastal Upwelling Experiment or have been described in the literature. Fig. 37 shows the development of a phytoplankton plume off Newport, Oregon, in August 1972. The similarity in orientation, position and length scale between the simulated and observed plume structure is striking.

Turbidity measurements made by Pak et al. (1970) in June 1967, indicate a suspended particle maximum existed within the same depth range and offshore location as the phytoplankton and detritus maxima shown in Figs. 30b and 34b. To explain this particle distribution, they proposed

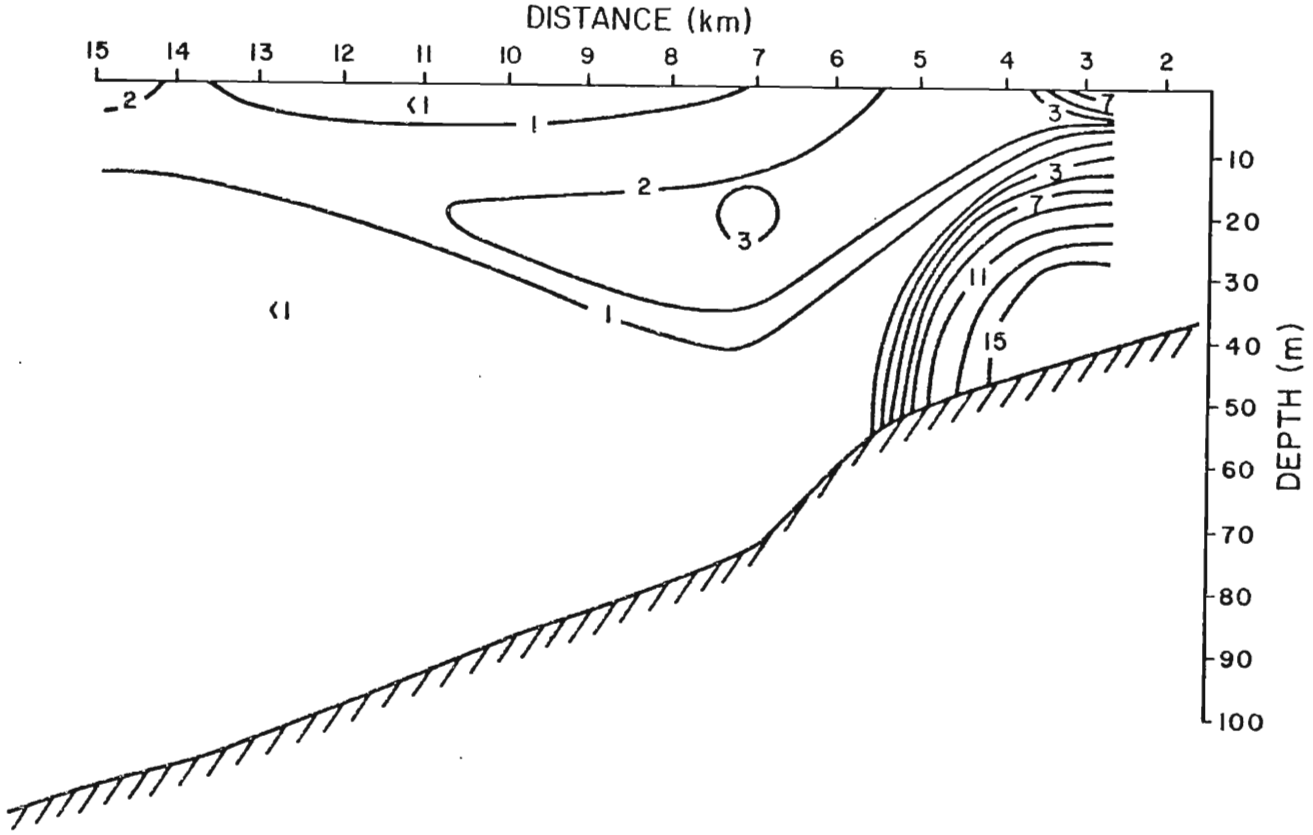

Fig. 37. (a) The phytoplankton spatial distribution in a transverse plane normal to the coast observed off Oregon on August 7, 1972. Phytoplankton biomass is expressed in terms of mg chlorophyll a m^{-3}.

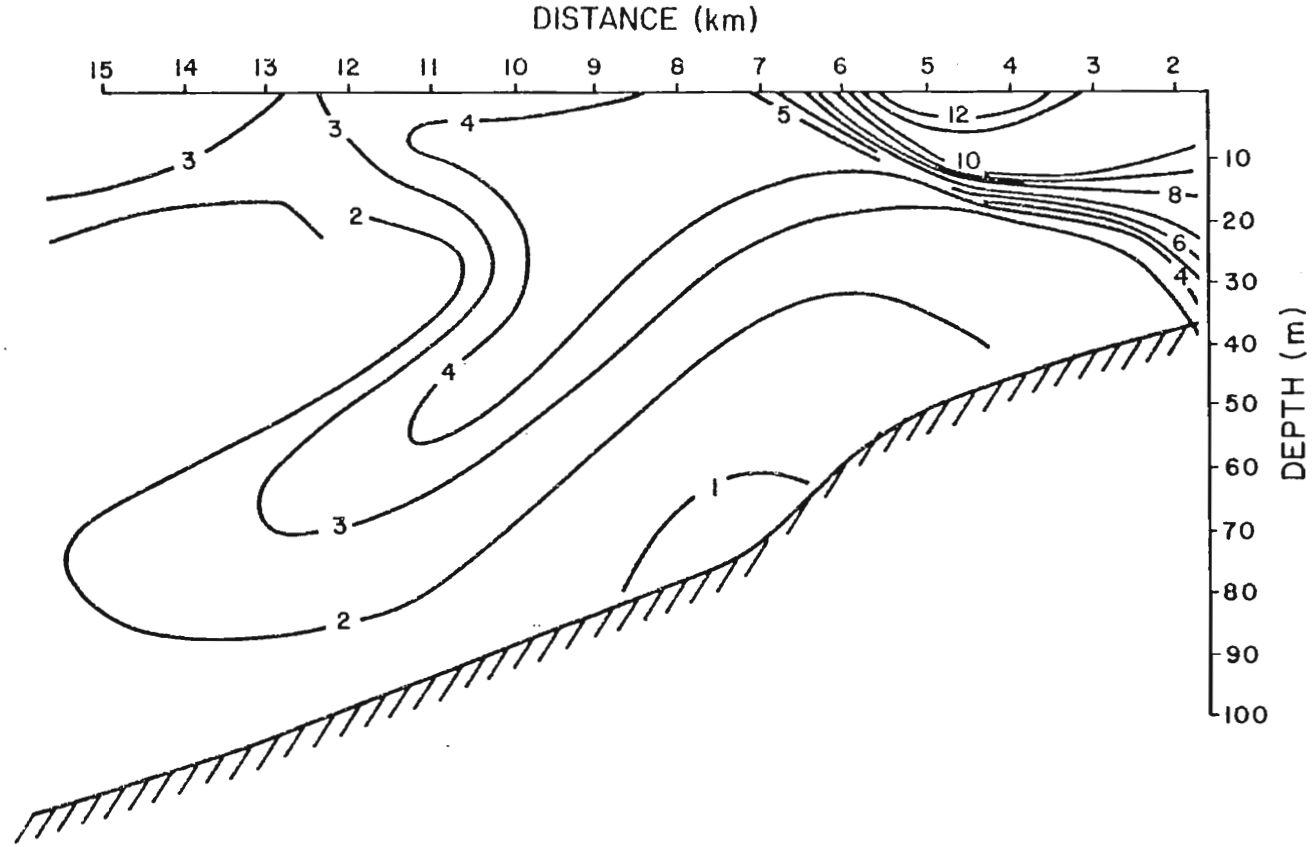

Fig. 37. (b) Same as (a) except observed on August 9, 1972 (from Small, in preparation).

a sequence of events in which nutrient rich water upwells close to shore, becomes increasingly concentrated with particles of biological origin as it moves offshore, and gradually sinks below the permanent pycnocline which slopes up to near the surface. This mechanism was adopted by Small and Ramberg (1971) and Anderson (1972) to explain the plume feature often observed in the phytoplankton distribution during upwelling. Kitchen et al., (1975) have shown the particle maximum in July 1973, was composed mostly of particles 20 to 50 μm in diameter nearshore and of increasingly smaller sized particles with progression offshore. They concluded the suspended particles in the upwelling region close to the coast were diatoms, which were progressively replaced by dinoflagellates in the offshore nutrient limited waters.

Peterson (1972) observed the zooplankton standing stock was greater in the oceanic region than on the continental shelf off Oregon in the summer. Only during winter was there a high zooplankton standing stock close inshore, where the primary production is greatest. Peterson suggested predation upon zooplankton nauplii and offshore water transport as reasons for low coastal herbivore biomass. The model solutions indicate offshore transport leads to a reduction of zooplankton standing stock over the shelf (Figs. 25a and 33a). Advective transport could
leads to a reduction of zooplankton standing stock over the shelf (Figs. 25a and 33a). Advective transport could
explain the observed high coastal zooplankton standing stock in winter when the Ekman surface flow is predominantly

onshore (Bakun, 1973).

Peterson and Miller (1975) found high zooplankton biomasses occurred within 10 km of the coast during the 1969-71 upwelling seasons, as did Myers (1975) in August 1973. Standing stocks were highest within 2 km of the beach, indicating the source of these animals was the coastal populations. If the (x,z,t) model had included in its coastal boundary conditions the inshore source of zooplankton, or if zooplankton were allowed to vertically migrate to depths where onshore flow occurs, the observations of Peterson, Miller, and Myers might have been more closely reproduced.

Measurements of the spatial distribution of nitrate by Ball (1970), Atlas (1973), and Myers (1975) indicate upwelling of water high in nitrate concentration occurs at the coast. Comparison of these observed nutrient fields with Figs. 21b and 33b shows good qualitative agreement. Few measurements of the ammonia field were made before the Coastal Upwelling Experiment. The ammonia data from 1972 and 1973 does indicate a maximum between 10 and 20 m depth seaward of 10 km. Not enough profiles were made, however, to validate the offshore ammonia maximum predicted in the model solutions (Figs. 22a and 34a). The NH_4 maximum is a temporary feature which decays when nutrient input by upwelling ceases and thus may easily be missed in field sampling. The spatial structure of ammonia should be more

upwelling ceases and thus may easily be missed in field sampling. The spatial structure of ammonia should be more thoroughly investigated in future observational programs.

Field measurements of net primary productivity by the C^{14} technique performed by Anderson (1964) and by Small et al, (1972) off Oregon during upwelling ranged from 0.5 to 1.5 g m^{-2} day^{-1}. If a C/N ratio of 7 is assumed (Small and Ramberg, 1971) the observed range in terms of nitrogen is 71 to 214 mg N m^{-2} day^{-1}. Gross primary productivities calculated for the model solutions range between 78 and 296 mg N m^{-2} day^{-1} during the strong upwelling case, and from 78 to 226 mg N m^{-2} day^{-1} during the intermittent upwelling case. This is excellent agreement between observation and model. The predicted increase in daily gross primary production of the water column after a strengthening of northerly winds for several days during the intermittent upwelling case (Fig. 28) is suggested in the CUE II productivity data (Small, in preparation). The bloom of phytoplankton upon relaxation of winds after a major wind event (Section 4.2) is a model feature clearly observed during the CUE field study.

5. SUMMARY, CONCLUSIONS AND CRITIQUE

Equations describing the mesoscale distribution and ecosystem dynamics of phytoplankton, herbivores, detritus and the nutrients, nitrate and ammonia, have been formulated for a time-dependent, two-dimensional, numerical model of phytoplankton patchiness during Oregon coastal upwelling. New formulations for herbivore egestion and ammonia-inhibition of nitrate uptake by phytoplankton are presented.

The goal of this research has been to provide a dynamical explanation for the spatial features which are consistently observed in the phytoplankton, nitrate and detritus fields during upwelling conditions off Oregon. While it is not implied that conclusive verification of the model lies in the cited observations, the similarity between model solutions and field data suggests the complex (x,z,t) model may include the basic biological, chemical and physical dynamics governing primary productivity in the Oregon upwelling ecosystem.

Production is a function of the availavility of light and nutrients, and its rate is governed by temperature. Because the physical and chemical environment in a coastal and nutrients, and its rate is governed by temperature. Because the physical and chemical environment in a coastal upwelling region is highly variable, production must be

modeled within a temporal, spatial framework. Smayda (1966) had only limited success in predicting daily primary production from an empirical equation relating phytoplankton biomass directly to the wind stress and surface temperature. Small et al., (1972) concluded there was no simple empirical relationship between daily primary production off Oregon and such environmental factors as incident radiation, photic depth or rate of upwelling. Iverson et al., (1974) were able to model phytoplankton standing crops observed in Auke Bay, Alaska, after allowing for the time-dependent supply of nitrate to the euphotic zone by wind-mixing. Walsh (1975) simulated phytoplankton and nitrate concentrations observed in the Peruvian upwelling region with a spatial, although time-invariant, ecosystem model.

A detailed mechanistic model is required to give adequate predictions of primary production. Nonspatial ecosystem models such as that of Cushing (1971) are useful for investigating the relationship between productivity and light, grazing and rate of upwelling, but they neglect the important influence of a variable environment upon primary productivity.

The dominant role of advection in determining the spatial configuration of plankton and nutrient fields in upwelling regions is obvious from the model solutions. To properly delineate the mesoscale phytoplankton plume off Oregon, a 2.5 m vertical and 1 km horizontal resolution of

the velocity field was required. Finer grids are necessary to model smaller scale phytoplankton patchiness.

The physical mechanisms which lead to the phytoplankton plume structure observed over the continental shelf off Oregon appear to be those suggested by Pak et al., (1970) and described dynamically by Mooers et al., (1976). The numerical upwelling model of Thompson (1974) simulates this circulation i.e., upwelling at the coast, offshore transport and downwelling in the region 10 to 25 km offshore. This physical model when coupled to the biological and chemical dynamics described in Section 2, reproduces the phytoplankton plume often observed off Oregon during the upwelling season. However, the two-cell circulation is but one of several upwelling patterns believed created by strong northerly winds off Oregon.

In spite of the successful reproduction of the biological and chemical features observed off Oregon during upwelling, this model is fundamentally limited in its ability to predict the distribution of its dependent variables in time and space. Numerical model solutions of a nonlinear, dissipative open thermodynamic system (such as the Oregon upwelling system) will diverge from the "real" solution if the initial state of the system is not specified exactly (Lorenz, 1969). In other words, one must know the actual initial conditions for all dependent variables for all time and space. The inevit-
other words, one must know the actual initial conditions for all dependent variables for all time and space. The inevitable discrepancy between the model prediction and observations stems from the fact that continuous physical processes

in the ocean are represented by finite approximations. Platt et al., (1975) estimate the limit to predictability of features with length scales of the order 10 km in the ocean is at best several days. After this period, the spatial solution and the observed fields may differ appreciably.

An important criticism of this model is the assumption that all parameter values have no spatial or temporal variability. For example, the light extinction coefficient for the seawater off Oregon was assumed constant with distance offshore. The extinction coefficient is known to decrease with distance from shore as turbidity caused by particles suspended in river runoff decreases (Small and Curl, 1968). If a spatially variable κ_w had been assumed, the subsurface phytoplankton maximum observed by Anderson (1969) in oceanic waters off Oregon may have been reproduced close to the seaward boundary of the model. Instead, this feature is missed altogether. Nevertheless, the model's spatial solutions in the region of interest are reasonable.

Longshore variation in all model variables has been ignored, although Peffley and O'Brien (1976) have demonstrated conservation of mass in the (x,z) plane is not achieved during Oregon upwelling. However, high altitude photographs (Keen and Pearcy, 1973) and airborne remote sensing of sea surface temperature (Holladay and O'Brien,
photographs (Keen and Pearcy, 1973) and airborne remote sensing of sea surface temperature (Holladay and O'Brien,
1975) show sea surface colors and temperature isotherms tend to be parallel to the coast for several tens of

kilometers. This suggests there is less longshore variability in the intensity of upwelling off the Oregon coast than observed in other upwelling regions - notably Peru, where phytoplankton are distributed in shallow tongues (Kelley et al., 1975). The model also ignores the possible influence of the Columbia River effluent tongue upon the physical and chemical environment off Oregon.

This model represents the most complex, time-dependent, spatial, numerical model of an upwelling ecosystem developed. A major strength of the model is the formulation of numerous physical, chemical and biological processes into an integrated framework. A major weakness is the treatment of individual phytoplankton and zooplankton species as members of a food web with invariable tropho-dynamic relationships. Few organisms play such a simple structured role in nature.

APPENDIX

Definition of Symbols and Scaling Relationships

Dimensional Quantity	Definition	Scaling Factor	Nondimensional Quantity
-	Temperature function parameters	-	a,b
c	Temperature function parameter	-	-
D	Detrital nitrogen	D/N_t	D'
d	Daylength fraction of a day	-	-
E_m	Maximum herbivore egestion coefficient	E_m/V_m	ρ
H	Characteristic vertical length scale	-	-
I_s	Light saturation parameter when $\theta = 0$ or $\eta = 0$	-	-
I_m	Light intensity at local apparent noon	-	-
K_h	Horizontal eddy diffusivity	-	-
K_v	Vertical eddy diffusivity	-	-
k_g	Half-saturation constant for growth	-	-
k_u	Half-saturation constant for nutrient [illegible] growth	-	-
k_u	Half-saturation constant for nutrient uptake	k_u/N_t	α

Dimensional Quantity	Definition	Scaling Factor	Nondimensional Quantity
L	Characteristic horizontal length scale	-	-
NH_4	Ammonia	NH_4/N_t	NH_4'
NO_3	Nitrate plus nitrite	NO_3/N_t	NO_3'
N_t	Total concentration of biologically limiting nutrient	-	-
P	Phytoplankton nitrogen	P/N_t	P'
P_t	Herbivore grazing threshold	P_t/N_t	P*
R_m	Herbivore maximum grazing rate	R_m/V_m	β
T	Temperature	-	-
t	Time	tV_m	τ
u	x-directed velocity component	u/U	u'
U	Typical value of the horizontal velocity	-	-
V_m	Phytoplankton maximum nutrient uptake rate	-	-
W	Typical value of the vertical velocity	-	-
w	z-directed velocity component	w/W	w'
w_s	Sinking velocity of detritus	w_s/W	w_s'
x	Tangent-plane Cartesian coordinates: x positive toward the coast	x/L	x'
Z	Zooplankton nitrogen	Z/N_t	Z'
	toward the coast	x/L	x'
Z	Zooplankton nitrogen	Z/N_t	Z'
z	Tangent-plane Cartesian coordinates: z positive upward	z/H	z'

Dimensional Quantity	Definition	Scaling Factor	Nondimensional Quantity
Γ	Herbivore excretion coefficient	Γ/V_m	γ
Δ	Herbivore egestion rate at phytoplankton concentration P_t	Δ/V_m	δ
-	Light function parameters	-	η, θ
κ_p	Light extinction per unit phytoplankton nitrogen	-	-
κ_w	Light extinction coefficient of pure seawater and any nonphytoplanktonic material	-	-
Λ	Ivlev constant	ΛN_t	λ
μ_m	Phytoplankton maximum growth rate	-	-
Ξ	Phytoplankton nutrient loss coefficient	Ξ/V_m	ξ
-	Pi	-	π
Υ	Herbivore egestion coefficient	Υ	υ
Φ	Detritus decomposition parameter	Φ/V_m	ϕ
Ψ	Nitrate uptake inhibition parameter	ΨN_t	ψ
Ω	Ammonia oxidation coefficient	Ω/V_m	ω

REFERENCES

Anderson, G. C., 1964. The seasonal and geographic distribution of primary productivity off the Washington and Oregon coasts. Limnol. Oceanogr., 9: 284-302.

Anderson, G. C., 1969. Subsurface chlorophyll maximum in the northeast Pacific ocean. Limnol. Oceanogr. 14: 386-391

Anderson, G. C., 1972. Aspects of marine phytoplankton studies near the Columbia River, with special reference to a subsurface chlorophyll maximum, in The Columbia River Estuary and Adjacent Ocean Waters, A. T. Pruter and D. L. Alverson, eds., Univ. of Washington Press, Seattle. pp. 219-240.

Anita, N. J., C. D. McAllister, T. R. Parsons, K. Stephens and D. H. Strickland, 1963. Further measurements of primary production using a large-volume plastic sphere. Limnol. Oceanogr., 8: 166-183.

Atlas, E. L., 1973. Changes in chemical distributions and relationships during an upwelling event off the Oregon coast. M.S. thesis. Oregon State Univ., Corvallis, 100 p.

Bainbridge, R., 1957. The size, shape and density of marine phytoplankton concentrations. Biol. Rev., 32: 91-115.

Bakun, A., 1973. Coastal upwelling indices, West Coast of North America, 1946-1971. U.S. Dept. Commer. NOAA Tech. Rep. NMFS SSRF - 671, 103 p.

Ball, D. S., 1970. Seasonal distribution of nutrients off the coast of Oregon, 1968. M.S. thesis. Oregon State Univ., Corvallis, 71 p.

Barber, R. T. and J. H. Ryther, 1969. Organic chelators: factors affecting primary production in the Cromwell current upwelling. J. exp. mar. Ecol., 3: 191-199.

Beers, J. R., W. R. Stevenson, R. W. Eppley and E. R. Brooks, [illegible] primary production in the Cromwell current upwelling. J. exp. mar. Ecol., 3: 191-199.

Beers, J. R., W. R. Stevenson, R. W. Eppley and E. R. Brooks, 1971. Plankton populations and upwelling off the coast of Peru, June 1969. Fish. Bull., 69: 859-876.

Caperon, J. and J. Meyer, 1972a. Nitrogen-limited growth of marine phytoplankton - I. Changes in population characteristics with steady-state growth rate. Deep-Sea Res., 19: 601-618.

Caperon, J. and J. Meyer, 1972b. Nitrogen-limited growth of marine phytoplankton - II. Uptake kinetics and their role in nutrient limited growth of phytoplankton. Deep-Sea Res., 19: 619-632.

Cassie, R. M., 1963. Microdistribution of plankton. Oceanogr. Mar. Biol. Ann. Rev., 1: 223-252.

Conover, R., 1966. Factors affecting the assimilation of organic matter by zooplankton and the question of superfluous feeding. Limnol. Oceanogr., 11: 346-354.

Corner, E. D. S. and A. G. Davies, 1971. Plankton as a factor in the nitrogen and phosphorus cycles in the sea. Adv. mar. Biol., 9: 101-204.

Corner, E. D. S., C. B. Cowey and S. M. Marshall, 1965. On the nutrition and metabolism of zooplankton. III. Nitrogen excretion by Calanus. J. Mar. Biol. Ass. U.K., 45: 429-442.

Criminale, W. O. and D. F. Winter, 1974. The stability of steady-state depth distributions of marine phytoplankton. Amer. Nat., 108: 679-687.

Curl, H., Jr. and G. C. McLeod, 1961. The physiological ecology of a marine diatom, Skeletonema costatum (Grev.) Cleve. J. Mar. Res., 19: 70-88.

Cushing D. H., 1971. Upwelling and the production of fish. Adv. mar. Biol., 9: 255-334.

Denman, K. L. and T. Platt, 1976. The variance spectrum of phytoplankton in a turbulent ocean. To be published.

Denman, K. L. and T. Platt, 1975. Coherence in the horizontal distributions of phytoplankton and temperature in the upper ocean. Mem. Soc. r. Sci. Liege, 7: 19-30.

Dubois, D. M., 1975. A model of patchiness of prey-predator plankton populations. Ecol. Model., 1: 67-80.

Dugdale, R. C., 1967. Nutrient limitations in the sea: dynamics, identification, and significance. Limnol. plankton populations. Ecol. Model., 1: 67-80.

Dugdale, R. C., 1967. Nutrient limitations in the sea: dynamics, identification, and significance. Limnol. Oceanogr., 12: 685-695.

Dugdale, R. C., 1975. Biological modeling I. in Modeling of Marine Systems, J. C. J. Nihoul, ed., Elsevier, New York, pp. 187-205.

Dugdale, R. C. and J. J. Goering, 1967. Uptake of new and regenerated forms of nitrogen in primary productivity. Limnol. Oceanogr., 12: 196-206.

Dugdale, R. C. and J. J. MacIssac, 1971. A computation model for the uptake of nitrate in the Peru upwelling region. Inv. Pesq., 35: 299-308.

Eppley, R. W., 1972. Temperature and phytoplankton growth in the sea. Fish. Bull., 70: 1063-1085.

Eppley, R. W. and J. J. Coatsworth, 1968. Uptake of nitrate and nitrite by Ditylum brightwelli - kinetics and mechanisms. J. Phycol., 4: 151-165.

Eppley, R. W. and W. H. Thomas, 1969. Comparison of half-saturation "constants" for growth and nitrate uptake of marine phytoplankton. J. Phycol., 5: 375-379.

Eppley, R. W., J. N. Rogers and J. J. McCarthy, 1969. Half-saturation constants for uptake of nitrate and ammonia by marine phytoplankton. Limnol. Oceanogr.,14: 912-920.

Fee, E. J., 1969. A numerical model for the estimation of photosynthetic production, integrated over time and depth, in natural waters. Limnol. Oceanogr., 14: 906-911.

Fowler, S. W. and L. F. Small, 1972. Sinking rates of euphsiid fecal pellets. Limnol.Oceanogr., 17: 293-296.

Frost, B. W., 1974. Feeding processes at lower trophic levels in pelagic communities. in The Biology of the Oceanic Pacific, C. B. Miller, ed., Oregon State Univ. Press, Corvallis, pp. 59-77.

Goering, J. J., R. C. Dugdale and D. W. Menzel, 1964. Cyclic diurnal variations in the uptake of ammonia and nitrate by photosynthetic organisms in the Sargasso Sea. Limnol. Oceanogr. 9: 448-452.

Holladay, C. G. and J. J. O'Brien, 1975. Mesoscale variability of sea surface temperatures. J. Phys. Oceanogr., 5: 761-772.

Hurlburt, H. E., 1974. The influence of coastline geometry and bottom topography on the Eastern Ocean circulation. Ph.D. thesis, Florida State Univ., Tallahassee, 103 p.

Huyer, A. and J. G. Pattullo, 1972. A comparison between wind and current observations over the continental shelf [illegible]

Huyer, A. and J. G. Pattullo, 1972. A comparison between wind and current observations over the continental shelf off Oregon, summer 1969. J. Geophys. Res., 77: 3215-3220.

Iverson, R. L., H. C. Curl, Jr. and J. L. Saugen, 1974. Simulation model for wind-driven summer phytoplankton dynamics in Auke Bay, Alaska. Mar. Biol., 28: 169-177.

Ivlev, V. S., 1945. The biological productivity of waters. Usp. soverm. Biol., 19: 98-120.

Jitts, H. R., C. D. McAllister, K. Stephens and J. D. H. Strickland, 1964. The cell division rates of some marine phytoplankters as a function of light and temperature. J. Fish. Res. Bd. Canada, 21: 139-157.

Johnston, R., 1964. Sea water, the natural medium of phytoplankton-II. Trace metals and chelation, and general discussion. J. Mar. biol. Ass.U.K., 44: 87-109.

Kamykowski, D., 1974. Possible interactions between phytoplankton and semidiurnal internal tides. J. Mar. Res., 32: 67-89.

Keene, D. F. and W. G. Pearcy, 1973. High-altitude photographs of the Oregon coast. Photogram. Engr., pp. 163-168.

Kelley, J. C., T. E. Whitledge and R. C. Dugdale, 1975. Results of sea surface mapping in the Peru upwelling system. Limnol. Oceanogr., 20: 784-794.

Kierstead, H. and L. B. Slobodkin, 1953. The size of water masses containing plankton blooms. J. Mar. Res., 12: 141-147.

Kitchen, J. C., D. Menzies, H. Pak and J. R. V. Zaneveld, 1975. Particle size distributions in a region of coastal upwelling analyzed by characteristic vectors. Limnol. Oceanogr., 20: 775-783.

Lassiter, R. R. and D. K. Kearns, 1973. Phytoplankton population changes and nutrient fluctuations in a simple aquatic ecosystem model, in Modeling the Eutrophication Process, E. J. Middlebrooks, D. H. Fulkenborg, and T. E. Maloney, eds., Utah Water Res. Lab., Utah State Univ., Logan, pp. 131-138.

Lehman, J. T., D. B. Botkin and G. F. Likens, 1975. The assumptions and rationales of a computer model of phytoplankton population dynamics. Limnol. Oceanogr., 20: 343-364.

Lorenz, E. N., 1969. The predictability of a flow which possesses many scales of motion. Tellus, 21: 289-307.

Lorenzen, C. J., 1972. Extinction of light in the ocean by phytoplankton. J. Cons. int. Explor. Mer., 34: 262-267.

MacIsaac, J. J., and R. C. Dugdale, 1969. The kinetics of nitrate and ammonia uptake by natural populations of marine phytoplankton. Deep-Sea Res., 16: 45-57.

MacIsaac, J. J., R. C. Dugdale and G. Slawyk, 1974. Nitrogen uptake in the Northwest Africa upwelling area: results from the CINECA - Charcot II cruise. Tethys, 6: 69-76.

Mooers, C. N. K., C. A. Collins and R. L. Smith, 1976. The dynamic structure of the frontal zone in the coastal upwelling region off Oregon. J. Phys. Oceanogr., 6: 3-21.

Myers, A. H., 1975. Vertical distribution of zooplankton in the Oregon coastal zone during an upwelling event. M.S. thesis. Oregon State Univ., Corvallis, 62 p.

Nihoul, J. C. J., 1975. Marine systems analysis. in Modeling of Marine Systems, J. C. J. Nihoul, ed., Elsevier, New York, pp. 3-39.

O'Brien, J. J. and J. S. Wroblewski, 1973. On advection in phytoplankton models. J. theor. Biol., 38: 197-202.

O'Brien, J. J. and J. S. Wroblewski, 1976. A simulation of the mesoscale distribution of the lower marine trophic levels off West Florida. in Systems Analysis and Simulation in Ecology, Vol. 4, B. C. Patten, ed., Academic Press, New York, pp. 63-110.

Okubo, A., 1971. Oceanic diffusion diagrams. Deep-Sea Res., 18: 789-802.

Packard, T. T. and D. Blasco, 1974. Nitrate reductase activity in upwelling regions. II. Ammonia and light dependence. Tethys, 6: 269-280.

Pak, H., G. F. Beardsley, Jr. and R. L. Smith, 1970. An optical and hydrographic study of a temperature inversion off Oregon during upwelling. J. Geophys. Res., 75: 629-636.

Park, K., 1967. Nutrient regeneration and preformed nutrients off Oregon. Limnol. Oceanogr., 12: 353-357.

Parsons, T. and M. Takahashi, 1973. Biological Oceanographic Processes. Pergamon Press, New York, 186 p.

Parsons, T. R., R. J. LeBrasseur and J. D. Fulton, 1976. Some observations on theory, models, of biological oceanographic Processes. Pergamon Press, New York, 186 p.

Parsons, T. R., R. J. LeBrasseur and J. D. Fulton, 1976. Some observations on the dependence of zooplankton grazing on cell size and concentration of phytoplankton blooms. J. Oceanogr. Soc. Japan, 23: 10-17.

Patten, B. C., 1968. Mathematical models of plankton production. Int. Rev. ges. Hydrobiol., 53: 357-408.

Peffley, M. B. and J. J. O'Brien. 1976. A three-dimensional simulation of coastal upwelling off Oregon. J. Phys. Oceanogr., 6: 164-180.

Peterson, W. K., 1972. Distribution of pelagic copepods off the coast of Washington and Oregon during 1961 and 1962 in The Columbia River Estuary and Adjacent Waters, A. T. Pruter and D. L. Alverson, eds., Univ. of Washington Press, Seattle, pp. 313-343.

Peterson, W. T. and C. B. Miller, 1975. Year-to-year variations in the planktology of the Oregon upwelling zone. Fish. Bull., 73: 642-653.

Piacsek, S. A. and G. P. Williams, 1970. Conservation properties of convection difference schemes. J. Comp. Phys., 6: 392-405.

Platt, T., 1972. Local phytoplankton abundance and turbulence. Deep-Sea Res., 19: 183-187.

Platt, T., 1975. The physical environment and spatial structure of phytoplankton populations. Mem. Soc. r. Sci. Liege, 7: 9-17.

Platt, T. and K. L. Denman, 1975. A general equation for the mesoscale distribution of phytoplankton in the sea. Mem. Soc. r. Sci. Liege, 7: 31-42.

Platt, T. and C. Filion, 1973. Spatial variability of the productivity: biomass ratio for phytoplankton in a small marine basin. Limnol. Oceanogr., 18: 743-749.

Platt, T. and D. V. Subba Rao, 1970. Primary production measurements on a natural plankton bloom. J. Fish. Res. Bd. Canada, 27: 887-899.

Platt, T., K. L. Denman and A. D. Jassby, 1975. The mathematical representation and prediction of phytoplankton productivity. Fish. Mar. Serv. Res. Dev. Tech. Rep. 523, 110 p.

Powell, T. M., P. J. Richerson, T. M. Dillon, B. A. Agee, B. J. Dozier, D. A. Godden and L. O. Myrup, 1975. Spatial scales of current speed and phytoplankton biomass fluctuations in Lake Tahoe. Science,189: 1088-1090.

B. J. Dozier, D. A. Godden and L. O. Myrup, 1975. Spatial scales of current speed and phytoplankton biomass fluctuations in Lake Tahoe. Science,189: 1088-1090.

Redfield, A. C., B. H. Ketchum and F. A. Richards, 1963. The influence of organisms on the composition of sea-water,in The Sea, Vol. 2, M. N. Hill, ed., Wiley Interscience, New York, pp. 26-77.

Reed, R. K. and D. Halpern, 1974. Radiation measurements off the Oregon coast July/August 1973. Coastal Upwelling Ecosystems Analysis Data Report 13. Univ. of Washington, Seattle. 51 p.

Richerson, P., R. Armstrong and C. Goldman, 1970. Contemporaneous disequilibrium, a new hypothesis to explain the "Paradox of the Plankton." Proceedings Natl. Acad. Sci. 67: 1710-1714.

Shaffer, G., 1974. On the North West African coastal upwelling system. Ph.D. thesis, Institude für Meereskunde, Universitat Kiel, Federal Republic of Germany. 177 p.

Small, L. F. and H. C. Curl, Jr., 1968. The relative contribution of particulate chlorophyll and river tripton to the extinction of light off the coast of Oregon. Limnol. Oceanogr., 13: 84-91.

Small, L. F. and H. Curl, Jr., 1972. Effects of Columbia River discharge on chlorophyll a and light attenuation in the sea. in The Columbia River Estuary and Adjacent Ocean Waters, A. T. Pruter and D. L. Alverson, eds., Univ. of Washington Press, Seattle, pp. 203-218.

Small, L. F. and D. A. Ramberg, 1971. Chlorophyll a, carbon, and nitrogen in particles from a unique coastal environment, in Fertility of the Sea, Vol. 2, J. D. Costlow, Jr., ed., Gordon and Breach, New York, pp. 475-492.

Small, L. F. and H. Curl, Jr. and W. A. Glooschenko, 1972. Effects of solar radiation and upwelling on daily primary production off Oregon. J. Fish. Res. Bd. Canada, 29: 1269-1275.

Smayda, T. J., 1966. A quantitative analysis of the phytoplankton of the Gulf of Panama. III. General ecological conditions and the plankton dynamics at 8°45'N, 79°23'W from November 1954 to May 1957. Inter-Amer. Trop. Tuna Comm. Bull., 11: 355-612.

Smayda, T. J., 1969. Some measurements of the sinking rate of fecal pellets. Limnol. Oceanogr., 14: 621-625.

Smayda, T. J., 1970. The suspension and sinking of phytoplankton in the sea. Oceanogr. Mar. Biol. Ann. Rev., 8: 353-414.

Smiles, M. C. Jr. and W. G. Pearcy, 1971. Size structure plankton in the sea. Oceanogr. Mar. Biol. Ann. Rev., 8: 353-414.

Smiles, M. C. Jr., and W. G. Pearcy, 1971. Size structure and growth rate of Euphausia pacifica off the Oregon coast. Fish. Bull., 69: 79-86.

Steele, J. H., 1974. The Structure of Marine Ecosystems. Harvard Univ. Press, Cambridge, Mass. 128 p.

Thompson, J. D., 1974. The coastal upwelling cycle on a beta-plane: hydrodynamics and thermodynamics. Ph.D. thesis, Florida State Univ., Tallahassee, 141 p.

Tomovic, R., 1963. Sensitivity Analysis of Dynamic Systems, McGraw-Hill, New York, 142 p.

Vollenweider, R. A., 1965. Calculation models of photosynthesis-depth curves and some implications regarding day rate estimates in primary production measurements, in Primary Productivity in Aquatic Environments. Mem. Ist. Ital. Idrobiol., 18, Suppl., C. R. Goldman, ed., Univ. of Calif. Press, Berkeley, pp. 425-457.

Von Brand, T., N. W. Rakestraw and C. E. Renn, 1937. The experimental decomposition and regeneration of nitrogenous organic matter in seawater. Biol. Bull., 72: 165-175.

Von Brand, T. and N. W. Rakestraw, 1940. Decomposition and regeneration of nitrogenous organic matter in sea water. III. Influence of temperature and source and condition of water. Biol. Bull., 79: 231-236.

Walsh, J. J., 1972. Implications of a systems approach to oceanography. Science, 176: 969-975.

Walsh, J. J., 1975. A spatial simulation model of the Peru upwelling ecosystem. Deep-Sea Res., 22: 201-236.

Walsh, J. J., 1976. A biological sketchbook for an eastern boundary current, in The Sea, Vol. 6, J. H. Steele, J. J. O'Brien, E. D. Goldberg, and I. N. McCowe, eds., Wiley Interscience, New York, in press.

Walsh, J. J. and R. C. Dugdale, 1971. A simulation model of the nitrogen flow in the Peruvian upwelling system. Inv. Pesq., 35: 309-330.

Walsh, J. J. and R. C. Dugdale, 1972. Nutrient submodels and simulatation models of phytoplankton production in the sea. in Nutrients in Natural Waters, J. Kramer and H. Allen, eds., J. Wiley and Sons, New York, pp. 171-191.

Walsh, J. J., J. C. Kelley, T. E. Whitledge and J. J. MacIsaac, 1974. Spin up of the Baja California upwelling ecosystem. Limnol. Oceanogr., 19: 553-572.

White, A., P. Handler and E. L. Smith, 1969. Principles of
MacIsaac, 1974. Spin up of the Baja California upwelling ecosystem. Limnol. Oceanogr., 19: 553-572.

White, A., P. Handler and E. L. Smith, 1969. Principles of Biochemistry, McGraw-Hill, New York, 1187 p.

Winter, D. F., K. Banse and G. C. Anderson, 1975. The dynamics of phytoplankton blooms in Puget Sound, a fjord in the Northwestern United States. Mar. Biol., 29: 139-176.

Wroblewski, J. S. and J. J. O'Brien, 1976. A spatial model of phytoplankton patchiness. Mar. Biol., 35: 161-175.

Yentsch, C. S. and R. W. Lee, 1966. A study of photosynthetic light reactions, and a new interpretation of sun and shade phytoplankton. J. Mar. Res., 24: 319-337.

VITA

Joseph Stanley Wroblewski was born June 8, 1948 in Chicago, Illinois. In 1970 he graduated with honors from the University of Illinois at Chicago Circle with a B.S. in Biological Science. He began his graduate study in the Department of Oceanography at Florida State University in September, 1970 and was awarded the M.S. degree in Biological Oceanography in 1972.

117